Catalysis and Photocatalysis over TiO$_2$ Surfaces Detailed from First Principles

By

Juan C. Garcia

Thesis submitted to the Faculty of the

Worcester Polytechnic Institute

in partial fulfillment of the requirements for the

degree of Doctor of Philosophy

in

Chemical Engineering

by

August 2014

APPROVED

Dr. N. Aaron Deskins, Advisor

Chemical Engineering Department, WPI

Dr. Ravindra Datta, Committee Member

Chemical Engineering Department, WPI

Dr. Pratap Rao, Committee Member

Mechanical Engineering Department, WPI

Dr, Nikolaos Kazantzis, Committee Member

Chemical Engineering Department, WPI

Dr. David Dibiasio, Head of Department

Chemical Engineering Department, WPI

Abstract

Catalysts are involved at some stage in the manufacture process of virtually all commercially produced chemical product. Among the materials used as catalysts, metal oxides are one of the most used due to their versatility and wide range of physical properties. Identifying the principles of surface to adsorbate charge transfer is key to a better understanding of metal oxide materials as both catalysts and gas sensors. Using density functional theory (DFT), we modeled the adsorption of small molecules over stoichiometric and reduced metal oxide surfaces of group IV metals and quantify the effect of electron transfer upon adsorption. We found that charge transfer only occurs during the adsorption process of an adsorbate more electronegative than the surface. We also found a correlation between the work function of the metal oxide, and the ionic adsorption of the oxygen molecule.

Mixed phase rutile/anatase catalysts show increased reactivity compared with the pure phases alone. However, the mechanism causing this effect is not fully understood. Using DFT and the +U correction we calculated the bands offsets between the phases taking into account the effect of the interface. We found rutile to have both higher conduction and valence band offsets than anatase, leading to an accumulation of electrons in the anatase phase accompanied by hole accumulation in the rutile phase. We also probed the electronic structure of our heterostructure and found a gap state caused by electrons localized in undercoordinated Ti atoms which were present within the interfacial region. Interfaces between bulk materials and between exposed surfaces both showed electron trapping at undercoordinated sites. Finally, we studied the effect of the size of gold nanoparticles in the catalytic properties of gold decorated TiO_2 surfaces. We found that the adsorption energy of several intermediates reactives in the CO oxidation and water gas shift reaction does not change with the size of the nanoparticles. In conclusion, the factor that affects the reactivity of the system is the density of undercoodinated gold atoms on the interface perimeter.

Table of Contents

List of Figures

.

List of Tables

Chapter 1: Introduction

Catalysts are involved at some stage in the manufacture process of virtually all commercially produced chemical product. Among the materials used as catalysts, metal oxides are one of the most used due to their versatility and wide range of physical properties. Some of the most interesting magnetic, optical, and electronic properties are found within this class of materials. Understanding the surface properties of metal oxides, their electronic structure, and reactivity with adsorbed molecules is crucial in many technological applications.[1]

The elimination of contaminants from waste effluents has become a primary issue due to the consequences to human health. Several methods have been developed to address this problem such as high temperature incineration, amended activated sludge digestion, anaerobic digestion. One of the most successful of such methods have been the supplementary and complementary use of semiconductor photocatalysts.[2] These materials use the energy of electromagnetic radiation to promote the excitation of electrons to the conduction band where they can diffuse to the surface and participate in reduction reactions. These materials also have application in photovoltaics for solar energy conversion, for instance in photo-electrolytic cells, since the pioneer work of Fujushima et al.[3] Another important application is in gas sensor devices, where the variation of the resistivity of the metal oxide with the adsorption of certain molecules is used as a

detection mechanism.

Among the metal oxide catalysts TiO_2 has become the prototype material. The interest in this material has grown over the years. The Fig. 1.1 shows the number of publications since 1988 until 2012, when the number of publication reached more than 10000. Fig. 1.1 also shows the number of publication using TiO_2 in photocatalysis.
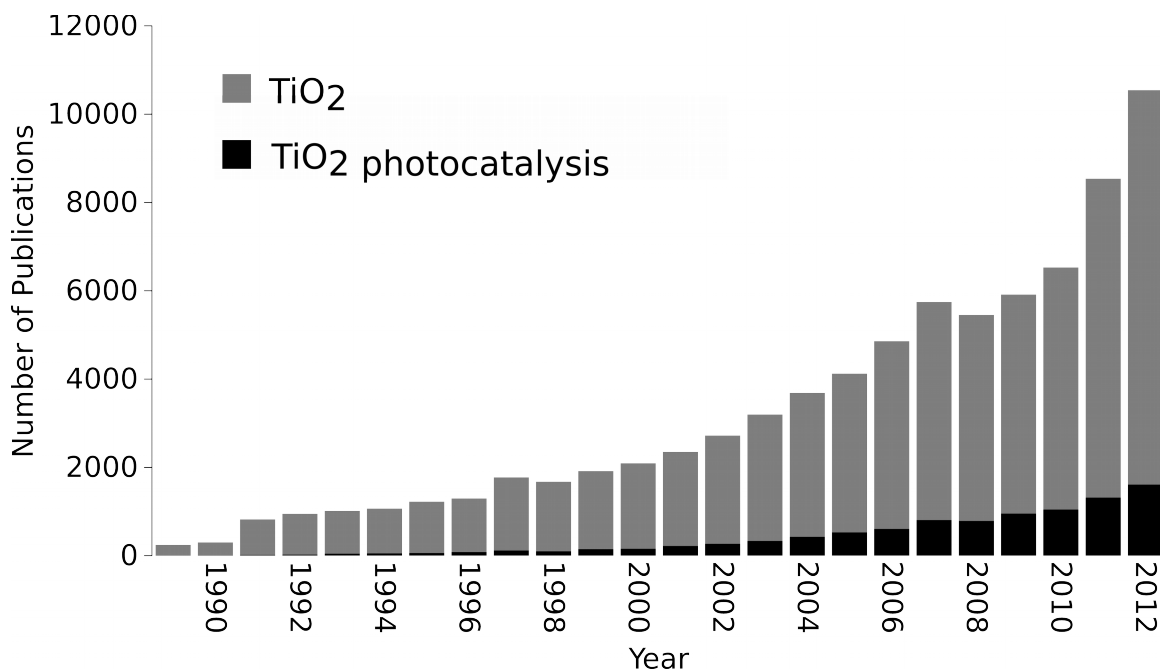
Fig. 1.1 Number of publications about TiO_2 and photocatalysis using TiO_2.

The design of catalytic materials has been traditionally a trial and error process. The process of design and development of heterogeneous catalysts relied on experiments. A candidate catalyst is synthesized, characterized and tested under the best conditions, usually followed by another characterization in situ.[4] This approach leads to a lengthy evolution.

The design of a material from pure theoretical methods would be a faster and cheaper process. However, despite the advanced state of theoretical and computational approaches several limitations still remain, due to the computational cost of the calculations. Then, to design optimal, inexpensive materials is required both experiments and molecular models to characterize the properties of new candidate materials.[5]

A well designed catalyst should have the characteristics of activity, stability, selectivity, and regenerability. All those attributes depends on the chemical and physical properties of the species involved in the reaction and the dynamics of their interaction. The knowledge of the processes taking place at a microscopic level play a fundamental role in the whole design scheme. The size, shape, and surface structure at the nanoscale, as well as on their bulk and surface composition influence the activity and selectivity of catalysts.[6] In addition, surface defects are highly important as they largely determine phenomena such as corrosion, adsorption, and catalytic behavior for many oxides. Defects often lead to excess electrons within the metal oxide lattice, or reduction of the material, and the ability of these electrons to affect surface chemistry has been the subject of several studies.[7–12]

In the present work, we examine the role of the morphology and composition of several metal oxide surfaces with emphasis on TiO_2 in the catalytic performance of such materials in a molecular scale. This will lead to a better comprehension of the microscopic process taking place during catalytic reactions. We are primary interested in the mechanisms of adsorption over stoichiometric and reduced surfaces, the reasons of

increased reactivity of mixed phase catalysts, the role of under coordinated metal atoms in the catalytic process and the effect of deposited metallic nanocluster in the reactivity of metal oxide surfaces.

In the next section we present a review of the literature, where the systems and processes under study are described and also the theoretical methods used. Then is established the scope of the present work and the overall goal and principal objectives. The chapter 2 shows the results obtained for the ionic adsorption process over group IV metal oxides surfaces, specifically TiO_2, ZrO_2 and HfO_2. Chapter 3 presents our work on the relative stability of electrons in mixed phases TiO_2 catalysts, which could explain the increased reactivity of the system. Finally, chapter 5 shows our findings in the effect of the size of gold nanoparticles supported on TiO_2 in the reactivity of such surfaces and chapter 6 presents the conclusions of our work.

1.1. Literature Review

This chapter presents an overview of the underlying principles governing the catalytic process on metal oxides. The study will be focused on the microscopic processes, since those are the key to understand the nature of the chemical transformation taking place in the surface of the catalyst. Initially, it is described the materials involved in this work and the mechanism of the processes and subsequently the theory to model them.

1.1.1. Metal oxide surfaces

Despite catalysts are often used in polycrystalline powder form the chemical reactions occur in specific sites in the facets of each micro crystal. Then, to understand the chemistry of this system we can study the reaction on the surfaces of the crystalline materials. The geometry of those surfaces, depend on the geometry of the bulk phase and the stability of the surfaces.[13]

The geometry of metal oxides can be understood used a simplified model where the bonds are considered to be ionics. Then, the forces in the lattice are between the positively charged metal atoms and the negative oxide O^{2-} anions, which are unstable in free space but are stabilized by the Madelung potential of the lattice.[13] The most stable configuration are usually with the metal cations surrounded by oxygen anions.

The configuration of metal oxide shows systematic features that are repeated in several different structure types. The stoichiometry and coordination of the ions determine the geometry of the lattice. The most common geometries of metal ions are tetrahedral, square planar, octahedral and cubic. Fig. 1.2 shows those configuration schematically.[14]
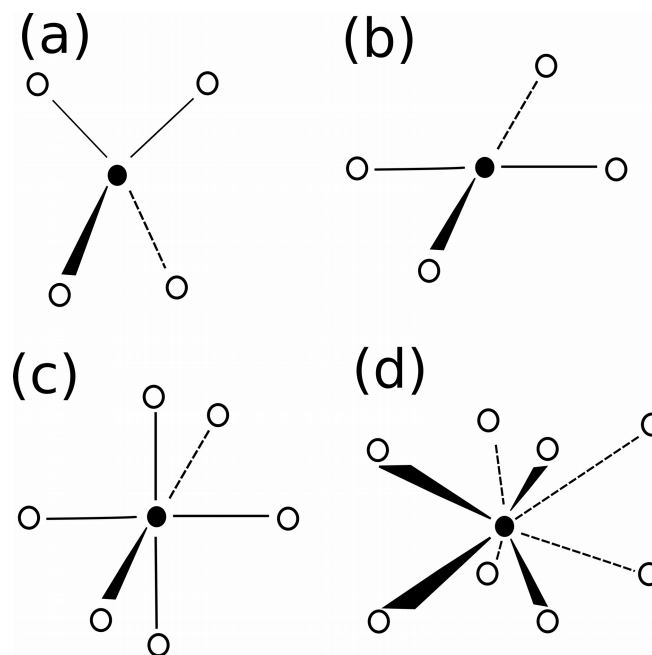
Fig. 1.2. Most common coordination geometries of metal atoms. The metal atoms are represented by black filled circles and O atoms are circles. (a) tetrahedral, (b) square plane, (c) octahedral, (d) cubic

Geometry of TiO_2 phases

Titanium dioxide presents three principal stable phases, namely, rutile, anatase and brookite. Rutile is the most stable phase, however anatase is most stable for particle size less than 11nm.[15] These polymorphs have different properties and exhibit different photocatalytic properties. Anatase transforms irreversibly to rutile at elevated temperatures.[16] The characteristic structural feature of TiO_2 phases is that of Ti^{4+} in an octahedral field of O^{2-} anions.[17] Since Brookite is rare compared to anatase and rutile and it has been less used as a catalyst we are going to focus on the description of rutile and anatase.

6

Bulk rutile has a tetragonal unit cell with two atoms per cell. The Ti atoms are located in the corners and center of the unit cell presenting a six coordinated structure, as is shown in Fig. 1.3 (a). The structure can be visualize as a chain of TiO_6 octahedron parallel to [001] direction(Fig. 1.3(b)).

<table>
<tr><td>(a)</td><td>(b)</td></tr>
</table>
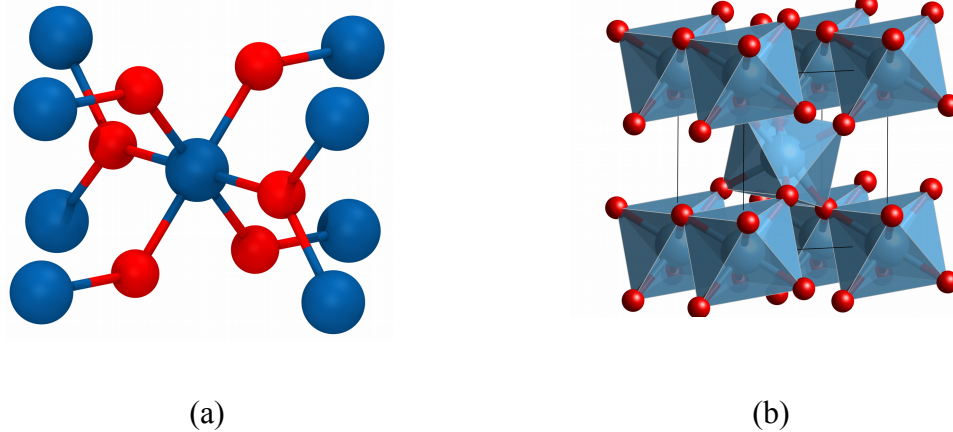
Fig. 1.3. TiO_2 rutile phase (a) unit cell (b) Polygon representation. Red spheres represent oxygen and blue spheres represent titanium.

The most stable surfaces of rutile are the (110) and (100) being the most thermally stable the (110).[18] The (110) surface it is shown in Fig. 1.4 (a) where can be seen the bridging oxygen atoms forming rows separated by rows of five coordinated Ti atom, while the Ti connected by the bridging oxygen are six coordinated.

<table>
<tr><td>(a)</td><td>(b)</td></tr>
</table>
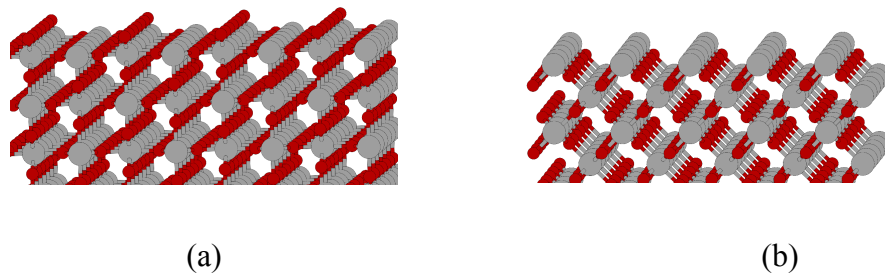
Fig. 1.4. Most stable rutile surfaces (a) (110) surface(b) (100) surface.

The anatase (101) surface presents a sawtooth like structure as is shown in Fig. 1.5. Titanium atoms at the terraces have fivefold and sixfold coordination, and titanium atoms at the step edges are fourfold coordinated. In the ridges there are twofold coordinated oxygen atoms.[19] To compensate the strain generated by the missing bonds in the surface the atoms relax to a new equilibrium position.
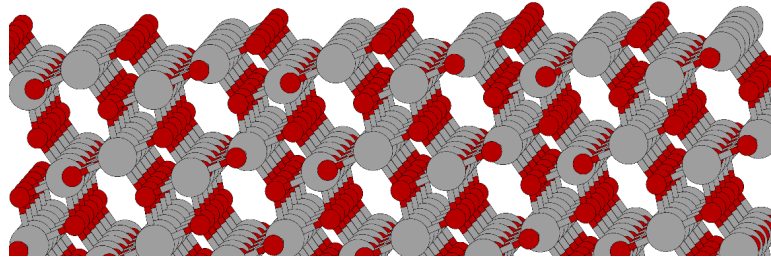
Fig. 1.5. Geometry of (101) anatase surface.

Rutile and anatase are n-type semiconductors. The effective electron mass has been found to be very large, 30-100 times greater than free electron. It is thought that the source of electronic conductivity in rutile is Ti^{3+} produced from the loss of oxygen.[3] The electronic structure calculated for the surfaces is very similar from that of the bulk. However, non-stoichiometric surfaces may present surface states.[19]

Electronic structure of TiO₂

Rutile TiO₂ is a semiconductor with a wide band gap of 3.0eV. The valence band is based predominantly on O 2p orbitals, while the conduction band is Ti 3d based.[20] The ionicity (the degree of ionic bonding) of rutile TiO_2 is of the order of 70%, meaning that it has a non-negligible covalent character. The anatase phase presents a band gap of 3.2eV.

The most simple electronic models of metal oxides assume electron electron repulsion as an average potential. However, in metal oxides this theory can break down due to the localization of electrons in the ions. The electron transfer from one ion to another require energy, which depends on the extra electron repulsion present in the receptor ion, this energy is know as the Hubbard U.[13]

Localized electrons tend to polarize the surrounding lattice. The electrons and the concomitant polarize lattice around them are know as polaron. If the polarization is strong enough the electron is unmobilized by the potential produced by the polarized lattice, this is know as a small polaron. The polaronic characteristic of the TiO₂ phases could have a strong influence in the photocatalytic process due to the change in stability and mobility of the charge carriers.[14]

1.1.2. Semiconductor photocatalysis

We can define photocatalysis as a photo-induced catalytic process.[21] In the present

work we are interested in such processes over solid semiconductors as heterogeneous catalysts. When molecules are formed, bonding and anti-bonding orbitals develop considering the Pauli exclusion principle. For instance, in a diatomic molecule each energy level of the isolated atoms splits into two molecular orbitals belonging to the pair, one lower in energy than the original atomic level and one higher. Usually only the less energetic orbital is occupied. When monomers are put together the energy necessary to photo-excite the electrons decreases. For n atomic orbitals in a molecule, n molecular orbitals are produced. As the number of molecular orbitals increases, the energy difference between the lowest bonding and the highest antibonding orbitals increases, while the space between each individual orbital decreases. For a big number of monomers as in crystalline solid a band of allowed energy is formed for occupied and unoccupied states. Those are the so called valence and conduction bands, which are separated by forbidden levels of energy known as band gap E_g.[21]

The photocatalytic process starts with the absorption of electromagnetic radiation, which excites an electron from the valence band to the conduction band, leaving a hole in the valence band. Fig. 1.6 shows a schematic representation of this process. In this process energy and momentum have to be conserved. The energy is conserved if the photons have the same energy of the band gap. The conservation of moment imply that the electrons must have the same momentum as the hole state plus the momentum of the photon. Since the wave vector of optical photons are negligible small, then the electron and holes have to have the same wave vector (k).[14] However, indirect optical transitions between two bands with different wave-vectors are possible with the participation of

phonons, but they are weaker than direct transitions.

The electron and holes can diffuse to the surface of the material and participate in chemical reactions. The mobility of the carrier is a significant property of semiconductor. The carrier in a semiconductor has an effective mass that is heavier than the free electron mass, owing to the presence of the periodic potential in the crystal. The electrons and holes may be trapped in the surface where react with acceptor and donor molecules.[3] The electrons and holes can also recombine there with the release of heat.
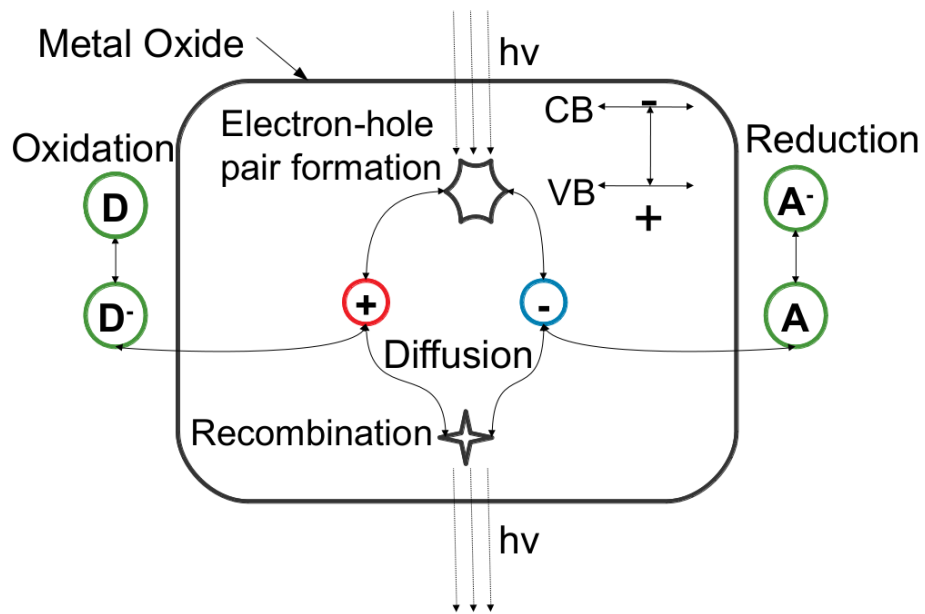
Fig. 1.6. Schematic diagram of the photocatalytic process.

1.1.3. Interaction of surfaces with small molecules

A catalyst increases the rate of a chemical reaction. Reactants bind to the surface of the catalyst, bonds are broken, and products are being formed leaving the catalyst unaltered. Thus a good catalyst must bind the reactants and at the same time facilitate the formation of products. In order for the products to desorb a good catalyst must not bind the products too strongly. In this thesis we focus on heterogeneous catalysis in which the reactants and the catalyst are in different phases. In this thesis the reactants and products are in the gas phase and the catalyst is in the solid phase.

When a molecule approaches catalyst surface, it starts interacting with the surface and form a bond. If the interaction is a long range one caused by dipoles, we say that the molecule is physisorbed on the surface. More importantly for this thesis, if the molecule goes even closer to the surface, direct interaction between the wave functions of the molecule and the catalyst happens, a much stronger, so called chemisorption takes place.

The binding mechanism of molecules on the TiO_2 surface affects its electronic structure.[17] Some factor as coverage, thermal stability and reactivity and adsorption structure determine the pathway of the reaction on the surfaces. Adsorption over TiO_2 has been extensively studied,[19,22–24] especially over the rutile phase. However, the anatase polymorph of TiO_2 is also a promising material because of its reactivity.[1,25] There are several theoretical studies on adsorption reactions and surface properties of anatase (101) surfaces.[26–29] DFT calculations also indicate that in the presence of O vacancies (Ov),

several absorbates have higher adsorption energies over anatase as compared to rutile, and the defects may act as nucleation sites for Au and Pt growth.[30] HfO$_2$ and ZrO$_2$ surfaces have been less studied than TiO$_2$, particularly using theoretical methods. However, significant attention has been paid to the deposition of thin zirconia/ hafnia films for microelectronics and catalysis.[31–37] Theoretical studies of HfO$_2$ and ZrO$_2$ surface adsorption have been performed, such as involving water and hydrogen,[38–41] Au,[42] or sulfuric acid.[43] Surface defects have also been modeled,[44–46] although charge transfer due to the presence of point defects has not systematically been explored over these oxides.

1.1.4. Molecular modeling methods

The two types of modeling methods most often used in heterogeneous catalysis are either based on quantum mechanics or based in parameterized interaction potential between atoms.[47] The objective of both methods is to find the spacial configuration of the atoms that minimize the total energy. Since, we are interested in the interaction between small molecules and the solid catalytic surfaces and the localization and transfer of charge, quantum mechanics methods are needed. The next section is a brief overview of the theory used in the calculations involved to get the results of the present work.

Electronic structure calculation

Ab initio calculations are difficult. The trouble is that the electrons have been observed to obey complicated and nonintuitive quantum mechanical laws. According to quantum theory, the electrons can only be described probabilistically. This means that the absolute positions and velocities of the electrons cannot be known exactly; rather, the whole system must be described by a mathematical object, namely, the wave function.[48] Experiments have shown that the wave function satisfies the Schrödinger equation to a very good approximation. Unfortunately, solving this equation to find the wave-function is not generally feasible. One difficulty comes from the nature of the electrons. They are fundamentally identical. This has more than just philosophical implications. It means that all physical quantities must be left unchanged when two electrons switch places. For this to be true, the wave-function can only change at most by an overall sign. The other complication arises from terms in the Schrödinger equation that describe how the electrons interact and repel each other. This mutual repulsion makes the solution grow exceedingly complex as the number of electrons increases.

The ultimate goal of most approaches in solid state physics and quantum chemistry is the solution of the time-independent, non-relativistic Schrödinger equation.[49]

$$\hat{H}\left(x_1, x_2, ..., x_N, R_1, R_2, ..., R_N\right) = E_i \Psi_i\left(x_1, x_2, ..., x_N, R_1, R_2, ..., R_N\right) \tag{1.1}$$

\

Where $\hat{H}$ is the Hamiltonian for a system of M nuclei and N electrons with coordinates x_i, R_i respectively. Ψ is the wavefunction and E the energy.

14

$$\hat{H} = -\frac{1}{2}\sum_{i=1}^{N}\nabla_i^2 - \frac{1}{2}\sum_{A=1}^{M}\frac{1}{M_A}\nabla_A^2 - \sum_{i=1}^{N}\sum_{A=1}^{M}\frac{Z_A}{r_{iA}} + \sum_{i=1}^{N}\sum_{j>1}^{N}\frac{1}{r_{ij}} + \sum_{A=1}^{M}\sum_{B>A}^{M}\frac{Z_{AB}}{R_A R_B} \quad (1.2)$$

Here, A and B run over the M nuclei while i and j denote the N electrons in the system. The first two terms describe the kinetic energy of the electrons and nuclei. The other three terms represent the attractive electrostatic interaction between the nuclei and the electrons and repulsive potential due to the electron-electron and nucleus-nucleus interactions.[49]

Due to their masses the nuclei move much slower than the electrons so we can consider the electrons as moving in the field of fixed nuclei. Therefore the nuclear kinetic energy is zero and their potential energy is merely a constant. This is called the Born-Oppenheimer approximation. Thus, the electronic Hamiltonian reduces to:[49]

$$\hat{H}_{elec} = -\frac{1}{2}\sum_{i=1}^{N}\nabla_i^2 - \sum_{i=1}^{N}\sum_{A=1}^{M}\frac{Z_A}{r_{iA}} + \sum_{i=1}^{N}\sum_{j>1}^{N}\frac{1}{r_{ij}} \qquad (1.3)$$

The solution of the Schrödinger equation with $\hat{H}_{elec}$ is the electronic wave function Ψ_{elec} and the electronic energy E_{elec}. The total energy E_{tot} is then the sum of E_{elec} and the constant nuclear repulsion term E_{nuc}.

$$\hat{H}_{elec}\Psi_{elec} = E_{elec}\Psi_{elec} \qquad (1.4)$$

$$E_{tot} = E_{elec} + E_{nuc} \qquad (1.5)$$

The variational principle

An important theoretical principle, upon which many calculations rely, is the

variational principle. It tells us how to look for ground-state solutions. The exact ground state wavefunction minimizes the expectation value of the Hamiltonian.[50]

$$E = \frac{\min_{\Psi} \left\langle \Psi | \hat{H} | \Psi \right\rangle}{\langle \Psi | \Psi \rangle} \tag{1.6}$$

A guessed normalized wave-function will always give a greater expectation value for the total energy. To make the problem operable a normalized trial solution is expanded in the complete basis of exact solutions for a chosen Hamiltonian:

$$|\Psi_{trial}\rangle = \sum_i c_i |\Psi_{trial}\rangle \tag{1.7}$$

$$\langle \Psi_{trial} | \Psi_{trial} \rangle = \sum_i |c_i|^2 = 1 \tag{1.8}$$

Then, the energy expectation value using the trial wave-function is:[50]

$$E_{trial} = \left\langle \Psi_{trial} | \hat{H} | \Psi_{trial} \right\rangle = \sum_i |c_i|^2 E_i \tag{1.9}$$

Density Functional Theory

Density functional theory (DFT) has been the most successful and widely used method in condensed matter physics, computational physics and quantum chemistry to describe properties of condensed matter systems, which include not only standard bulk materials but also complex materials such as molecules, proteins, interfaces and nanoparticles. The main idea of DFT is to describe a many-body interacting system via its particle density and not via its many-body wavefunction. Its significance is to reduce the

16

3N degrees of freedom of the N-body system to only three spatial coordinates through its particle density.

The basis of DFT is the well known Hohenberg-Kohn (HK) theorem, which claims that the wave-function and all physical properties derived from it are uniquely characterized by the ground-state electron density $\rho(r)$. The map between external potential and the electron density is one to one and unique up to an arbitrary constant shift in the potential.[38] The Hohenberg-Kohn second theorem states that it is possible to define a universal functional for the energy E[ρ] depending on the electron density $\rho(r)$. The true ground state energy is the global minimum of the energy functional, and the density \rho(r) which minimizes the functional is the exact ground state density.[51]

In 1965, Kohn and Sham (KS) introduced an orbital method for the quantitative modeling of electronic structure.[52] In order to evaluate the kinetic energy of N noninteracting particles given only their density distribution $\rho(r)$, they simply found the corresponding potential $v_{eff}(r)$, and used the Schrödinger equation.

$$\left(-\frac{1}{2}\nabla^2 + v_{eff}\left(r\right)\right)\psi_i\left(r\right) = \varepsilon_i\psi_i\left(r\right) \tag{1.10}$$

where:

$$\rho\left(r\right) = \sum_i^N |\psi_i\left(r\right)|^2 \tag{1.11}$$

It is necessary to determine the set of wave functions ψ_i that minimize the KS energy functional $E\left[\rho\left(r\right)\right]$. These are given by the self-consistent solutions to the KS

equations, which are a set of eigenvalue problems as shown in equations 1.10 and 1.11.

The effective potential $v_{eff}(r)$ is the sum of the potential produced by the ions $v_{ions}(r)$, the Hartree potential v_H represented in equation 1.12 and the exchange correlation potential $v_{xc}(r)$ which account for the non classical effects, which will be described in the next section.[53]

$$v_H(r) = \int \frac{\rho(r)}{|r - r'|} d^3 r' \tag{1.12}$$

The exchange correlation functional

In DFT, the total energy is expressed as a functional of the density:

$$E[\rho(r)] = T[\rho(r)] + V_{ee}[\rho(r)] + \int d^3 r v_{ions}(r)\rho(r) \tag{1.13}$$

Where $T[\rho(r)]$ is the kinetic energy and $V_{ee}[\rho(r)]$ is the electron electron interaction energy. This interaction can be computed as the sum of the Hartree potential defined in equation 1.12 and the energy for exchange correlation $E_{xc}[\rho(r)]$.[53]

The exchange-correlation energy has been referred to as nature's glue because it is responsible for keeping much of matter together by counteracting some of the Coulomb repulsion.[54] The exchange- correlation contribution reduces the interaction energy because it accounts for the tendency of electrons not to collide. The exchange-correlation potential is defined by:

$$v_{xc} = \frac{\delta E_{xc}\left[\rho\left(r\right)\right]}{\delta\rho\left(r\right)} \qquad (1.14)$$

Then the effective potential $v_{eff}\left(r\right)$ in equation 1.10 can be computed as:

$$v_{eff}\left(r\right) - v_{ions}\left(r\right) + v_H\left(r\right) + v_{xc}\left(r\right) \qquad (1.15)$$

The equation 1.10, must be solved using a self-consistent scheme. An initial guess for the density is made and a effective potential is constructed from it. The resulting KS equation is solved for the KS orbitals ψ_i, and the orbitals are then used to find a new density with equation 1.11. The new density gives a new potential and we calculate again. This procedure is re-iterated until the density changes less than some chosen criteria.[53]

If the $E_{xc}\left[\rho\left(r\right)\right]$ used in the calculation is exact, the calculated density is also exact. However, an exact exchange correlation energy is unknown. Then, we have to use an approximation which has a higher computational cost for increased detail and accuracy.

The efficiency of an electronic structure method is often characterized by the way a calculation effort grows with the number of electrons, N . Ideally, an electronic structure calculation for N electrons would be as complicated as a calculation for one electron times N . This is called order N and is for the most part not possible yet without a compromise in accuracy. DFT typically scales as N^3 but in some cases as N.

1.2. Problem statement

A more fundamental understanding of the catalytic processes in the microscopic scale is required to design better catalysts. The size, phase, interfaces and defects can change the electronic density distribution in the lattice. It is necessary to know the effect of the morphology of the catalysts in the electronic structure in order to gain some insights in the catalytic process over metal oxides.

Our approach is the use of first principles calculation to elucidate the microscopic mechanism involved in the catalytic processes over group IV metal oxides. In this section we establish the objectives and scope of the present work. Our overall goal is to understand the catalytic and photocatalytic processes over TiO_2 from first principles.

Fig. 1.7 shows a schematic representation of the system modeled in the present work. The red spheres represent oxygen atoms, pink spheres represent a metal, the blue sphere represent a C atom and the yellow spheres represent Au atoms. It is shown the three aspects of the problem addressed in this work. First, we analyzed the ionic adsorption process over group IV metal oxides. Second, we studied the relative energy of electrons in mixed phase TiO_2 catalysts in order to explain the increased reactivity of the system. Finally, we analyzed the influence of the size of Au nanoparticles on the adsorption energy over different sites of several small molecules.
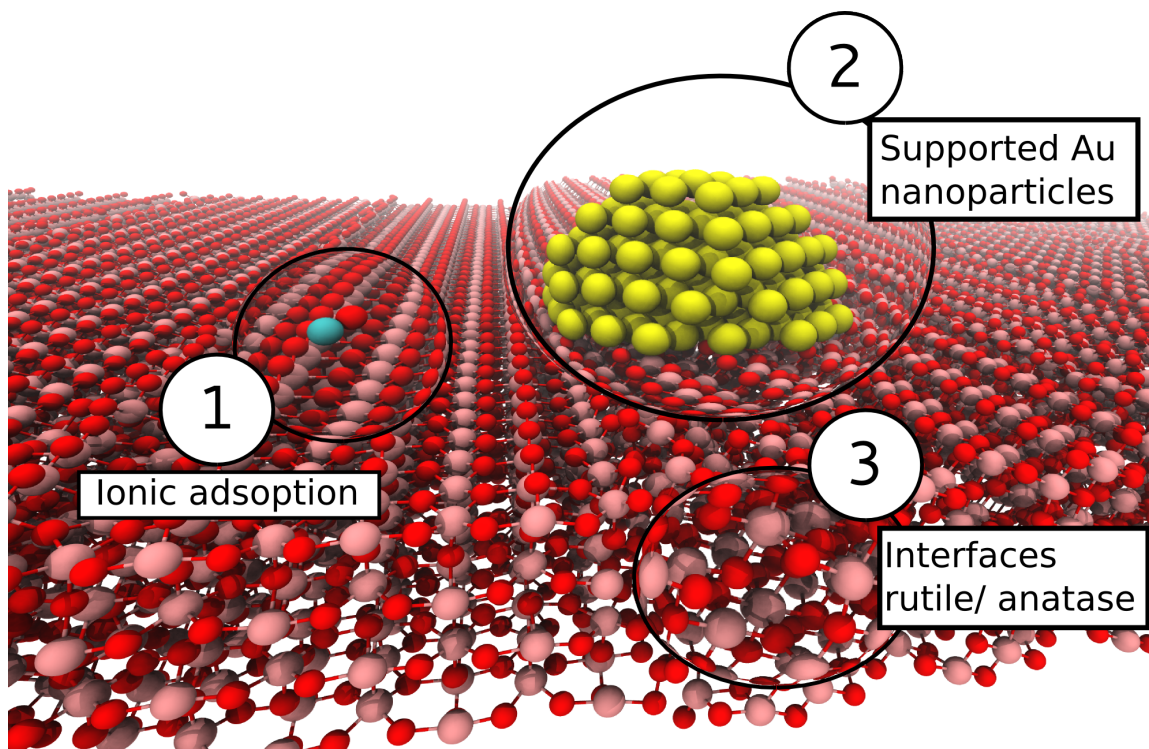
Fig. 1.7. Schematic representation of a mixed phase TiO_2 rutile/anatase surface showing a CO molecule and a gold nanoparticle over the surface. The three principal aspects of the problem addressed in this thesis are highlighted.

1.2.1. Charge transfer processes over TiO_2

The adsorption and desorption of reactive intermediates play a fundamental role in the definition of a pathway for any reaction. The strength of the interaction between the adsorbate and the surface defines the final output of products. The nature of this interaction may vary according with the structure of the species participating in the process.

The knowledge of the details of the adsorption process would allow the identification of a descriptor for the interaction process. For example, correlating the

strength of the binding with a property of the system. Identifying the principles of surface to adsorbate charge transfer is key to a better understanding of metal oxide materials as both catalysts and gas sensors. The extra charge in the adsorbate might stabilize the molecules at the solid surface and also weakens the bonds promoting the dissociation or reaction with another molecules. However, the whole mechanism of charge transfer is poorly understood.

The mechanism responsible for gas sensing effects is not fully understood, but is associated with electron transfer to absorbates, forming negatively charged anions, or ionosorption. Catalytic surface reactions may also involve electron transfer from the oxide to the absorbates. For instance, the reduction of an organic molecule over a catalytic surface requires the transfer of electrons from the solid to the adsorbate.

Using density functional theory, we modeled the adsorption of small molecules over stoichiometric and reduced metal oxide surfaces of group IV metals and quantify the effect of electron transfer upon adsorption. Surface reduction was accomplished through creation of oxygen vacancies, which lead to unpaired electrons within the oxide lattice, and which may eventually transfer to absorbates. We examined the TiO_2 anatase (101), tetragonal HfO_2 (101), and tetragonal ZrO_2 (101) surfaces. We first focused on O_2 (a known electron scavenger) adsorption at surface cation sites and expect to analyze the formation of anionic O_2 species. Our objective is to quantify the nature of the ionosorption process of small molecules on TiO_2 surfaces and compare with other group IV metal oxides.

1.2.2. Electronic properties of mixed phase TiO$_2$ catalysts

TiO$_2$ photocatalysts consisting of two phases have shown increased catalytic activity over single-phase catalysts (rutile or anatase), even up to ten times more activity.[55–60] the reason for the increased reactivity is still in debate (see a recent review article[61]) but could involve several factors, including bulk charge separation, interfacial charge transfer effects or special interfacial reaction sites. The electron hole recombination rate decreases because one or several of such factors produce a energy barrier for the process.

There have been a debate on the mechanism of chemical reaction on mixed phase TiO$_2$ catalysts due to the increased observed reactivity. However, there is experimental evidence that the phase junction formed between anatase and rutile in the surface of the catalyst can enhance the photocatalytic activity for photo-catalytic reaction, for instance, H$_2$ production.[62]

In this work we modeled using DFT the interface between rutile and anatase phases of TiO$_2$ in order to further identify the mechanism of the increased reactivity of these mixed-phase catalysts. This information could lead to the design of heterostructure with better catalytic performance.

Relative stability of electrons and holes in mixed phase bulk   TiO$_2$

There have been several attempts to explain the increased activity of the mixed

phases catalysts.[61] the most accepted hypothesis is that presence of the two phases lowers the electron-hole recombination rate, which increases the number of surface electron/holes, and therefore the surface reactivity.[17,25,63] The conduction band (CB) minimum of anatase has been proposed to be higher that the CB minimum of rutile.[25,63,64] The valence band (VB) maximum, according with this hypothesis, are very similar for both phases. Therefore, the photo-excited electrons may selectively migrate to the rutile phase, while holes may migrate to the anatase phase, which effectively lowers the recombination rate. However, some experimental work suggests that photo-generated electrons may migrate from rutile to anatase, due to trapping sites in the anatase lattice.[65] The preferred phase of the electrons (or holes) is determined by the relative energy of the two phases' conduction bands (or valence bands). Strong interfacial regions between the phases has been suggested to facilitate charge transfer.[66–68] Other work attributes special four-coordinated Ti interfacial sites as contributing to the increased photo reactivity.[25,62,65,69]

Band offsets at semiconductor heterojunctions are known fundamental parameters which govern the transport properties of electrons, and the differences in energy of the bands determines the direction and magnitude of the electrical current.[70] The estimation of the band offsets for semiconductor interfaces is crucial to understand the behavior of a metal oxide mixed phase catalysts. In order to determine offsets using electronic structure techniques it is typically necessary to simulate an interface between the two materials.[71] There have been successful attempts to model interfaces.[72–74] These models mostly use

bulk properties of the different constituents. However, the detailed atomic and electronic properties at the interface are know to influence band offsets.[75] The geometry of the interface could induce the formation of trapping sites and dipoles, which could affect the band structure. The power of electronic structure calculations is that one can determine band offsets between two materials, and quantify the nature of the interfacial region.

The way the electrons localized in each phase in fundamental to understand the physics of the system and build a model that emulate the real system as well as possible. We modeled several of the possibles equilibrium geometries of the interface between anatase and rutile and line up the band energies of both phases based on a common reference in order to get the band offsets. Our objective is to determine the thermodynamically favorable flow direction of electrons on mixed phases TiO_2, taking into account the influence of the interface structure.

Stability of electrons in special sites on mixed phases TiO_2 catalysts

The trapping of electrons in special sites in the materials could lead to increased reactivity due to the availability of those electrons to be transfer to absorbates.[64,76] The chemical reactivity of TiO_2 has been correlated to the interfacial surface area.[77] Based on this, interfacial regions are likely locations of unique active sites for charge trapping, transfer, and chemical reactions.[64]

The four coordinated Ti atoms are unstable in any bulk phase of crystalline TiO_2, however they could be stabilized in an interfacial region or surface. In the interfacial

region the geometry is amorphous, leading to several different configuration for the Ti atoms. Under coordinated Ti atoms and the surrounding O atoms could act as a potential well where a localize electron sits in a small polaron like structure.

We identified undercoordinated atoms within the interfacial region of the mixed material. We analyzed the localization of charge in those sites using the spin density and the projected density of states (PDOS). The spin density indicates the presence of unpaired electrons in the orbitals of the atom. Those allowed states should lie within the band gap of the material below the energy of the Fermi level. Our specific objective is to analyze the influence of morphology in the relative stability of electrons on mixed phases catalysts and TiO_2 nanostructures.

Reactivity of mixed phase TiO_2 surfaces

Most semiconductor photocatalytic processes end in recombination of the electrons instead of producing chemical energy. Therefore, research involving titanium dioxide focuses on making the catalyst more active and efficient in ultraviolet as well as visible light. By making the catalyst more active in visible light, the process is more practical for use in gas and water waste purification, energy renewal, and storage.

The mechanism of photocatalysis over mixed phase TiO_2 is still in debate. The experimental results show an enhanced reactivity in this system. Besides, there are several experiment that corroborate the charge transfer process from one phase to another.

However, there has not been a clear theoretical description of a surface. This is partially due to the difficulty to model a big enough supercell with an interface. The supercell has to be big because it is necessary to match two phases with different cell parameters in a periodic supercell. Another factor is the intrinsic difficulty to build a reasonable model for the geometry of the interfacial region between each solid phase.

The increased catalytic activity of mixed-phase TiO_2 catalysts has been proposed to be due to the synergistic activation of the rutile phase by anatase.[65] The rutile phase extends the photoactive range into the visible, and electron transfer from rutile to anatase trapping sites lower charge recombination rate.

The reactivity is usually linked with the strength of the adsorption of the intermediates with the catalyst. In a mixed phase catalyst there may be several distinguishable regions presenting different affinity to each intermediate. The mechanisms of adsorption and surface affinities of organic compounds has been shown to differ significantly when comparing adsorption to pure phase TiO_2 crystalline planes versus mixed phase TiO_2.[65] The strength as well as the nature of the intermolecular force between the adsorbate and the surface play a role in the reactivity of the catalyst. Our objective is to analyze the physical parameter that affect the ionic adsorption of small molecules in mixed phase TiO_2 surfaces.

1.2.3. Gold nanoclusters over TiO₂ surfaces

Despite the chemically inert nature of gold the high catalytic activity of gold supported on metal oxide is well know. However, the microscopic processes taking place in that material are not understood. For instance, it is not clear where the active sites are and their nature. [78]

The oxidation of CO on gold supported on TiO₂ is a example of the synergistic effect of the materials. Pure TiO₂ adsorb CO weakly, however,it can be oxidize at room temperature with gold cluster deposited on the surface. [19]

It is accepted that gold must be in small particles to be active, where quantum size effects significantly alter the electronic structure of the particle. There is evidence that the reactivity of the system does not increase with the size of the gold nanocluster after certain critical size. This could be evidence of the role of the coordination in the chemical process.

The interaction between gold clusters and the substrate has been shown to play a significant role,[79] but an understanding of this phenomenon is still missing. Electron transfer between support and cluster might further modifies the electronic structure of the metal. The interface between the metal particle and the support creates new reaction sites that favor the catalytic reaction. The metal particle provides adsorption sites for at least one of the reactants, while the support may participate as a reactant reservoir.[80]

We explained the role of the interaction between the gold nanocluster and the surface. In order to accomplish this task we performed DFT+U calculation to identify the

activity of several possible active sites. The electron transfer and the availability of those electrons in special sites may produce the preferential adsorption on those sites. Our objective is to explain the influence of the morphology of gold nanocluster decorated TiO_2 surfaces on the reactivity of the system.

Chapter 2: Detailing Ionosorption over TiO₂, ZrO₂, and HfO₂ from First Principles

2.1. Introduction

The study of metal oxides is an area of rich active research, because some of the most interesting magnetic, optical, and electronic properties are found within this class of materials. Understanding the surface properties of metal oxides, their electronic structure, and reactivity with adsorbed molecules is crucial in many technological applications.[1] In addition, surface defects are highly important as they largely determine phenomena such as corrosion, adsorption, and catalytic behavior for many oxides. Defects often lead to excess electrons within the metal oxide lattice, or reduction of the material, and the ability of these electrons to affect surface chemistry has been the subject of several studies.[7,9–12,81]

Metal oxides are often used either as catalyst supports or directly as catalysts for a variety of applications.[2] Electron transfer from the metal oxide plays a fundamental role in many catalytic processes, such as photocatalytic oxidation of organic contaminants and other reactions over TiO_2.[9] Oxygen acts as a well-known electron scavenger in these processes, and without its presence the photocatalyst would deactivate due to negative charge accumulation.[9,82,83] Detection of gases is also a subject of growing importance with domestic, environmental and industrial applications.[84] Metal oxides have attracted attention for gas sensing applications due

to their sensitivity and relatively low cost. The design of better gas sensing devices depends in part on knowledge of the sensing mechanism. The gas sensing mechanism is associated with surface reactions of absorbed molecular and atomic ions (O_2^- and O^-) that have scavenged electrons and then can react with a reducing gas such as CO, releasing electrons.[85] After the adsorption of a molecule on the surface the concentration of electrons in the conduction band decreases due to surface electron transfer which leads to increased electrical resistance of the material. This process in turn leads to a change in the conductivity of the oxide, allowing the indirect detection of the gas.

These gas-sensing effects have been explained by the ionosorption model.[86] This is illustrated in Fig. 2.1, which shows the initial adsorption, electron transfer, and final anionic state of the adsorbate. Electrons from the conduction band of the solid become captured by adsorbates, leading to ionization of the adsorbate, or anion formation. The bond formed in this process thus has strong ionic character, as the negatively charged adsorbate interacts with positively charged surface metal cations. SnO_2 sensors are the prototype oxide-based gas sensor involving ionosorption. There is however a great interest in understanding the mechanism in other oxides in order to develop better gas-sensing devices.[87–89]

31
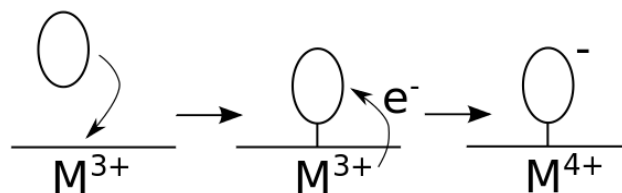
Fig. 2.1. Illustration of the ionosorption process showing adsorption, then electron transfer to form an anionic adsorbate. M represents a metal cation site.

Defects can have a strong effect on surface processes because they can provide electrons for charge-transfer processes, such as shown in Fig. 2.1. Defects can also serve directly as reaction sites, such as an oxygen vacancy being filled by H_2O or O_2, but the current work does not address the direct reactivity at these reaction sites. Rather, the role of defects as electron-donating centers is only considered. For instance, oxygen vacancies lead to a reduced surface with excess electrons, that introduce defect states in the band gap.[90] In TiO_2 for each removed oxygen atom, two electrons remain in the lattice of the Ti atoms and two Ti^{4+} are reduced to Ti^{3+}. Other defects such as interstitial Ti atoms or H atoms also lead to unpaired electrons.[7,9,81,91] The reduction of the surface can change the adsorption energy of atoms and molecules[10,81,92,93] and the current work concerns the transfer of unpaired electrons to adsorbates due to the presence of surface O vacancies (O_v) and what role these electrons play in adsorption and chemistry over group IV metal oxide surfaces.

Adsorption over TiO_2 has been extensively studied,[19,22–24] especially over the rutile phase. However, the anatase polymorph of TiO_2 is also a promising material because of its reactivity.[1,25] There are several theoretical studies on adsorption

reactions and surface properties of anatase (101) surfaces.[26–29] DFT calculations also indicate that in the presence of O vacancies (O_v) several adsorbates have higher adsorption energies over anatase compared to rutile and the defects may act as nucleation sites for Au and Pt growth.[30] HfO_2 and ZrO_2 surfaces have been less studied than TiO_2, particularly using theoretical methods. However, significant attention has been paid to the deposition of thin zirconia/hafnia films for micro-electronics and catalysis.[31–37] Theoretical studies of HfO_2 and ZrO_2 surface adsorption have been performed, such as involving water and hydrogen,[38–41] Au,[42] or sulfuric acid.[43] Surface defects have also been modeled,[44–46] although charge transfer due to the presence of point defects has not systematically been explored over these oxides.

Previous work by Deskins et al.[81] examined charge transfer over the rutile (110) surface with density functional theory (DFT). They found a correlation between the number of excess electrons and the strength of O_2 adsorption. The number of excess electrons in the surface was moderated by the number and type of defect (O vacancy, surface hydroxyl, or interstitial Ti atom). They also demonstrated that significant charge transfer occurs only for species with large electronegativities greater than the electronegativity of the rutile (110) TiO_2 surface. Other computational work also showed similar electron transfer events over the rutile (110) surface.[10,12]

In the present work we examine charge transfer to adsorbates over reduced surfaces of the anatase phase of TiO_2, and tetragonal phases of HfO_2 and ZrO_2 (all group IV metal oxides) using DFT. We compare these three metal oxides and determine the details of electron transfer for them, including what factors influence charge transfer

33

to adsorbates and on which surfaces electron transfer has the largest effect. We first examined O_2 adsorption, then considered several other adsorbates. We provide several new insights that may be helpful for the future design and study of gas sensors and catalytic metal oxides.

2.2. Methodology

The DFT computations were performed with the CP2K[94,95] package. It uses the Gaussian and plane waves approach (GPW) with periodic boundary conditions. Valence electrons were described by a double-ζ basis set, specifically optimized to perform accurate molecular calculations. This basis set is well suited for the condensed phase.[96] Core electrons were described by Goedecker-Teter-Hutter (GTH) pseudopotentials.[97–99] Within the pseudopotential approximation only valence electrons are represented explicitly in the calculations, with the valence-core interaction being represented by non-local pseudopotentials. The gamma point supercell approach was used, necessitating the use of large supercells. Calculations have been performed using the Perdew-Burke-Ernzerhof (PBE) functional for the exchange correlation term of the electron-electron interaction,[100] and all calculations were spin polarized.

Table 2.1 shows calculated and experimental bulk lattice parameters for the studied metal oxides. These lattice parameters were found using a 3x3x3 bulk lattice cell. Optimized bulk lattice parameters were found to agree well with experimental

data; the maximum deviation was 1.9% for the *a* parameter of ZrO_2, while the other parameters showed deviations of less than 1%.

Table 2.1 Comparison of calculated and experimental lattice parameters for tetragonal HfO_2 and ZrO_2, and anatase TiO_2

	TiO_2	HfO_2	ZrO_2
a [Å]	3.76	3.62	3.57
a exp [Å]	3.79	3.64	3.64
b [Å]	9.52	5.23	5.26
b exp [Å]	9.54	5.27	5.29
Experimental Reference	[101]	[102]	[103]

Periodic slab models were used for all the metal oxide surfaces. Each slab size was set to be (3 x 2) in the [0 1 1] and [0 1 0] directions respectively, and six atomic layers thick with ~20 Å vacuum spacing between slabs. The total lateral size of each surface slab was 11.28 Å by 20.47 Å for anatase (101), 10.71 Å by 12.71 Å for HfO_2 (101) and 10.87 Å by 12.32 Å for ZrO_2 (101). Fig. 2.2 shows the slab models used. The bottom O-M-O trilayer (three atomic layers) was kept fixed and all other atoms were free to relax during optimization. Typically one surface O atom was removed to create a reduced surface.

To compare the reducibility of the surface we computed the formation energy of an oxygen vacancy E_{vac} according to:

$$E_{vac} = E_{1/2 O_2} + E_{reduced\ slab} - E_{clean\ slab} \tag{2.1}$$

where $E_{1/2O2}$ is the energy of a oxygen atom computed as one half of the energy of a oxygen molecule, $E_{reduced\ slab}$ is the energy of the metal oxide surface with an oxygen vacancy, and $E_{clean\ slab}$ is the energy of the stoichiometric slab. Positive energies indicate endothermic processes so that the energy of an oxygen vacancy is smaller for a more reducible surface;. The work function, defined as the energy needed to move an electron from the Fermi level to vacuum, was computed for each metal oxide slab. This was done in order to roughly compare the surfaces' relative electronegativity. The methodology used was based on the method proposed by Fall.[71] For each reduced slab we calculated the average electrostatic potential perpendicular to the surface as a function of the z coordinate value. This was used to establish the vacuum energy level, or the flat electrostatic region outside the slab. The work function was then found by taking the difference between the vacuum level and Fermi level (calculated from the eigenvalues).

Adsorption energies E_{ads} were calculated using the following expression:

$$E_{ads} = E_{surf+\ adsorbate} - E_{surf} - E_{adsorbate} \qquad (2.2)$$

Where $E_{adsorbate}$ is the energy of the isolated molecule in the vacuum, E_{surf} is the energy of the bare slab, and $E_{surf+adsorbate}$ is the total energy of the molecule adsorbed on the slab. We calculated adsorption energies over both stoichiometric and reduced surfaces. Bader charge analysis was performed in order to analyze the charge distribution.[104–107] For all the adsorbates we modeled the adsorption over the metal atoms, or the cationic sites, as opposed to over O atoms. Several adsorption geometry

36

configurations were found for each adsorbate but the most stable geometries are analyzed herein. Previous research found that the exact physical location of the defect relative to the adsorbate had little effect on the surface chemistry,[81] so we did not consider this matter further. Adsorbates were placed sufficiently far away from an O vacancy to preclude direct reactivity of adsorbates with the O vacancy; the O vacancy only serves to reduce the surface.
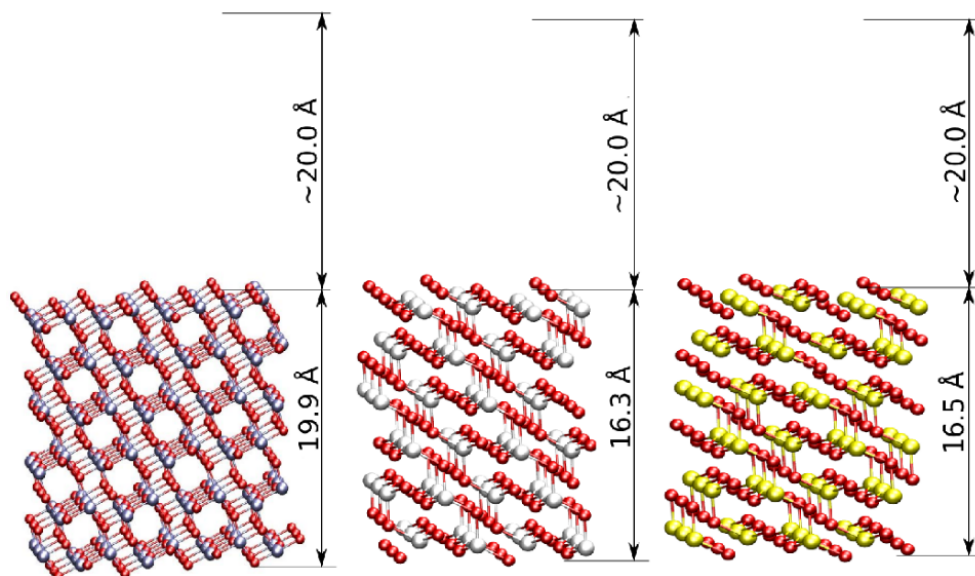
Fig. 2.2 Slab models used in the current work. Surfaces of (a) anatase TiO_2 (101), (b) tetragonal ZrO_2 (101), and (c) tetragonal HfO_2 (101). Slab thicknesses are indicated as well as vacuum spacings. The red spheres represent oxygen, the blue spheres represent Ti, the white spheres Hf, and the yellow spheres represent Zr. The same color scheme is used in the remaining figures.

In order to confirm the validity of our model, we performed several convergence tests. We determined a suitable slab thickness by calculating the adsorption energy of O_2 (in the side-on configuration as discussed in Section 2.3.2) as a function of slab thickness. The results, as shown in Fig. 2.3, indicate that the

37

adsorption energy is converged for six layers or larger (each layer being an O-M-O trilayer, or three atomic layers). We therefore used a six-layer slab in the current work.
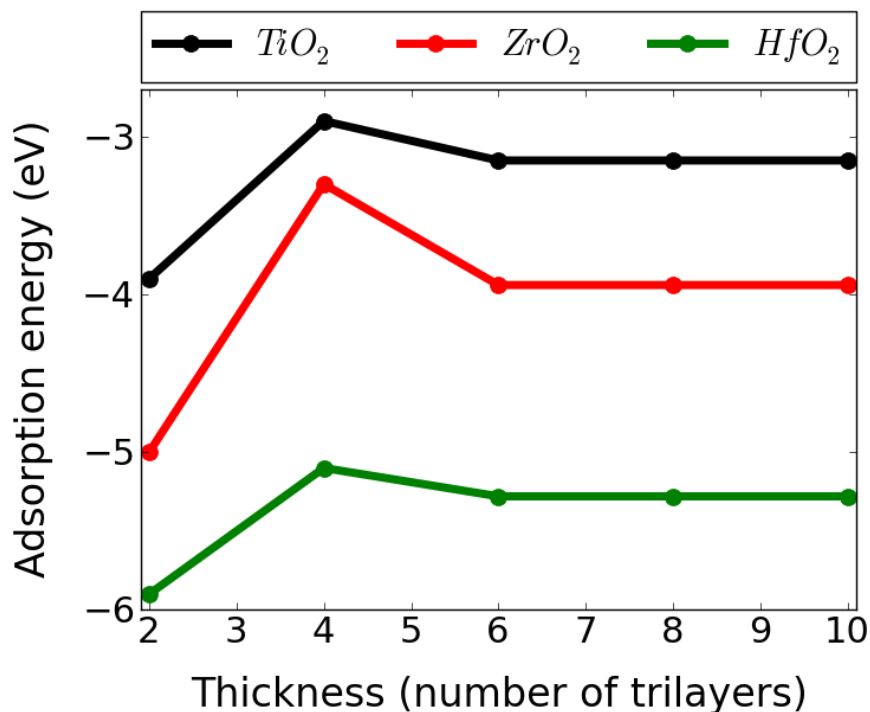
Fig. 2.3 Convergence of the adsorption energy of O_2 over reduced surfaces of TiO_2, ZrO_2 and HfO_2 as a function of slab thickness. Each layer on the plot is an O-M-O trilayer, or three atomic layers.

The use of a single k-point may introduce errors in our calculations because of an insufficient k-point mesh. We tested this possibility by determining adsorption energies for slabs with larger dimensions in the x- and y- directions. By increasing the supercell size the distance between k-points decreases, or k-point density increases.

Convergence is reached when increasing the supercell shows little or no change in calculated properties. We calculated the adsorption energy of O_2 while changing the surface size and the results are summarized in Table 2.2. Our results indicate that the use of a (3x2) surface cell gives sufficient k-point sampling.

Table 2.2. Adsorption energy of O_2 [eV] over stoichiometric surfaces using different surface cell sizes.

Metal Oxide	Surface size		
	3x2	3x3	4x3
TiO_2	-1.37	-1.37	-1.36
ZrO_2	-0.55	-0.54	-0.55
HfO_2	-1.36	-1.36	-1.35

2.3. Results and discussion

2.3.1. Nature of the reduced surfaces

Our reduced surfaces showed similar properties to previous research. Our calculated formation energy of an oxygen vacancy in the anatase (101) surface (4.87 eV) was similar to the value reported in previous DFT work (4.15eV).[108] The slight difference in formation energy could be due to our larger slab as well as basis set or pseudopotential choice. For the (101) surface of tetragonal ZrO_2 our formation energy was calculated to be 7.14 eV and previous DFT work reported a value of 8.4 eV.[109] This latter study used an embedded atom cluster approach. Another paper[91] calculated the value to be 5.48 eV, using the plane waves method , contrasted

with the hybrid basis set method that we used. The literature thus reports O_v formation energies using a variety of methods and simulation parameters, and our calculated vacancy formation energies fit the range of reported values.

Graphs of the spin density (the difference between the spin up and spin down densities) for the ZrO_2 and HfO_2 surfaces are shown in Fig. 2.4. These graphs demonstrate the presence of unpaired electrons mainly localized on the 3d levels of the neighboring Hf and Zr atoms, which coincide with previous work.[110–112] The DFT method did not show localized electrons on the anatase surface. The GGA approach tends to delocalize the electrons in TiO_2;[90,91] this is a known limitation that can be avoided with the DFT+U method, which will be discussed later. Our results in modeling reduced surfaces indicate that our simulation approach is in adequate agreement with previous DFT work, and that our approach is therefore to be reasonable.
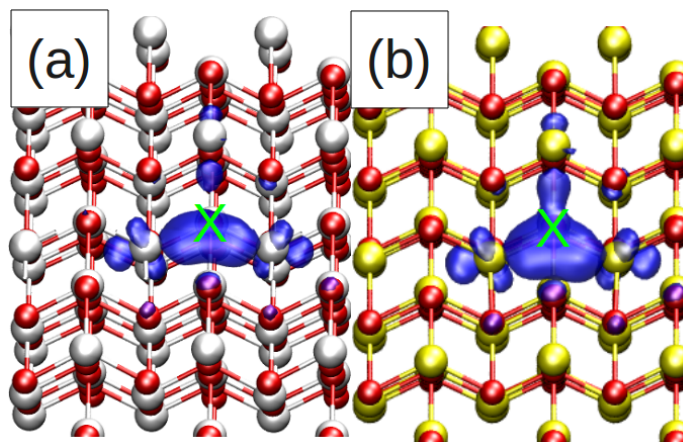
Fig. 2.4 Spin density plots in the region near the oxygen vacancies of the surfaces (a) t−ZrO_2 (101) and (b) t−HfO_2 (101). The location of an oxygen vacancy is indicated by an X.

2.3.2. Adsorption of O_2

We used molecular oxygen as a prototype molecule for our initial analysis. Oxygen is nearly ubiquitous in gas-sensing and catalytic environments, and is a known electron scavenger. Oxygen can adsorb on the surfaces in several configurations. It can be adsorbed with one end of the molecule on the surface, or laying on its side on the surface. These configurations can be observed for TiO_2 in Fig.2.5.
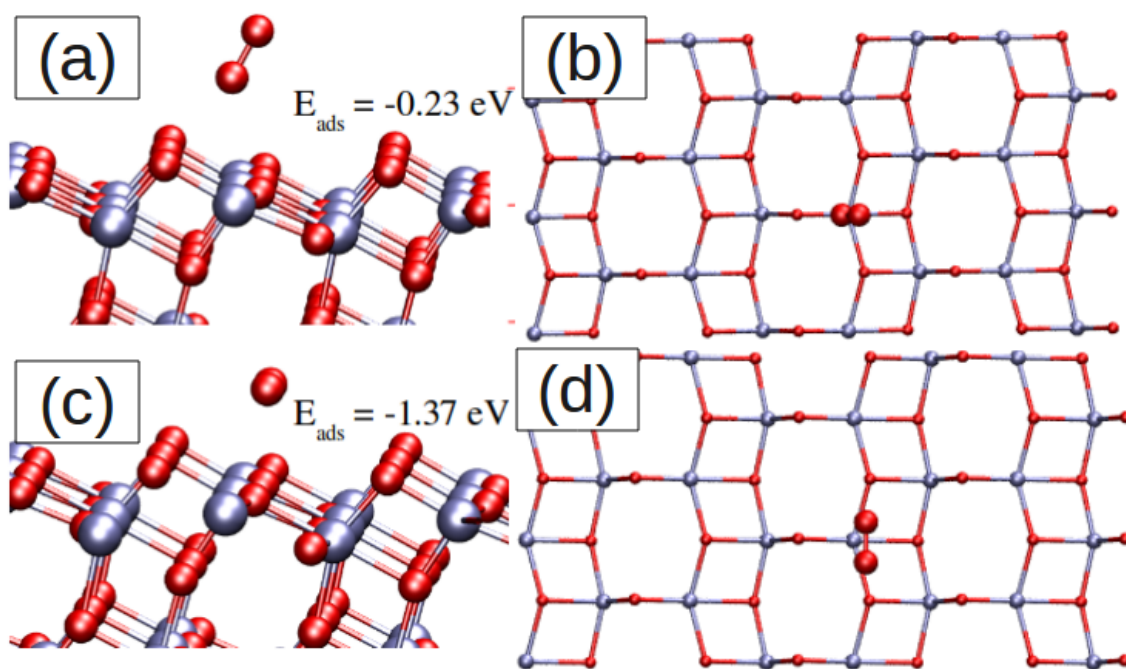
Fig. 2.5 Stable configurations for oxygen adsorbed over the stoichiometric (101) surface of TiO_2 anatase. (a) side view of end-on surface configuration. (b) top view of end-on surface configuration. (c) side view of side-on surface configuration. (d) top view of side-on surface configuration.

We checked several configurations and the most stable configuration over all the metal oxides studied was with O_2 laying nearly flat on the surface (the side-on configuration in Fig. 2.5c). This is true on both the stoichiometric and the reduced surfaces. We report adsorption energies for O_2 over both stoichiometric and reduced surfaces in Table 2.3. ΔE in the table is defined as the difference in adsorption energy between the reduced and stoichiometric surfaces. In previous work[110] the adsorption energy of oxygen on a stoichiometric anatase (101) surface in the side-on configuration was calculated to be -0.90eV and in the end-on configuration -0.58eV, while we calculated these values to be -1.37 eV and -0.23 eV, respectively. Despite the difference between this previous work and our results the trends coincide with a more stable molecule in the side-on configuration. The differences in numerical results could be possibly due to the methodologies used, as the calculations reported by Zeng et. al.[110] were performed with relativistic SBJK pseudopotentials and basis set, and the B3LYP exchange correlation functional. However Aschauer et. al.[111] calculated the side-on configuration adsorption energy for a stoichiometric surface to be -1.5eV which is close to our value of -1.37 eV. In another work[113] the adsorption energies were calculated using DFT methods in the generalized gradient corrected approximation (GGA) with the PBE exchange and correlation functional, the results were -2.37eV for the side-on configuration over a reduced surface and -0.34eV for oxygen molecule in the end-on configuration over a stoichiometric surface, which match the trend of our calculations.

Table 2.3. Adsorption energies (eV) and O-O bond lengths (Å) of molecular oxygen over stoichiometric and reduced surfaces. ΔE is defined as the difference in adsorption energy between the reduced and stoichiometric surfaces.

Metal Oxide	Side-on configuration					End-on configuration				
	Stoichiometric Surface		Reduced Surface		ΔE	Stoichiometric Surface		Reduced Surface		ΔE
	Ads. Energy	Bond Length	Ads. Energy	Bond Length		Ads. Energy	Bond Length	Ads. Energy	Bond Length	
TiO_2	-1.37	1.24	-3.15	1.44	-1.78	-0.23	1.23	-0.24	1.23	-0.01
ZrO_2	-0.55	1.24	-3.94	1.48	-3.39	-0.18	1.22	-0.18	1.23	0
HfO_2	-1.36	1.23	-5.28	1.5	-3.91	-0.2	1.23	-0.2	1.22	0

We observed that adsorption is significantly enhanced over the reduced surfaces compared to stoichiometric surfaces, as shown by the large negative values of ΔE for the side-on configuration of O_2. ΔE is the difference in adsorption energies over reduced and stoichiometric surfaces. Negative values for ΔE indicate that adsorption is preferred over reduced surfaces. Because we considered O_2 binding to cationic metal sites, charge transfer from the surface to adsorbate (giving negatively charged ionic O_2) leads to stronger binding between cationic metal and anionic O_2 (see Fig. 2.1). The electrons available for transfer to O_2 directly result from the O_v defects, so binding is enhanced over the reduced surfaces. As we discuss below, this charge-transfer process will become more evident.

Likely the side-on configuration is most stable because it produces stronger ionic bonding between the surface and O_2, since each O atom can interact with a

surface metal cation (see Fig. 2.5d). We also observed that the adsorption energy differences between the reduced and stoichiometric surfaces follow the trend | ΔE_{TiO2}| < | ΔE_{ZrO2} | < | ΔE_{HfO2} |. More will be said of this in later sections. We examined the nature of O_2 adsorption by looking at the O-O bond lengths, which are given in Table 2.3. The observed bond lengthening over the reduced surfaces suggests a weakening of the O-O bond, which is indicative of charge transfer taking place between O_2 and the surface. Gas-phase O_2 has a calculated bond length of 1.22 Å, while superoxide species O_2^- has a typical bond length of 1.23 Å and peroxide species O_2^{2-} has a typical bond length of 1.48 Å.[111] The adsorbed O_2 bond lengths over reduced surfaces match the O_2^{2-} bond lengths well, while O_2 bond lengths over stoichiometric surfaces match gas phase O_2 bond lengths Again, the reduced surfaces have unpaired electrons available for transfer to the O_2, while the stoichiometric surfaces have no such unpaired electrons.

For comparison, we also analyzed the end-on adsorption configuration, with the molecule pointed away from the surface (and slightly bent) as is shown in Fig. 2.5. This was the second most stable configuration over all the metal oxides. The O_2 bond length over all surfaces (reduced and stoichiometric) for end-on adsorption was always similar to the bond length of gas-phase oxygen molecule (~1.2 Å). This suggests that large charge transfer is not occurring with the end-on configuration and weaker ionic interactions occur between O_2 in this geometry and the surface. The difference in adsorption energies over stoichiometric and reduced surfaces are all nearly zero for the end-on configuration, again suggesting little electron transfer

44

whether over reduced or stoichiometric surfaces. To first order the adsorption energy can be written as:

$$E_{ads} \approx E_{electron\,transfer} + E_{electrostatic\,interactions} \qquad (2.3)$$

The transfer of electrons to O_2 involves a certain positive energy cost ($E_{electron\,transfer}$) that is compensated by the favorable electrostatic interactions ($E_{electrostatic\,interactions}$) between the newly formed anion and surface cation. Thus E_{ads} is exothermic, or negative, when $E_{electrostatic\,interactions}$ is more negative than the positive $E_{electron\,transfer}$ value. In the end-on configuration only one O atom interacts with a surface metal cation, and thus any compensating electrostatic interactions between negatively charged O_2 and cation are minimized. Electron transfer does not occur for end-on geometry because the anionic O_2 would not be stabilized enough on the surface to overcome energetic barriers for electron transfer, or $E_{electrostatic\,interactions}$ is smaller than $E_{electron\,transfer}$ In contrast, a much larger ionic character can be assigned to O_2 in the side-on configuration (which has very favorable electrostatic interactions between both O atoms and a surface cation or large $E_{electrostatic\,interactions}$), and this is reflected by the stronger adsorption energies and bond distances of this configuration.

To confirm the charge transfer process, we also performed Bader charge analysis. Table 2.4 shows the charges of the oxygen molecule adsorbed over the stoichiometric and reduced surfaces. In all the cases the oxygen molecule over a reduced surface has a more negative charge in the side-on configuration, indicating that electrons are transferred from the surface to the O_2 molecule. The charge value

near -2 is evidence of peroxide O_2^{2-} species formation . For the end-on configuration there is negligible charge transfer. We note that defining a Bader volume to calculate Bader charges is not without difficulty and obtaining O_2 charges to be exactly -2 is problematic and some charges are slightly lower than -2. Nonetheless the charges do show that greater charge transfer occurs over reduced surfaces. We also note that some charge transfer occurs over stoichiometric surfaces, but these electrons come from filled electronic states in the metal oxides, and are much less energetically transferable than unpaired electrons in reduced surfaces. $E_{electron\ transfer}$ is very high over stoichiometric surfaces, which is why the adsorption energy is lower compared to reduced surfaces which have lower $E_{electron\ transfer.}$

Our results show that stronger binding occurs when O_2 becomes an anion, or when ionosorption takes place, and that this adsorption process occurs over all the group IV metal oxides studied. The configuration of the O_2 during the adsorption process determines directly whether the ionosorption process can take place or not. This geometry-dependence may have great influence on on the surface chemistry of the metal oxide surfaces, especially when considering co-adsorption of other molecules or higher surface adsorption coverages. These latter two effects may influence stable adsorption geometries, and hence the electron transfer process. Further research is needed to clarify the influence of coverage and co-adsorbates on ionosorption over metal oxides. We next endeavor to explain the different behavior of the metal oxides considered in this study.

Table 2.4. Bader charges (e⁻) of oxygen adsorbed over the stoichiometric and reduced surfaces.

Metal Oxide		Stoichiometric	Reduced
TiO_2	side-on	-0.58	-2.12
	end-on	0.01	0.01
ZrO_2	side-on	-1.16	-2.01
	end-on	0.02	-0.01
HfO_2	side-on	-0.04	-1.17
	end-on	0.01	0.01

2.3.3. Comparison of O₂ adsorption on the different metal oxides

Understanding the charge transfer processes over the various metal oxides involves several complexities, but we provide some analysis comparing the different surfaces. In order to discover any trends we computed the O_v formation energy over each surface. These results are shown in Table 2.5. The most reducible of the studied surfaces is anatase and the reducibility decreases with tetragonal ZrO_2 being more reducible than HfO_2 (101) surfaces. The reducibility is roughly a measure of the M-O bonding strength in the surface.

Covalent systems would tend to have smaller vacancy formation energies. In contrast, strongly ionic systems would tend to have larger vacancy formation energies. The differences in electronegativity between O and metal atom for atomic Ti, Zr, and Hf are -1.90, -2.11 and -2.14,[112] indicating a rough order of ionic character for the metal oxides. Thus, oxides of TiO_2 are to be the least ionic, while oxides in HfO_2 are the most ionic in character. This trend is reflected in the O_V formation

energies and O_2 adsorption energies. The most ionic system (HfO_2) has the strongest O_2 surface binding (-5.28 eV) due to the largest anion-cation interactions ($E_{electrostatic\ interactions}$ in Equation 2.3). Conversely the least ionic system (TiO_2) has the weakest adsorption energy (-3.15eV) due to the weakest ionic interactions between the O_2 anion and Ti cation.

Table 2.5. Formation energy of an oxygen vacancy on the surface of the studied metal oxides

Metal Oxide	Energy [eV]
TiO_2	4.87
ZrO_2	7.14
HfO_2	7.47

The work function is also another parameter for comparison. The work function represents the energy required to remove an electron from the material (or $E_{electron\ transfer}$ in Equation 2.3), and it is expected that materials with lower work functions will lead to easier/more facile electron transfer. Table 2.6 shows our calculated work functions for the studied metal oxides; the work function trends match the trends of O_2 adsorption over reduced surfaces very well. For example, TiO_2 has the largest work function value, so removal of electrons from TiO_2 is hardest (largest $E_{electron\ transfer}$), which in turn leads to the O_2 adsorption energy being the weakest. HfO_2 has the smallest work function and has the strongest (most stable) adsorption energy, indicating charge transfer is easiest for this oxide. The relative electronegativities of the surface and adsorbate have been used as key parameters to understand charge transfer between surface and adsorbate as in previous

48

work.[81] Electrons flow from less electronegative species to more electronegative species. Thus, the difference between the electronegativity of the surface and the adsorbate is indicative of the degree or possibility of electron transfer. The absolute electronegativity can be taken approximately to be equal to the work function. We see that metal oxides with higher electronegativities (as approximated by the work function) lead to less stable ionosorption. Referring to Equation 2.3, raising $E_{electron\ transfer}$ lowers the adsorption energy, or makes the process more endothermic.

Table 2.6. Calculated work functions (eV) for the studied metal oxide surfaces

Metal Oxide	Work function
TiO_2	6.91
ZrO_2	6.31
HfO_2	6.15

We have provided two correlations that explain the trends in O_2 adsorption energy over these reduced metal oxide surfaces. The oxygen vacancy formation energy is largest for HfO_2 which indicates a strongly ionic oxide, and the adsorption energy of O_2 over HfO_2 is also most exothermic, particularly due to strong ionic bonding. HfO_2 also has the lowest work function, so removal of an electron from HfO_2 is easiest, and thus charge transfer proceeds most readily over HfO_2. These two properties of a metal oxide may be useful to predict charge transfer behavior and trends in other metal oxides.

49

2.3.4. DFT + U analysis of the surfaces

We next tested the effect of DFT+U on ionosorption. The prediction of delocalized defect states in anatase is not consistent with experimental data.[114,115]The need for self-interaction corrections in order to describe the polaronic nature of excess electrons in TiO$_2$ has been discussed by several authors.[90,91] Corrected computations were carried out within the DFT method modified with on-site Coulomb correction terms, or DFT + U . We applied a U value to all the metal atoms (Ti, Zr, Hf) . Fig. 2.6 shows the electron localized in the 3d orbitals of the Ti atoms neighboring the oxygen vacancy after applying DFT+U in anatase TiO$_2$. The oxygen vacancy gave two unpaired electrons in the oxide, and in our solution they are both localized on different Ti atoms with opposite spins.
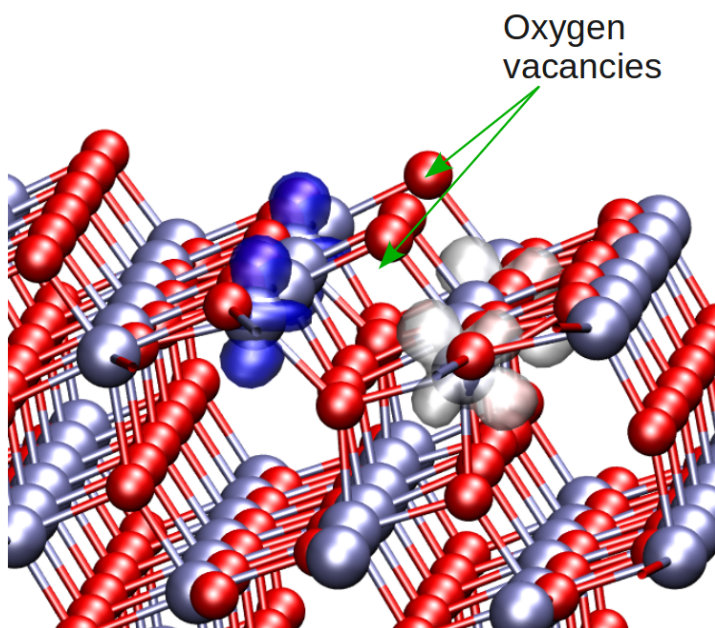
Fig. 2.6 Electron spin density localized in the 3d orbitals of Ti atoms in anatase neighboring an oxygen vacancy using DFT+U with U = 5 eV. The white surface represents the spin up density and the blue surface the spin down density. Two unit cells are represented in the [0 1 0] direction in order to see the oxygen vacancies.

The adsorption energies of oxygen over the reduced metal oxide surfaces using DFT+U and a range of U values are shown in Fig. 2.7. Our results indicate little change in adsorption energies for U = 5 eV, but the adsorption energies increase for U = 8 eV. This trend is consistent with previous work.[81] At sufficiently large U values the transfer of electrons to the O_2 molecule becomes hindered ($E_{electron\ transfer}$ becomes larger) because the larger U values stabilize the electrons in the oxide lattice. Increasing the U value lowers the defect state energy location within the band gap; small U values give defect states near the conduction band, while large U values give defect states near the valence band. U values in between give defect states in the band gap. The U value becomes a way to control the unpaired electrons' stability within the lattice, and influence ionosorption. Lastly, DFT+U has the largest effect on TiO_2. Standard DFT gives solutions with delocalized electrons in TiO_2, while solutions of ZrO_2 and HfO_2 have localized states(see section 2.3.1). DFT+U has the largest effect on TiO_2 since it induces electron localization and considerably modifies the electronic nature of the unpaired electrons, much more so than in ZrO_2 and HfO_2. This modification of TiO_2 due to DFT+U is clearly indicated by the large change in adsorption energy at increasing U values.
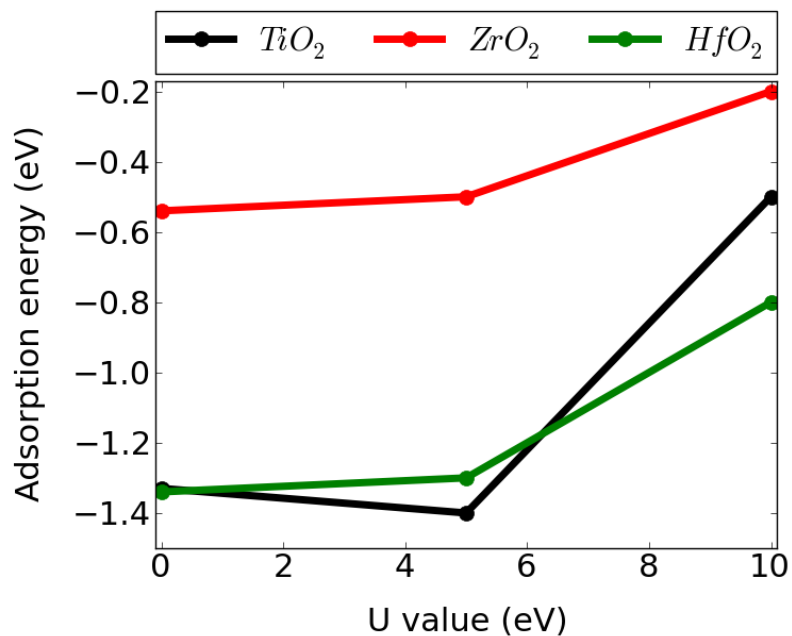
Fig. 2.7 Adsorption energies (eV) of molecular oxygen over the reduced metal oxide surfaces using the DFT + U method.

2.4. Adsorption of Other Molecules

Previous work by one of the authors examined a variety of molecules adsorbed over the rutile (110) surface.[81] It was shown that significant electron transfer did not occur for species with low electronegativity (e.g. H_2O). The main criteria for this analysis was how the adsorption energy changed over the stoichiometric compared to over the reduced surface. Significant change in adsorption energy would indicate electron transfer from the reduced surface to the adsorbate, or ionosorption taking place. We also modeled adsorption of several species over the anatase TiO_2, ZrO_2, and HfO_2 surfaces in order to assess how the electronegativity of the adsorbate influences

the strength of adsorption.

Fig. 2.8 shows the differences between the energy of adsorption of various species on the stoichiometric and the reduced surface for the (101) surface of the anatase phase of TiO_2. Fig. 2.9 and 10 contain similar results for ZrO_2 and HfO_2, respectively. As before, the difference in energy of adsorption is defined as $\Delta E_{ads} = E_s - E_r$, where E_s is the energy of adsorption on the stoichiometric surface and E_r the energy of adsorption on the reduced surface, similar to ΔE in Section 2.3.2. Again, adsorption over cationic metal sites only was considered, since this type of binding will be most affected by electron transfer. Electronegativity values were taken from Pearson.[116]
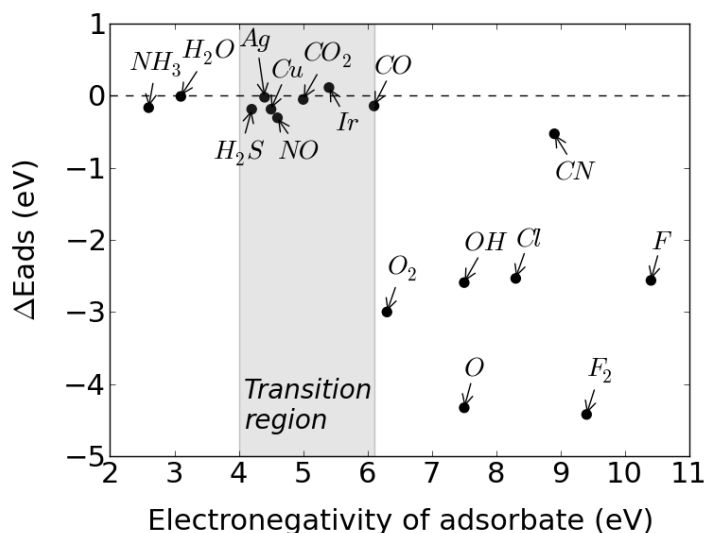
Fig. 2.8 Differences in adsorption energies over clean and reduced surfaces (ΔE_{ads}) as a function of adsorbate electronegativity for the TiO_2 anatase (101) surface.

We observed large negative values of ΔE_{ads} for several species, which is indicative of a strong effect due to the presence of excess electrons and enhanced

53

charge transfer over the reduced surfaces. Several species with low values of electronegativities were not affected by the reduction of the surface. A transition region (such as shown in Fig. 2.8) indicates when ΔE_{ads} starts to become non-zero. In essence, when the electronegativity of the adsorbate is roughly lower than the electronegativity of the surface, the transfer of charge is not a favorable process and the reduced surface behaves as a stoichiometric surface. Ionosorption does not occur and covalent bonding is dominant. We note that the ΔE_{ads} values are stronger for anatase compared to rutile TiO_2[81] (for example ΔE_{ads} is -0.6 eV over rutile for atomic O, while -4.5eV over anatase). At this point, it is very likely that the specific surface structure (e.g. coordination numbers or orbital levels) will influence the adsorption energies; generally anatase is more reactive than rutile.[25] We observed similar effects over ZrO_2 and HfO_2 (see Fig. 2.9 and Fig. 2.10), in that the electronegativity value of the adsorbate is a large indicator of whether increased binding over reduced surfaces will occur.
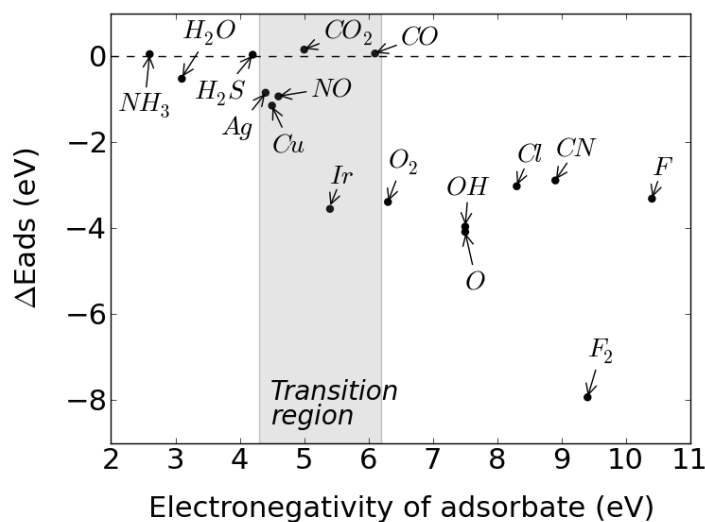
Fig. 2.9 Differences in adsorption energies over clean and reduced surfaces (ΔE) as a function of adsorbate electronegativity for the ZrO_2 (101) surface.
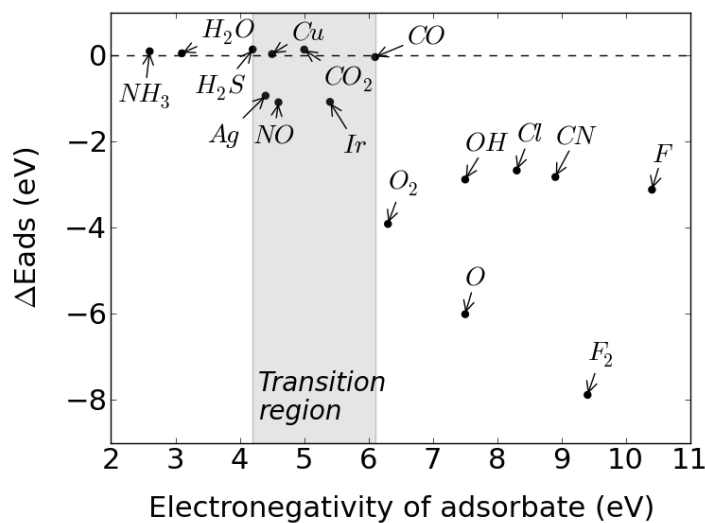
Fig. 2.10 Differences in adsorption energies over clean and reduced surfaces (ΔE) as a function of adsorbate electronegativity for the HfO_2 (101) surface.

In previous work[81] the electronegativity of the rutile (110) surface was approximated as the work function of the surface. We find that our calculated work

55

function values (see Table 2.6) do not exactly match the transition region, which we attribute to the limitations of calculating the work function as well as breakdown of the assumption that work function and electronegativity are equivalent. However, we have observed that the work functions and transition regions are relatively close, which supports the idea that adsorbates with electronegativies less than the surface electronegativities will not ionoadsorb.

Ionosorption has now been observed with four metal oxide surfaces: rutile TiO_2 (110),[81] anatase TiO_2 (101), tetragonal ZrO_2 (101), and tetragonal HfO_2 (101). We expect this to be a very general phenomena with ionic transition metal oxides, but further work needs to be performed in order to confirm how widespread this occurs. We have only considered O vacancy defects, but other electron-donating defects (such as interstitial atoms) likely also lead to ionosorption, as previously observed[81] . Clearly defects may strongly affect surface adsorption and surface chemistry in several different ways, and thus any theoretical modeling of these surfaces should take into account the possibility of ionosorption. For example, simply using a stoichiometric slab may lead to wrong results with electronic structure calculations. Furthermore there is also much experimental work focusing on understanding defects and their role in oxide surface chemistry,and certainly future research will provide more details on metal oxide ionosorption.

2.5. Conclusions

We have presented evidence that suggests ionosorption should occur over group IV metal oxides (TiO_2, ZrO_2, and HfO_2) with electron-donating defects. Increased binding of O_2 is observed when the surface is reduced and unpaired electrons are present in the surface slab. These electrons transfer to O_2 forming an anion that may favorably interact with surface metal cations. This electron transfer process is dependent on the adsorption geometry, as we observed that not all stable O_2 adsorption modes lead to electron transfer. We have examined the details of the ionosorption over the different metal oxides, and two parameters correlate with the adsorption energies of O_2: surface vacancy formation energy and surface work function. HfO_2 has the largest O vacancy formation energy of the studied oxides, but also has the most exothermic O_2 adsorption energy, which is explained by the larger ionic nature of HfO_2. Larger ionic character will lead to stronger binding between the cationic metal sites and anionic adsorbates. HfO_2 also has the lowest work function which indicates that electron transfer from HfO_2 is easiest. Correspondingly, anatase TiO_2 has the lowest O vacancy formation energy, the largest work function, and the least exothermic O_2 adsorption energy. Increased binding is also observed for several other adsorbates, but only when the adsorbate electronegativity is significantly large, which indicates that the electronegativity of the adsorbate should be larger than the electronegativity of the surface. Certainly our results reinforce the idea that electrons and charge transfer are important when surface chemistry over early transition metal

oxides is studied, and future work may examine this concept over other metal oxides.

Acknowledgement

Chapter 3. The Nature of Interfaces and Charge Trapping Sites in Photocatalytic Mixed-Phase TiO$_2$ from First Principles Modeling

3.1. Introduction

The physical and chemical properties of TiO$_2$ have been extensively studied, due to its wide range of applications. It is used as a photocatalyst, a gas sensor, in medical implantations, in hydrophobic glass, and corrosion protection.[1] It has become the prototypical material for photocatalytic processes, and its rutile (110) surface is a prototype for surface science studies of metal oxides. TiO$_2$ photocatalysts consisting of two intimately connected phases have been demonstrated to show increased catalytic activity over single-phase catalysts (whether they be rutile or anatase), in some cases, with even up to ten times more activity.[55–57,59,60,117] The reason for the increased reactivity is however still under debate (see for example a recent review article[61]), but could involve several factors, including bulk charge separation, interfacial charge transfer effects, or special interfacial reaction sites, such as low coordinated Ti. While EPR studies of rutile-anatase systems have indicated that low coordinated Ti sites are likely to trap electrons,[118] the details of the interface are extremely difficult to obtain from experiments and hence, first principles simulations can be invaluable in this regard. In this chapter we

modeled using density functional theory (DFT) the interface between rutile and anatase phases of TiO_2 in order to further explain the mechanism of the increased reactivity of these mixed-phase catalysts.

The process of heterogeneous photocatalysis over semiconductors starts with the generation of electron-hole pairs due to photoexcitation of an electron to the conduction band, creating a hole in the valence band. These electrons and holes may then diffuse to the surface, and transfer to adsorbed species initiating surface reduction/oxidation reactions.[92] Alternatively, the electron-hole pair may recombine with a concomitant release of energy. This competitive recombination pathway is undesired since it lowers the concentration of active electrons and holes. Much research on TiO_2 photocatalysis has focused on either increasing the production of more electron-hole pairs through for instance band-gap engineering,[119] or attempting to reduce the recombination rates.[25,120,121]

Mixed phase photocatalysts appear to be a superior material over single phase TiO_2 and there have been several attempts to explain the increased activity of the mixed phase catalysts.[61] The most accepted hypothesis is that presence of the two phases lowers the electron-hole recombination rate (through preferential charge migration to the various phases, or increased charge separation), which increases the number of surface electrons/holes, and therefore the surface reactivity.[63,122,123] The preferred phase of the electrons (or holes) is determined by the relative energy of the two phases' conduction bands (or valence bands).The alignments of the conduction band (CB) minimum and valence band maximum of rutile and anatase have been under intense debate, with different studies indicating contradictory results.[63,66,122] Most recent results suggest that

60

the rutile VB and CB lie higher than the anatase VB and CB.[124,125] Therefore, this is consistent with experiments suggesting that photo-generated electrons may migrate from rutile to anatase, due in part to trapping sites in the anatase lattice.[57] A recent combined experimental and theoretical work[126] also confirms the higher energy level of the rutile phase conduction and valence bands. Strong interfacial regions between the phases have been suggested to facilitate charge transfer.[62,67,68] Other work attributes special four-coordinated Ti interfacial sites as contributing to the increased photo reactivity.[63,65,69,118]

Band offsets at semiconductor heterojunctions are known fundamental parameters which govern the transport properties of electrons, and the differences in energy of the bands determines the direction and magnitude of the electrical current.[70] The estimation of the band offsets for semiconductor interfaces is crucial to understand the behavior of a metal oxide mixed phase catalysts. In order to determine offsets using electronic structure techniques it is typically necessary to simulate an interface between the two materials.[71] However, in practice, this is rarely done, in part due to the difficulty and complexity of modeling an interface between two different crystal phases (in contrast to, e.g. interfaces in III-V layered materials with the same phase[72–74]). There have been some attempts to determine offsets, primarily using the bulk energy levels (suitably referenced) of the different constituents.[124,127] However, the detailed atomic and electronic properties at the interface are known to influence the band offsets[36] and key photocatalytic properties. A recent paper predicted the band offsets of rutile and anatase modeling an interface with the QM/MM approach, but did not give details on the interfacial

region.[125] The geometry of the interface could induce the formation of trapping sites and dipoles, which could affect the band structure. While these are difficult to probe experimentally and are not treated in simple bulk band alignment studies, the power of modern electronic structure calculations is that one can determine band offsets between two materials in an explicit interface model, and quantify the nature of the interfacial region.

We present electronic structure calculations (DFT) of realistic rutile-anatase interfaces. We calculated the relative stability of electrons in each phase, taking into account the presence of the interface. The electronic structure of the interface is also studied and the nature of under-coordinated Ti sites is shown. The bulk of the analysis is performed on interfaces formed by bringing two surfaces together so that no exposed surface regions exist (bulk interface), but an interfacial structure with exposed surfaces is also used. Our analysis of the interfacial region for all interfaces provides key information on the interface and its role during photocatalysis.

3.2 Methodology

In this work, we modeled interfaces formed by bringing together surfaces of rutile and anatase TiO_2. Interfacial simulations involving periodic boundary conditions require finding common lattice vectors between the two materials in the two directions parallel to the surfaces being combined. Generally this means compressing or expanding the surface lattice parameters of one of the materials to match the surface lattice parameters of the

other material. This can lead to excessive strain if the mismatch between the two materials is great due to a large distortion of one of the materials. One method to overcome such strain is near-coincidence-site lattice (NCSL)[128] theory. Rather than combining single surface cells together to form the interface, in NCSL theory the interface is constructed by combining surfaces composed of multiple cells. For instance, an interface can be formed between the (001) rutile and (100) anatase surfaces that consists of 18.2 Å x 22.7 Å and 18.0 Å x 22.3 Å surface cell sizes for rutile and anatase, respectively. This large interface minimizes the misfit between the two surfaces, giving misfit percentage values (a measure of the strain created by putting the two surfaces in a common periodic cell) of 3.47% and -0.92% in the x- and y-directions[33]. The difficulty therefore of modeling such interfaces is predominantly the large system size, requiring robust computational resources.

In order to facilitate computational difficulties, geometries of the interfaces between bulk rutile and anatase were taken from the work of Deskins et al.[129] wherein slabs were modeled through molecular dynamics simulations with an empirical forcefield. Using empirical forcefields allows for a large sampling of the geometry space in tractable simulation time. The interfaces in this previous work were constructed by bringing together surfaces with thousands of atoms in size together and then subjecting them to an annealing procedure in order to better obtain realistic structures. The interfaces were simulated at 1300 K, and then slowly annealed to low temperature. Such simulations are beyond the capabilities of current DFT methods given the large size of the system. For an interface between the rutile (001) and anatase (100) surfaces, the

supercell had 2472 atoms and the total size of the slab was 18.2 Å by 60.2 Å in the x- and

y-directions respectively. The slab was 22.7 Å in the z direction with a ~20 Å vacuum

spacing between slabs. Fig. 3.1 shows the supercell slab model used. An alternative

interface that was used in this work was formed between the rutile (110) and anatase(101)

surfaces and had 1136 atoms. There are other interfaces between various surfaces that

could have been used, but these contained larger number of atoms[129], and therefore more

difficult to model.
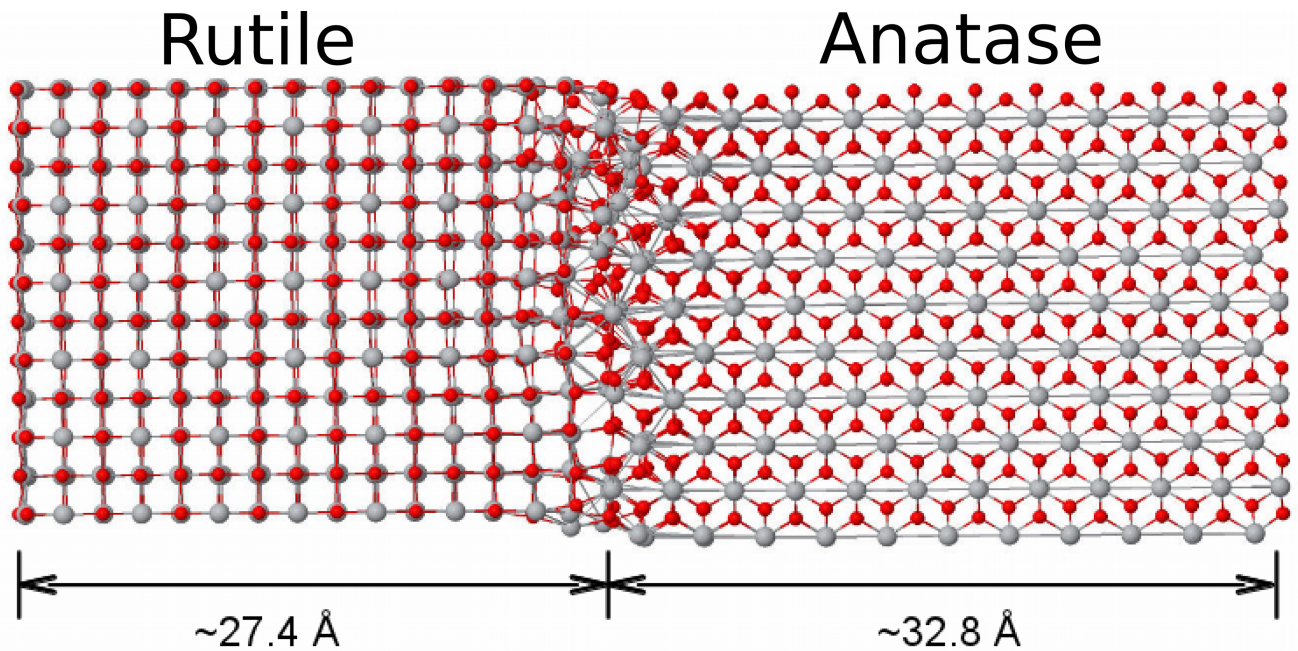
Fig. 3.1 Slab model of the interface between bulk materials used in the current work formed by bringing together the rutile (001) and anatase (100) surfaces. The thickness of each phase is indicated. The red spheres represent oxygen, the grey spheres represent Ti. The same color scheme is used in the remaining figures.

We also modeled interfaces between rutile and anatase with exposed surfaces, where for instance surface chemistry may occur (see Fig. 3.7). This structure was not used to calculate band offsets, but to identify the properties of the interfacial region. The

structure of this interface was created using a molecular dynamics. approach Interatomic interactions were represented by the Buckingham potential with the parameters from the work of Matsui and Akaogi.[130] The calculations were performed with the DL_POLY[131] code. A cutoff distance of 9.0 Å was used for the short-range interactions. We performed all calculations in the NPT ensemble. We started our molecular dynamic simulation at 800K for 400 ps using a timestep of 0.001 ps. Then, the temperature was lowered in 100 K increments for 200 ps at each temperature until 0 K was reached. Then, we optimized the structure a 0 K for 200 ps. The final structure was simulated at the DFT level. This surface interface had 1056 atoms and the simulation box had dimensions of 14.86 Å, 55.20 Å, 30.00 Å in the x-, Y- and y-directions respectively. The vacuum space between surfaces was 20 Å.

Due to the large size of the systems and computational limitations, we only calculated single-point energies and wavefunctions of the slab at the DFT level. Even such single-point calculations were difficult, and typically took several days on a 256-processor cluster. The majority of calculations were performed with code CP2K, which implements the Gaussian and plane waves (GPW) method.[94,95] Valence electrons are described by a double-ζ basis set.[96] Core electrons were described by Goedecker-Teter-Hutter (GTH) pseudopotentials[97] with 12 and 6 valence electrons respectively for Ti and O. The gamma point supercell approach was used. Calculations were performed using the Perdew-Burke-Ernzerhof exchange correlation (PBE) functional[98,99] and were all spin-polarized. The auxiliary planewave basis set was expanded up to an energy cutoff of 300 Ry.

A few calculations on the interface were performed with VASP.5.2[132–135] using three dimensional periodic boundary conditions with a plane wave basis set and a cut off energy of 400 eV. Projector augmented wave potentials[136,137] are used to describe the core-valence interaction, with 4 and 6 valence electrons and Ti and O, respectively. The PBE exchange-correlation functional[100,138] was used.

One potential problem with DFT simulations is that generalized gradient approximation (GGA) exchange correlation functionals incorrectly describe the band gaps of semiconductors and often do not account for electron localisation, arising from the well known self-interaction error (SIE).[90,91] SIE can lead to incorrect electronic levels (e.g. band gaps) and electronic delocalisation, and to overcome this issue with approximate DFT we used the so-called +U correction to DFT (DFT+U) on the 3d states of the Ti atoms.[139,140] DFT+U has been used successfully to model several TiO_2 systems.[78,141–144] An alternative approach is to use hybrid exchange correlation functionals but such calculations are very time-consuming, often an order of magnitude or more slower than GGA-based DFT. Furthermore, previous work shows that DFT+U and hybrid methods give similar results.[145,146] The little additional computational time of the +U correction justifies its use in the current simulations.

The strength of the U correction may influence the calculated valence band minimum and thus calculated band gaps.[147] Appropriate U value choice may also depend on simulation parameters such as basis set, pseudopotential, k-point mesh, etc. The nature of our system makes the selection of a suitable U value difficult due to the presence of two phases. We tested several U values, including assigning different U values to Ti

atoms in the two phases. We found that choice of U value did not change our overall conclusions as summarized in Table 3.1, where it was found that the electronic bands of anatase are always higher than those of rutile. We therefore used different U values for each phase to reproduce the experimental band gaps for bulk calculations. This results in a U value of 8.4 eV for rutile and 6.3 eV for anatase. For atoms in the interfacial region (defined within 2 Å of interface divide) we assigned an average U value to these Ti atoms (7.4 eV). U values for Ti atoms in oxides in the range of 2 to 8 eV have been reported[148] for different oxides, oxidation states and exchange correlation functionals. A recent paper[149] used an iterative procedure to determine a Hubbard U value of 7.5 eV which is very close to our average U value 7.4 eV.

Table 3.1. Electronic bands offsets as calculated using the method in Section III.B as a function of U parameter for a rutile(001)/anatase(100) interface. Valence band offset (VBO) and conduction band offset (CBO), and band gaps for the anatase-rutile interface using CP2K are given. In all cases the rutile valence and conduction bands lie higher than the anatase bands.

U [eV]		VBO [eV]	CBO [eV]	Band gap [eV]	
Anatase	Rutile	VBO [eV]	CBO [eV]	Anatase	Rutile
0.0	0.0	0.81	0.46	2.11	1.77
4.0	4.0	1.05	0.54	2.84	2.34
8.0	8.0	1.21	0.66	3.47	2.92
10.0	10.0	1.31	0.70	3.89	3.28
6.3	8.4	0.41	0.21	3.20	3.00

3.3 Results and Discussion

3.3.1 Nature of the Interface

Our procedure to produce the interface does not simply rely on bringing two surfaces together to form a heterostructure and then allowing optimization (a common approach). Rather, rearrangement and relaxation of the interfacial region is accomplished through the simulated annealing approach discussed in the methodology section. While time-consuming, such an approach gives interfaces that are more likely representative of those present between real TiO_2 nanoparticles. During synthesis and reaction conditions the interfacial atoms between particles are likely to overcome any energetic barriers for rearrangement and find more stable configurations. A standard optimization procedure is unlikely to find any such configurations. The final relaxed interfacial region exists as a transition between the two phases since rutile is more stable than anatase, and is disordered (see Fig. 3.1). These interface regions have been observed experimentally and are suggested to be crucial for the anatase-to-rutile phase transition.[150–152] The local surface structure of the two materials, e.g. (001), (100), etc., is largely removed as surface atoms lose their ordered structure and rearrange to form bonds with the corresponding counter surface.

The interfacial region has a distribution of four-, five-, and six-coordinated Ti atoms. Ti atoms in bulk TiO_2 are six-coordinated. There is no unambiguous way to define coordination, but we assigned coordination numbers based on a simple rule of counting a neighboring atom closer than less than sixty percent of the sum of the van der Waal radii

of each pair of atoms (2.0 Å for Ti, 1.3 Å for O), or 1.98 Å. For instance in the rutile (001)/anatase (100) interface (Fig. 3.1) the distribution of coordination on the interfacial Ti atoms (defined as XYZ) was found to be as follows: 72.2 % Ti_{6c}, 22.2 % Ti_{5c}, and 5.6 % Ti_{4c}, where the subscript designates the coordination. Four-coordinated Ti atoms have been implicated as contributing to increased photo-reactivity[153–155] and we discuss their role in future sections of this thesis. The distribution of four-coordinated Ti atoms seems to be random for all the interfaces that we studied; that is no discernible trend for position of under-coordinated Ti atoms was found.

We note that recent papers have modeled interfaces between rutile and anatase using density functional theory. The first such papers by Xia et al.[156] addressed the thermal properties of the rutile-anatase interface in order to further clarify the anatase to rutile transition. Kullgren et al.[157] calculated the electronic offset between rutile and anatase and found that rutile does indeed have a higher valence and conduction band offsets than anatase. They found that mobile electrons will be accumulate in anatase and mobile holes in rutile, and this is reinforced by the inherent self-trapping mechanisms for electrons in rutile and holes in anatase Li et. al.[158] studied mixed phase TiO_2 composite slabs using DFT. They concluded that the HOMO and LUMO states are separated in different phases, which could be the key to improved photoactivity.The current work is unique in that the interfacial region is examined in detail including the electronic structure which is crucial for these mixed-phase catalysts. None of the previous papers have identified interfacial electronic trapping sites (discussed further below) that are predicted to exist experimentally. The current work also utilizes a large bulk interface,

for instance of the size 18.2 Å by 22.7 Å, containing 2472 atoms. The problem with smaller interfaces is that they introduce excess strain as lattices are compressed or stretched to fit together. Relaxation may also be hindered if the interface is too small since the atoms do not have the configurational freedom to fully move and reach more stable configurations. The limited number of unique atoms and periodic boundary conditions may prevent the realization of realistically optimized structures. Thus, bigger interfaces are likely to give results more comparable to experimental results.

3.3.2. Electronic Offsets between the Phases

The key to aligning energy levels of two materials is to find a common reference level. Such an absolute reference can only be present when the energies in the bulk semiconductor can be referenced to the vacuum level or some other common level. Since typical bulk calculations are carried out for an infinite crystal, no such reference is available; the calculated energy bands are referred to an average electrostatic potential within the solid, which is only defined with respect to an arbitrary constant.[159,160] In order to align the energy levels of the two phases, we used the macroscopic average of the electrostatic potential in the supercell as proposed by Baldereschi et al.[72] and Fall et al.[71] This method filters the microscopic periodic oscillations and gives the macroscopic electrostatic properties.

The valence band offset, ΔE_{VBO}, is defined as the difference between the valence band maximum (VBM) of the two phases, and was calculated using the following

expression:

$$\Delta E_{VBO} = E_{\nu} - \Delta_V \qquad (3.1)$$

where ΔE_{ν} is the difference between the two bulk band edges as calculated by the DFT program. In this case the eigenvalues are measured with respect to the average of the electrostatic potential of each individual bulk material. The second term ΔV is the difference in the bulk electrostatic potential as calculated through the electronic distribution and charge on the ion cores. This term accounts for the different reference levels of the two materials and also may contain interfacial effects. ΔV was calculated as follows.

To compute the electrostatic potential along the z-direction of the interfacial slab, electrostatic data generated by CP2K was processed in order to compute the planar electrostatic potential average $\overline{V}$ with the following expression:

$$\overline{V}(z) = S^{-1} \int_S V(\vec{r}) \, dx dy \qquad (3.2)$$

In equation (3.2), S is the area of the plane perpendicular to the z direction, and x, y are contained in that plane. After computing the planar electrostatic average, $\overline{V}$, it was required to determine the macroscopic average of the electrostatic potential in the slab. To achieve this goal we used a local averaging scheme. This was performed taking an arithmetic average of the nearest neighbors of the point. The result of such procedure is shown in Fig. 3.2. Once the electrostatic potential average was computed, the difference was taken from the electrostatic values in the bulk-like region of each phase, where the potential was virtually constant (~15 Å and ~50 Å in Fig. 3.2) to give ΔV. We

also performed separate bulk calculations for each phase and computed the difference between the energy of HOMO (valence band maximum) and the average electrostatic potential (which is aligned to the interface average electrostatic potential). In this manner we have the energy of the valence band maxima referenced to the average potential for each phase.
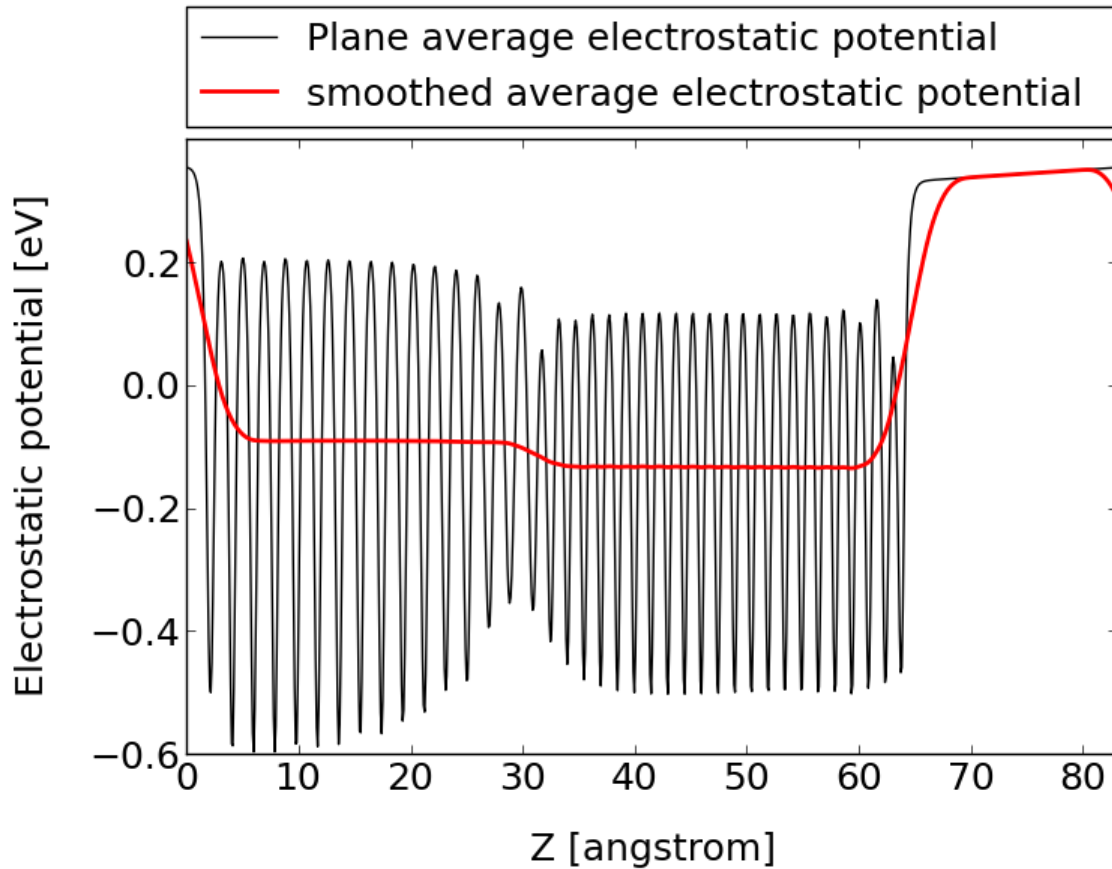
Fig. 3.2. Average electrostatic potential variation along the z axis of the mixed phase rutile (001) / anatase (100) slab using CP2K and U values of 8.4/6.3 eV for rutile/anatase. The black line represents the average potential in planes perpendicular to the z axis ($\overline{V}$) and the red line a smoothed average. The difference between the two smoothed averages in the middle of the slabs gives ΔV.

A sample result showing the calculated bulk offsets is shown in Fig. 3.3. We

calculated rutile to have a higher conduction band offset than anatase by 0.21 eV, and a higher valence band offset of 0.41 eV for U values of 8.4/6.3 eV respectively for rutile/anatase. This alignment would produce an accumulation of bulk migrating electrons in the anatase phase accompanied by hole accumulation in the rutile phase, suggesting that charge separation does indeed occur for a TiO_2 heterostructure. Table 3.1 summarizes results using various U values, and we found that the direction of offset (rutile higher than anatase) does not change based on the U value choice, only the magnitude of the offset. Thus, the DFT+U results are all consistent with the picture in Fig. 3. 3 for electronic band offsets. The results for the other studied interface, an interface between the rutile (110) and anatase(101) surfaces, present the same trend with a CBO of 0.18 eV.
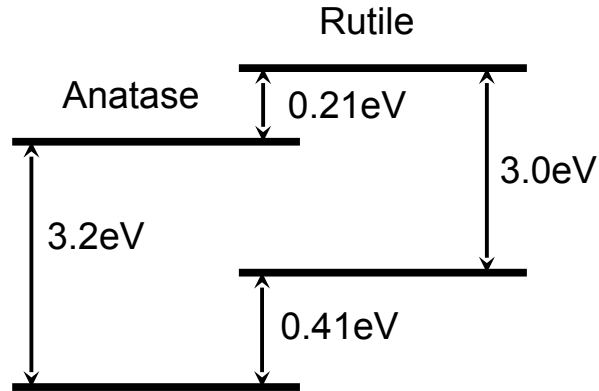
Fig. 3.3. Schematic representation of the band alignment between rutile and anatase as calculated by DFT+U (U = 8.4/6.3 eV for rutile/anatase) and the rutile (001)/anatase (100) interface.

In contrast, previous experimental work[15] argued that the anatase CB was higher than the CB of rutile. However, this previous work did not actually measure the offset between the two materials, but inferred the offset based on other measured properties,

such as x-ray diffraction data.

Theoretical work generally agrees with our current work. The exception appears to be the work of Kang et. al.[161] who computed through DFT a different band alignment than our work, and suggested that anatase has a higher VB and CB. They used the LDA exchange correlation functional (no U correction) and modeled particles, rather than bulk TiO_2 which could explain the disagreement with our work. On the other hand, other recent theoretical results agree with our conclusions. Using the branching point energy or charge neutrality level as a common reference[70,162] Deak et al.[124] found the rutile CB to be higher than the anatase CB by 0.3 to 0.4 eV. This work is based on a more crude alignment procedure (no common cell between rutile and anatase was modeled) but the agreement with our work is encouraging. Later work by this group[157] also found the rutile CB to be higher than the anatase CB by modeling rutile/anatase interfaces utilizing an alignment scheme similar to the current work. Our values are also reasonably consistent with those from embedded cluster hybrid DFT results.[125] In previous DFT work Deskins et al.[163] also predicted the same trends in phase preference of the charges based on the thermodynamics of electron/hole transfer to the two phases. Furthermore Li et al.[164] developed a theoretical model where the electrons in TiO_2 have small polaron character in the rutile phase. Their model also predicted that the rutile CB lies higher than the anatase CB. We conclude that the alignment scheme from theory is fairly consistent, but that more work may be needed to reconcile experimental observations and theoretical predictions.

In order to further examine the effect of the interface we performed an analysis of

the projected density of states (PDOS) for the slab, with the density of states calculated for different regions of the interface model. Fig. 3.4 shows the PDOS around the VB and CB of the slab. The PDOS for each atom type was found, then the PDOS were added together to get the DOS of the rutile, anatase, and interface regions. The bulk rutile and anatase PDOS were taken ~10 Å away the interface, or in the middle of the anatase and rutile regions of the slab (representative of the bulk phases), while the interfacial PDOS included atoms within 2 Å of the interfacial divider. The results from the PDOS agree with our previous offset results (Fig. 3.3) in that the bulk CB and VB of rutile are both higher than of anatase. We also observed a interfacial gap state (discussed in the next section) just below 0 eV.
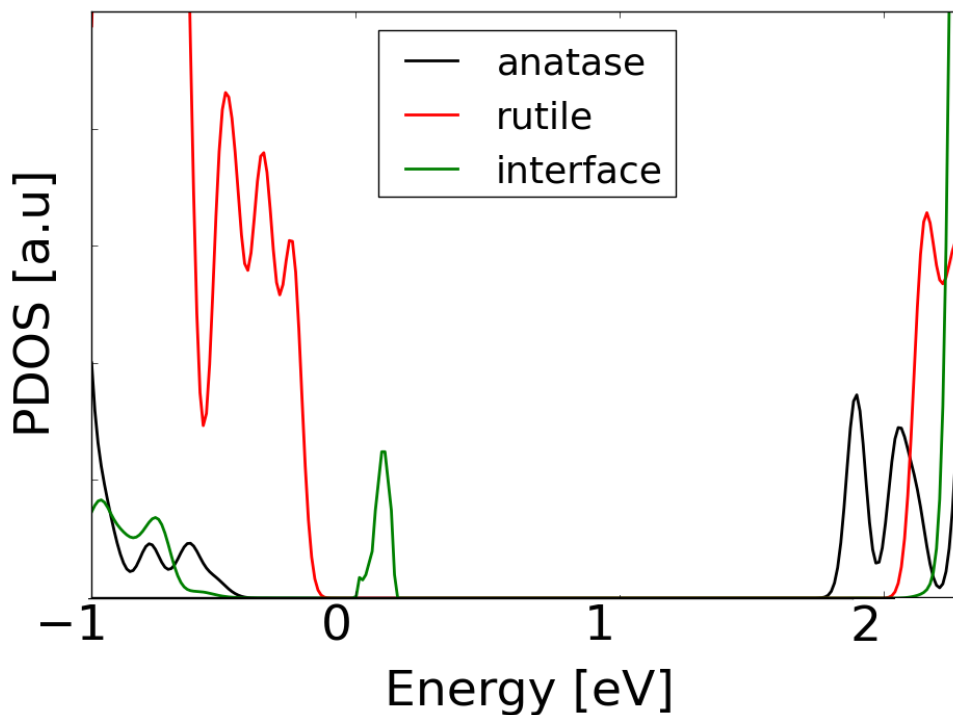
Fig. 3.4. Projected density of states (PDOS) plot for the anatase phase, rutile phase and the interface region using U = 8.4/6.3 eV for the rutile (001)/anatase (100) interface using the CP2K code. 0 eV corresponds to the Fermi level.

75

3.3.3. Charge Trapping at Four-Coordinated Ti

As mentioned above, a gap state is observed in the PDOS, as shown in Fig. 3.4, which represents the localization of electrons within the interfacial region. In our model slab the interfacial region has a disordered structure due to the transition from one phase to the other, and the Ti atoms have a variety of coordination numbers.[129] We identified five Ti atoms that were four-coordinated (Ti_{4c}) for the rutile (001)/anatase (100) interface and several electrons localized at some of these sites, as shown in Fig. 3.5. Large electron spin density is found in d orbitals on Ti_{4c} atoms. The gap state observed in Fig. 3.4 corresponds to the localization of electrons at these Ti_{4c} sites. There are some electrons localized on other interfacial Ti atoms besides the two Ti_{4c} atoms, but there is much less electron density on these atoms. We did not observe unpaired electrons away from the interface (bulk rutile and anatase) region of the slab.

Not all Ti_{4c} atoms in the interface had localized excess electrons and in fact we observed no localized electrons for the rutile (110)/anatase (101) interface which only had two Ti_{4c} in the interface. These results show that merely the presence of Ti_{4c} does not guarantee electron localization and formation of gap states; such processes are structure dependent. The greater number of Ti_{4c} in the rutile (001)/anatase (100) interface however leads to a greater chance of electron localization which is why electron localization is observed for this interface while no localization occurs for the rutile (110)/anatase (101) interface.
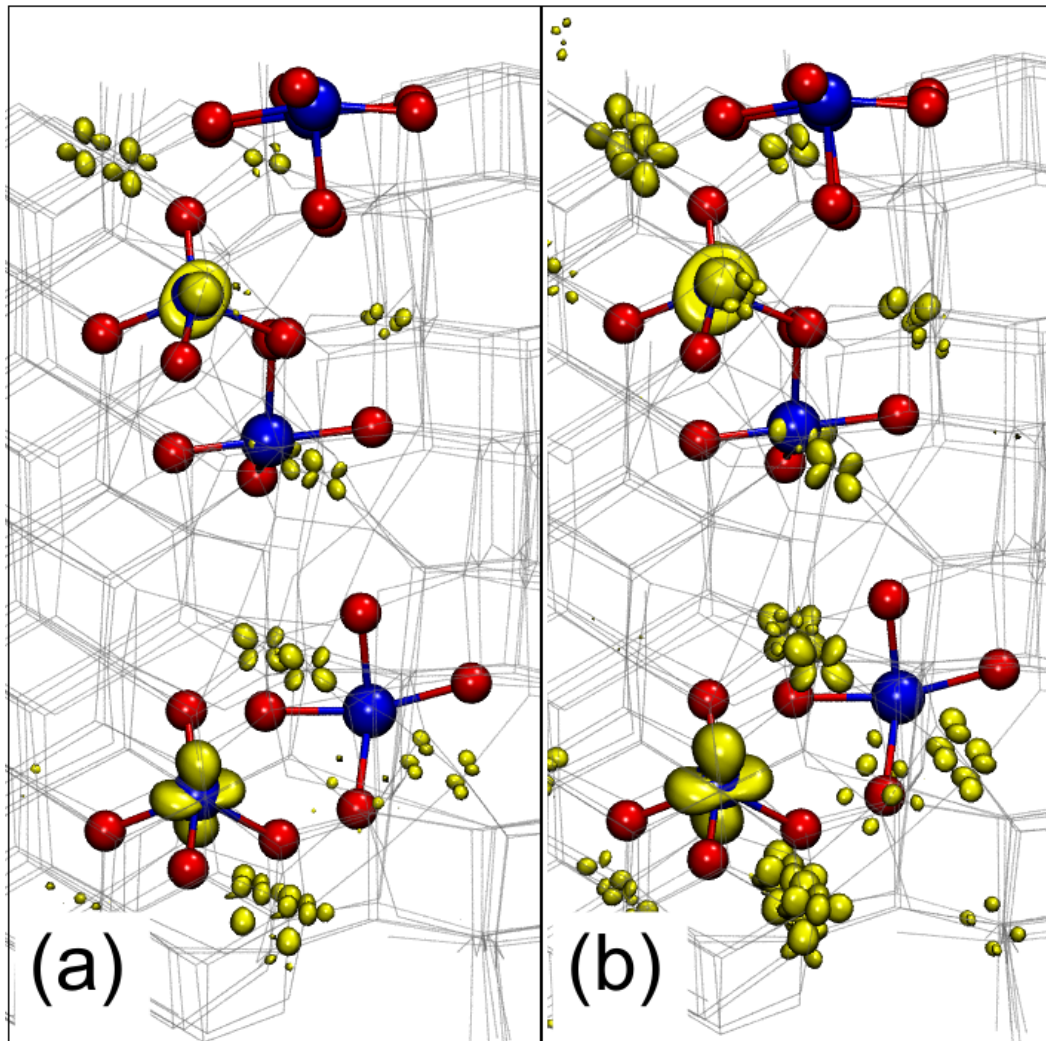
Fig. 3.5 (a) Electron spin density plot (isovalue = $0.017e/Å^3$) of electrons localized in the 3d orbitals of four coordinated Ti atoms in the interfacial region for a neutral slab. The results are from a rutile (001)/anatase (100) interface with U = 8.4/6.3 eV for rutile/anatase. (b) An electron spin density plot (isovalue = $0.03e/Å^3$) for a slab having a net -1 charge. No +U correction was applied to these calculations. The blue spheres represent four coordinated Ti atoms while red spheres are their nearby O atoms. The yellow contours represent the spin up density.

One issue arising from these calculations is the nature of the hole states. Since unpaired electrons localized at specific Ti_{4c} sites, forming Ti^{3+} cations, hole states on O atoms must also have formed in the slab due to electron deficiency. We found these hole

states to be delocalized across several O atoms rather than confined to specific atoms. This delocalization of the holes could possibly be mitigated by applying DFT+U to the O orbitals,[165] but should not change the conclusions on electron localization. In order to further remove the issue of hole states and address the stability of photoexcited electrons at or near the interfacial region, we simulated a slab that had a net charge of -1, in contrast to previous results thus far which involved neutral slabs. A similar approach was used to model polaron formation in bulk TiO_2.[165] Electron spin density plots of the interfacial region using a charged slab are shown in Fig. 3.6(b). In agreement with our previous results on neutral slabs, excess electronic charge occurs at several Ti_{4c} sites. In fact, the extra electron even localizes at Ti_{4c} sites even when no U correction is applied (U = 0 eV or standard GGA-based DFT) indicating the strong tendency of electrons to localize at Ti_{4c} sites and become trapped. A Ti^{4+} atom in bulk TiO_2 is surrounded by six O^{2-} atoms in a stable octahedral environment. Ti_{4c} atoms are deficient in coordination, and therefore deficient in surrounding negative charge and filled bonding. Apparently this deficiency leads to a destabilization such that addition of an excess electron stabilizes the Ti_{4c}. Such behavior is also seen with surface atoms which have unsaturated bonds, where electron trapping may occur.[166] Previous DFT results have shown that Ti_{4c} can exist on nanoparticle surfaces and can act as sites to trap electrons.[154] The importance of undercoordinated Ti atoms as electron traps has also been discussed from experiments.[118,153]

Undercoordinated Ti have been shown by modeling results to be very reactive for catalysis.[167] At the interface between anatase particles undercoordinated Ti also have been

78

shown to form trapping states[154] (a similar finding to our current work except that we considered both rutile and anatase phases). Our results thus show that excited electrons could migrate to the interfacial region and become trapped at Ti_{4c} sites. Generally trapping sites are proposed to increase hole/electron recombination but it is still unclear whether these interfacial sites have a inhibitory or beneficial effect on photocatalysis. These unpaired electrons may potentially be available to participate in chemical reactions at exposed areas of the interface, and could be photocatalytic "hot spots".[153] These Ti_{4c} sites have been shown experimentally[118] to exist in the transition region between rutile and anatase, and have been postulated as increasing the reactivity of mixed-phase TiO_2. We note that distorted tetrahedral shapes were also observed for four-coordinated Ti on anatase particle surfaces[154]. Our results do indeed confirm the special nature of the interface and the existence of Ti_{4c}, as well as their trapping nature. Synthesis of TiO_2 materials with increased interfacial Ti_{4c} atoms may be an avenue to develop more active photocatalysts and more experimental and theoretical work is needed to further clarify the nature of under-coordinated atoms for photocatalysis.

3.3.4. Exposed Surfaces of Mixed Phase TiO₂

Our studies on the increased reactivity of mixed phase surfaces have been explained so far by modeling bulk materials. In this section we discuss results on modeling a surface of a mixed phase anatase/rutile material, or a three-phase system (anatase, rutile, vacuum). Such interfaces would be present for instance at the intersection

of two nanoparticles (rutile and anatase). This approach requires a large supercell in order to accommodate the two pure phases plus the interfacial region. The amorphous character of the interface between the phases adds an additional complication for the molecular model of the surfaces.

We modeled a slab with two different interfaces running parallel to the [010] direction. The exposed surfaces are the (110) surface for rutile and (101) for anatase, which are shown in Fig. 3.6. Those are the most stable surfaces for each phase. The slab has two interfaces due to the present periodic boundary conditions in the x and y directions. There is a vacuum space in the z-direction of ~20 Å between slabs. This geometry was built using molecular dynamics and the cooling approach described in the methodology section.
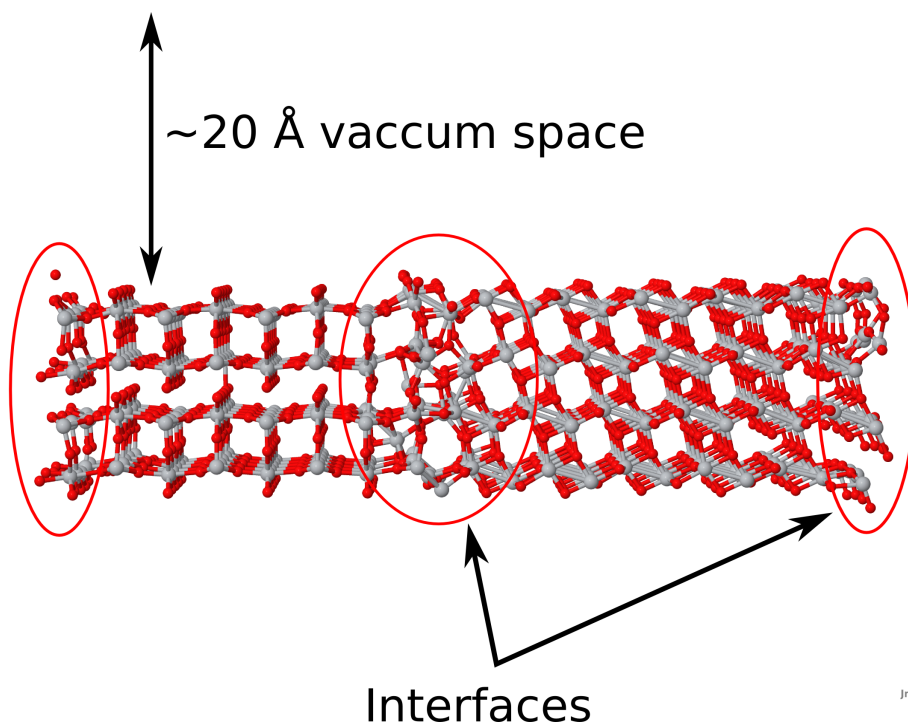
Fig. 3.6. Slab model of the mixed phase exposed surface.

Localization of charge was observed in this system in the interface. This can be visualized with a spin density plot, as shown in Fig. 3.7. From this figure it is clear that the unpaired electrons are more stable within the interfacial region than in the pure phases alone. Electrons seem to be trapped in this disordered region. It is important to highlight that there are no unpaired electrons in the regions of pure rutile or pure anatase. Therefore, the interfacial regions are potentially more reactive, since those electrons could be transferred to adsorbates on the surface near the interfaces.
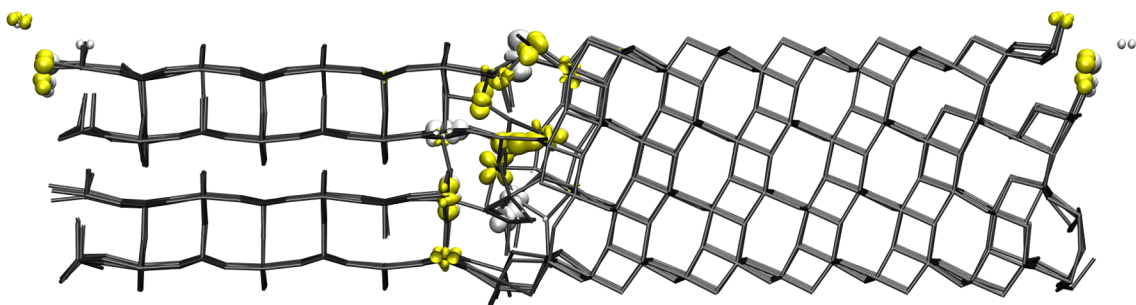
Fig. 3.7 Spin up and down density plot showing the whole slab (isovalue = 0.017e/Å^3). The yellow contours represent the spin up density and the white surfaces represent the spin down density. The grey lines represent the bonds between atoms.

To further clarify the interfacial region Fig. 3.8 shows only the Ti atoms in the interfacial region and the spin density isosurfaces for the electrons with spin up and down. The majority of the atoms in this interface model are five- and four-coordinated, the purple and green spheres in Fig. 3.8, but even six and three-coordinated atoms are found. The electrons can be seen localized mostly on the five and four coordinated Ti atoms. There are also unpaired electrons in one of the two three coordinated Ti Atom and

in one of the two six coordinated Ti atoms in this region.   In general the distortion of the

lattice seems to favor the stability of unpaired electrons on undercoordinated Ti atoms.

The results of a slab with exposed surfaces gives very similar results to bulk interfaces,

which confirms the electron trapping character of the interfacial region. We also modeled

a charge with -1 charge, which would be representative of a photo-excited slab, and

found the same electronic structure.
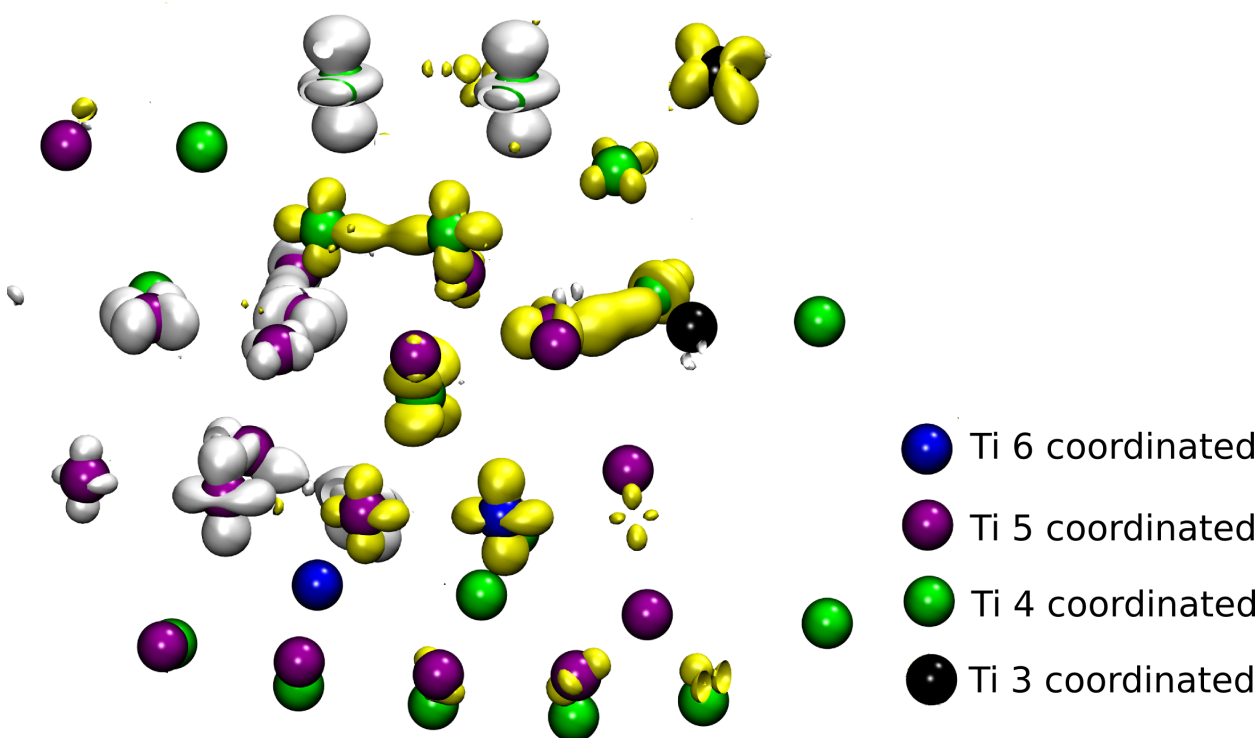
Fig. 3.8 Electron spin density plot (isovalue = 0.017e/Å^3) of the interfacial region for a slab with vacuum-exposed surfaces. The results are from a rutile (001)/anatase (100) interface with U = 8.4/6.3 eV for rutile/anatase. The blue spheres represent six coordinated Ti atoms, the purple spheres represent five coordinated Ti atoms, the green spheres represent four coordinated Ti atoms and the black spheres represent three coordinated Ti atoms. The yellow contours represent the spin up density and the white surfaces represent the spin down density.

3.4. Conclusions

We have simulated the interface between the anatase and rutile phases of TiO_2 using DFT+U in order to better characterize the nature of mixed-phase TiO_2 photocatalysts. We modeled realistic structures that contained thousands of atoms, rather than smaller, possibly irrelevant interfaces. Our results show that the rutile conduction and valence bands are higher than the anatase bands. This has important implications for TiO_2 photocatalysis, indicating the preferred direction of electron/hole flow (electrons to anatase, holes to rutile). Such preferred migration could lower the electron/hole recombination rate, which would increase photo-reactivity. Our results are also particularly novel in that we show how electron trapping can occur in the interfacial region in bulk and exposed slabs at undercoordinated Ti sites. Such sites have been experimentally predicted, but theoretical work now confirms their existence. Trapped electrons produce a gap state, which may influence photoexcitation, and these trapping sites may also strongly influence electron/hole recombination and/or reactivity. Finally, we acknowledge that we have modeled interfaces formed from stoichiometric surfaces. We cannot exclude the possibility that defects (such as O vacancies or Ti interstitials) may affect the electronic properties of mixed-phase interfaces, and future work may examine interfaces with such structures.

Chapter 4: Size Effects of TiO$_2$ supported Gold Nanocatalysts

4.1. Introduction

Dispersed metal nanoclusters supported on different materials have unique properties as catalysts for several chemical reactions.[168] Gold is an inert metal at the macroscopic level, however it becomes reactive at the nanoscale.[169–172] Hence this metal has been of much interest to the scientific community. Gold dispersed on metal oxides have been used as novel catalysts for several commercially important chemical reactions. A lot of work has been performed on nanosized Au dispersion. However, a complete understanding of these catalysts has not been reached.

When gold is dispersed on certain metal oxides the chemistry of the system changes depending on the support material and Au particle size.[79] For instance, when the gold particles present sizes of about 3nm the turnover frequencies for certain reaction as the oxidation of CO are very high.[173]This work addresses the effect of the size of the gold particle and its performance as a catalyst using density functional theory.

As mentioned, an example of the synergistic effect of the dispersion of gold on metal oxides is the CO oxidation reaction. CO oxidation on gold supported over metal oxides has been studied as a model reaction for its simplicity and technological relevance. During the last several decades, there has been a significant increase in the research on

fuel cells since it can offer a cleaner alternative for conventional internal combustion engines. The hydrogen rich gas mixture obtained by the partial oxidation or steam reforming of a hydrocarbon fuel usually contains byproducts, mainly carbon monoxide. Among the many approaches to reduce CO concentration in the reformed gas mixture, selective catalytic oxidation of CO to CO_2 has been found to be the most effective way to remove the trace amount of CO from hydrogen.[174] Bulk gold alone is not active for CO oxidation and TiO_2 is not active either for thermal CO oxidation. Nevertheless, gold supported on TiO_2 is an active catalyst for CO oxidation at room temperature.[175] Higher activities have been found by oxide-supported small gold particles less than about 5 nm size, with the highest rates being shown at sizes of about 2 to 3 nm.[176] Molecular modeling has been a useful tool in testing the feasibility of the proposed active sites and reaction mechanisms.[6]

Another model reaction example is the water gas shift reaction (WGSR) which has been carried out commercially over catalysts based on Ni or Cu at 900 K and 600 K respectively. Supported gold nanoclusters catalysts operate at temperatures as low as 473 K.[175] DFT calculations predict a very high barrier for the dissociation of H_2O on Au(111) or isolated Au nanoparticles.[178] In the metal-oxide supported gold system the adsorption and dissociation of water takes place on the oxide and CO adsorbs on the gold nanoparticles. Experimental evidence indicates that gold-oxide interfaces catalyze the reaction of OH with CO to yield HCOO or CO_3 intermediates and then H_2 and CO_2.[178] Williams et. al.[179] proposed a model were the active sites are the Au atoms in corner sites. This model successfully fit experimental data. Gold nanoparticles supported on metal

oxides has found several other applications beyond the mentioned CO oxidation and WGSR. It is also well know for its ability of oxidize alcohols and effect other complex organic transformations.[33] Moreover, The application of gold catalysis in organic synthesis is promising but still in early stages of development, and further work is expected in this area.

One of the important aspects of Au catalysis is the role of the support. The periphery between the Au cluster and the support is potentially very active.[19] Experimental studies on CO oxidation suggest that inert supports, such as SiO_2, Al_2O_3, MgO, are less active than reducible transition metal oxides.[180] Such reducible supports also are more sensitive to variations in the size of the gold particles. This difference in activity could be attributed to the size of the Au-oxide interface which changes with Au particle size. For instance, in CO oxidation molecular oxygen could adsorb on the reducible metal oxides as a superoxide. Then, dissociation of the molecularly adsorbed oxygen could take place at the metal support interface. These oxygen atoms could become a reservoir in the vicinity of the gold clusters where the CO molecules could adsorb, and participate in the CO oxidation reaction.[180]

Chen et. al.[181], unlike the aforementioned authors, suggests that the role of the support is crucial as a promoter of Au nucleation, but it is not directly involved in the bonding of O_2 and CO. The interaction of the gold nanocluster with Ti^{3+} defects sites in TiO_2 could yield $Au^{\delta-}$ which could be crucial for O_2 activation. Since, those Ti sites promote the nucleation of gold particles they populate the perimeter of the gold atoms.

However, DFT calculations have identified an active role of the support. The positively charged Ti at the interface enhances electron transfer from the supported Au to the adsorbed O_2.[182] A more recent work[183] using DFT supports this theory claiming that the periphery of the supported Au clusters on TiO_2 surfaces will be oxidized with O atoms at all Ti atoms underneath the Au cluster. Those oxygen atoms are stabilized in the substrate by charge transfer from the adsorbed Au cluster. Another work also claims that CO absorbs along the $[1\bar{1}0]$ direction of the rutile (110) surface while the [001] direction remain inactive[184] The work by Remediakis et al.[185] also suggests that charge can accumulate between the Au atoms at the bottom of the clusters and Ti atoms from the support. Those electrons trapped in the O deficient substrate supply the bonds at the interface.

Another characteristic of Au nanoparticles that may affect their catalytic ability is the presence of highly active surface, edge, or corner sites. The effect of undercoordination of gold atoms has been investigated previously. Lopez et. al.[186] have discovered a number of details on the catalytic activity of gold dispersed on metal oxides. They found that the main effect of decreasing the size of the gold nanocluster is to increase the total number of undercoordinated gold atoms. This is proposed to be the principal effect on the activity of the catalyst. The support have a smallest effect on the reactivity. Mavrikakis et. al.[187] also found the density of undercoordinated gold atoms to give the increased reactivity of the system. As mentioned, one way to increase the density of corner and edges, is to decrease the size of the gold clusters. Those corner and edges have been found to be very catalytically active.[169] Other work has shown that a change in

the coordination of Au atoms produces a modified electronic structure. The undercoordinated Au atoms have high lying metal d states, which can interact better with the adsorbate valence state than the low lying states of the higher coordinated atoms of the close packed surface.[171]

The number of undercoordinated Au atoms depends on the shape of the nanoparticle, and the interaction between the gold and the metal oxide support determines the size and shape of the gold nanoparticles.[188] Supports with different interfacial binding energies between the Au particles and metal oxide produce different sizes and shapes and therefore different activities. Defects on the oxide surfaces, such as oxygen vacancies, have a key role in the adsorption, nucleation, and growth of gold particles. High resolution STM and DFT calculations confirmed that bridging oxygen vacancies are the active nucleation centers for the growth of Au nanoclusters on TiO_2.[172] Therefore, the size of the particle depends on the density of oxygen vacancy defects on the surface.[189] The Au particles nucleate in vacancies and them diffuse trough the surface until they coalesce with other particles generating multiple attaching sites to the surfaces, which stabilize the particle. Besides the anchoring of gold particles promoted by oxygen vacancies, defect sites might play an important role in charge transfer to gold particles. Electron transfer from the metal oxide produces negatively charged gold particles which present enhanced catalytic activity for CO oxidation.[170] Charged particles in general can play a role in the activation of intermediates in several chemical reactions.

One particular work has shown contrasting results with regards to the role of

oxygen vacancies. Matthey et. al.[190] claim that oxygen vacancies do not stabilize Au nanoparticles under real reaction conditions at usually high oxygen pressures. They suggest that the Au particles are stabilized via Au–O–Metal bonds. They propose that Au nanoparticles dispersed on reducible oxides are better catalysts than those supported on nonreducible oxides, because reducible oxides are more capable of forming oxygen rich surfaces. DFT calculations evidence high Au-oxide support adhesion on oxidized TiO_2 surfaces but not on reduced or stoichiometric TiO_2 surfaces. The Au clusters become cationic and is capable of binding molecular and atomic oxygen at perimeter sites next to the support and CO further away from the support.

Even though it is usually assumed that CO absorbs on the gold nanoparticles,[191] experimental evidence indicates that O-O bond scission is activated by the formation of a $CO-O_2$ complex at dual Ti-Au sites at the Au/TiO_2 interface. DFT calculation confirms this model and the activation energy. The $Au-Ti^{4+}$ site at the Au/TiO_2 interface has been found to be crucial in activating O_2 because it allows for electron transfer from Au to Ti and subsequent electron transfer to O_2, promoting O-O bond activation.[192] Another recent DFT work[193] has confirmed that O_2 is strongly adsorbed and activated on the Ti^{5c} (five coordinate) site next to the perimeter of the Au nanoparticle and also in the sites away from the perimeter.

There is experimental evidence that suggests that the effect of supporting Au nanoparticles on a TiO_2 support is the same that supporting TiO_2 nanoparticles on bulk gold.[194] Then, the electronic interactions are likely the key aspect of the catalytic activity

in Au–TiO$_2$. The Au nanoparticle can donate electrons to the O$_2$ molecule making it more reactive. This effect also left a positive charge in the gold atoms increasing the stability of the absorbate. A switch in the polarity of the metal oxidation state (cationic → anionic) during cluster reaction has been identified experimentally.[195]

As discussed above, there are various theories as to why Au nanoparticles behave so actively as catalysts. To reiterate, the following are some of the important points. Undercoordinated Au atoms may have unique electronic levels that enable surface reactions. The interaction between the Au and support metal oxide is crucial since it determines the shape and stability of Au nanoparticles. Sites at the interface between Au and metal oxide may also be especially reactive. In the current work we use DFT to model Au nanoparticles on TiO2 surfaces in order to understand the nature of such catalytic systems. We focus on the role of undercoordinated sites and how size affects their catalytic ability.

4.2. Methodology

The DFT computations were performed with the CP2K[95,196] package. CP2K uses the Gaussian and plane waves approach (GPW)[95] with periodic boundary conditions. Valence electrons were described by a double-ζ basis set, specifically well suited for the condensed phase.[96] Core electrons were described by Goedecker−Teter−Hutter (GTH) pseudopotentials.[97–99] The gamma point supercell approach was used.. Calculations have been performed using the Perdew−Burke−Ernzerhof (PBE) functional for the exchange

correlation term of the electron−electron interaction,[100] and all calculations were spin polarized.

Transmission electron microscopy studies have shown that deposited Au particles morphology can be described by a truncated cubo-octahedron.[179] We modeled the three smallest possible truncated cubo-octahedro gold particles. The model TiO_2 rutile (110) surface was made large enough to allow a separation between the periodic images of the gold clusters of at least 3 Å. All the calculation were performed at the DFT level. A four tri-layer slab of the rutile TiO_2 (110) surface was used for the calculations. The size of the TiO_2 surfaces was 7x4 for the small and medium size Au nanoparticles and 10x5 for the biggest nanoparticle. The simulation boxes were 20.9Å by 26.2Å by 30.0Å and 29.8Å by 32.7Å by 40.0Å respectively. The two top tri-layers were allowed to relax and the two bottom tri-layer were kept fixed.

The typical size of the gold particles in relevant systems is between 1 nm and 5 nm. However, a typical size used in many previous DFT reports to model gold particles dispersed in metal oxides is usually less than 1nm.[184,186,193,197–203] We used the three smallest possible truncated cubo octahedra gold particles, with 25, 119 and 331 atoms, which have 0.9 nm, 1.8 nm, 2.7 nm diameters respectively. Fig. 4.1 shows the gold nanoparticles with the corner sites highlighted

Adsorption energies E_{ads} were calculated using the following expression:

$$E_{ads} = E_{surf+absorbate} - E_{surf} - E_{absorbate} \qquad (4.1)$$

92

In the above equation $E_{absorbate}$ is the energy of the isolated molecule in the vacuum, E_{surf} is the energy of the bare slab, and $E_{surf+absorbate}$ is the total energy of the molecule adsorbed on the slab. For a better visualization of some results we defined the binding energy as $E_{binding} = -E_{ads}$. Several adsorption geometry configurations were found for each adsorbate, but the most stable geometries are analyzed herein.

4.3. Results and discussions

Since the interaction between the gold nanoparticle and the oxide surface seems to play a key role in the reactivity, it is very important to obtain a stable configuration for this system. We chose a truncated cubo-octahedral shape, because this is a known stable configuration for gold supported particles. This particle has been identified using transmission electron microscopy (TEM) as a good representation of the average particle.[179]

(a)   (b)   (c)
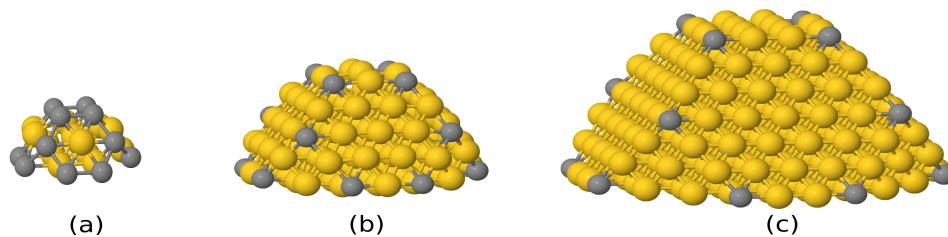
Fig. 4.1 Truncated cubo-octahedral Au nanoparticles (a) 25 atoms, (b) 119 atoms, (c) 331 atoms. Yellow spheres represent gold atoms and the gray spheres represent gold atoms in corner sites

4.3.1. Supported nanoparticles

We modeled the gold nanoparticles supported on the TiO_2 rutile (110) surface. This is the most stable and studied surface of TiO_2. The stability of the supported nanoparticles influences the possible reaction sites on the support, metal particle, and the interface perimeter. In order to obtain a reasonable Au/TiO_2 system we optimized the geometry of the model nanoparticle on the TiO_2 surface using several different initial configurations.

We obtained several stable configurations with different angles between the perimeter atoms of the Au nanoparticles and the $[1\bar{1}0]$ direction. Fig. 4.2 shows the adsorption energies of the 119 Au atoms nanoparticle on the rutile TiO_2 (110) surface for different stable configuration of the cluster. The most stable configurations have the perimeter atoms aligned along the $[1\bar{1}0]$ direction. The nanoparticles stabilize with the perimeter close to the line of bridging O atoms on the TiO_2 surface. We used this stable geometry for the rest of the simulations. We used the same procedure with the 25 Au atoms nanoparticle. However, we did not use this procedure for the biggest nanoparticles because of limitations in computational time. We used a initial geometry for the 331 Au atoms where the perimeter atoms were aligned along the $[1\bar{1}0]$ direction.

Fig. 4.3 shows the most stable configuration of the Au nanoparticles with 25, 119 and 331 atoms. The smallest particle stabilizes with a more spherical shape (see Fig. 4.3 (a)). It is important to mention that the configuration shown for the smallest particle is not

94

the most stable. The most stable configuration was a bilayer of gold atoms. However, we wanted to compare particles with approximately the same shape and different size in order to understand geometric and electronic effects. In contrast the bigger nanoparticles are stable in the truncated cubo octahedral shape (see Fig. 4.3 (b) and (c)).
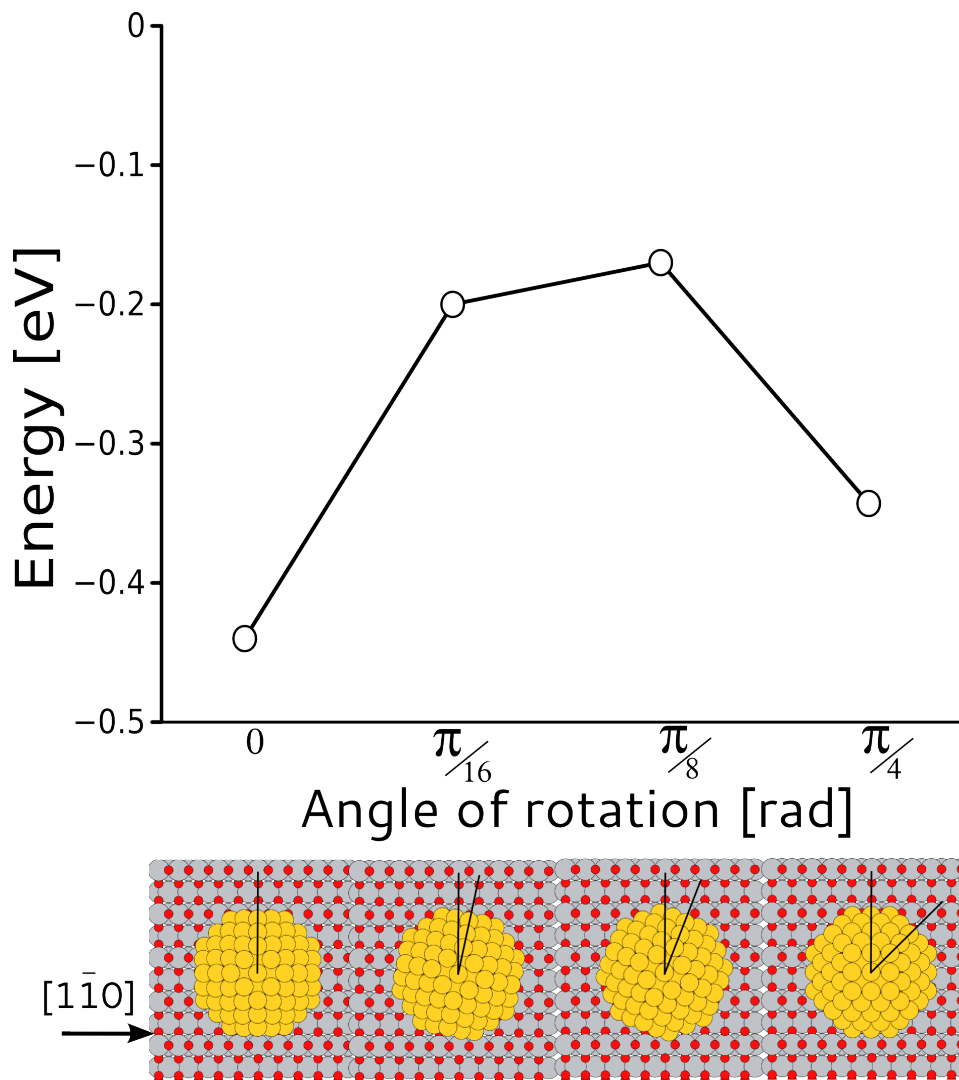
Fig. 4.2 Adsorption energies of the 119 Au atoms nanoparticle on the rutile TiO2 (110) surface at different angles with respect the [001] direction.
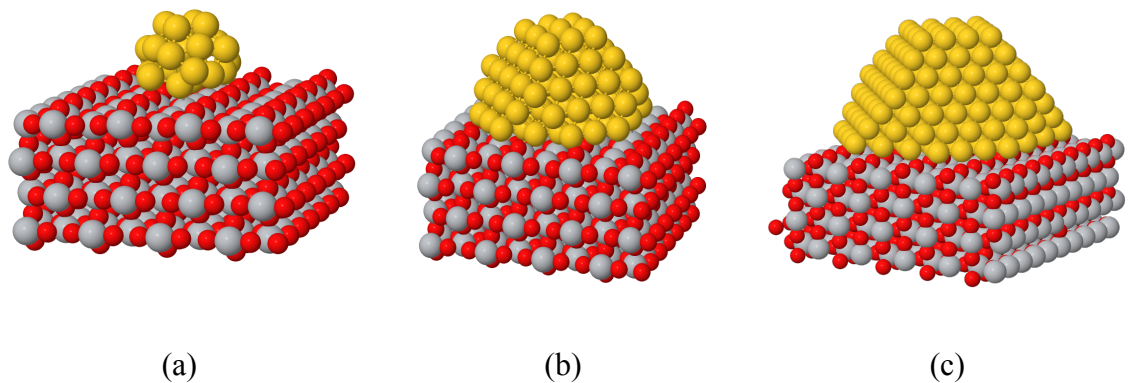
Fig.4.3 Gold nanoparticles on TiO2 (110) surface. (a) 25 atoms, (b) 119 atoms, (c) 331 atoms.

4.3.2. Size dependence of H_2 adsorption

The influence of the size of the Au nanoparticle on reactivity has been extensively studied using experimental methods. However, at the atomic scale the effect of changing the size of the Au cluster is not completely clear. The computational cost needed to model realistic systems has typically hindered the simulation at the DFT level. In the present work we used particles with sizes close to the size of experimentally observed Au nanoparticles supported on metal oxides. In order to make the simulations possible we used up to 1000 computer processors for each system. Even with these computational resources, some simulations took more than 12 days of computation.

We modeled H_2 adsorption over the three Au/TiO_2 systems. The adsorption configurations of H_2 on three different sites on the 25 gold atoms nanoparticle are shown in Fig. 4.4. The adsorption sites are a corner Au atom in the interface between the Au nanoparticle and the TiO_2 surface, a corner atom in the Au particle and one site on the (111)-like surface of the Au nanoparticle. Fig. 4.5 shows the binding energies of H_2 on

three different sites over the 25-atom Au nanoparticle. The least stable adsorption site occurs along the particle face, the (111)-like facet, while corner and corner-interface sites are more stable.

<div align="center">(a)   (b)   (c)</div>
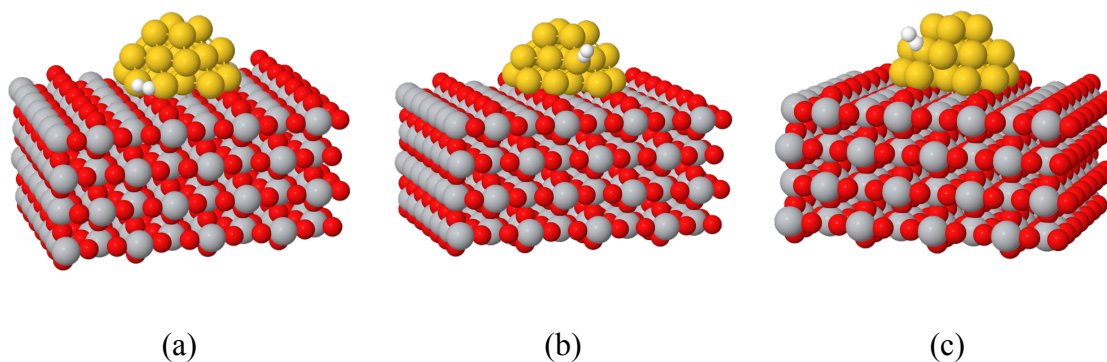
Fig. 4.4 Hydrogen molecule adsorption configuration on the 25 Au atoms particle (a) Adsorption at a corner interface site, (b) adsorption at a corner site, and (c) adsorption on the gold surface face.
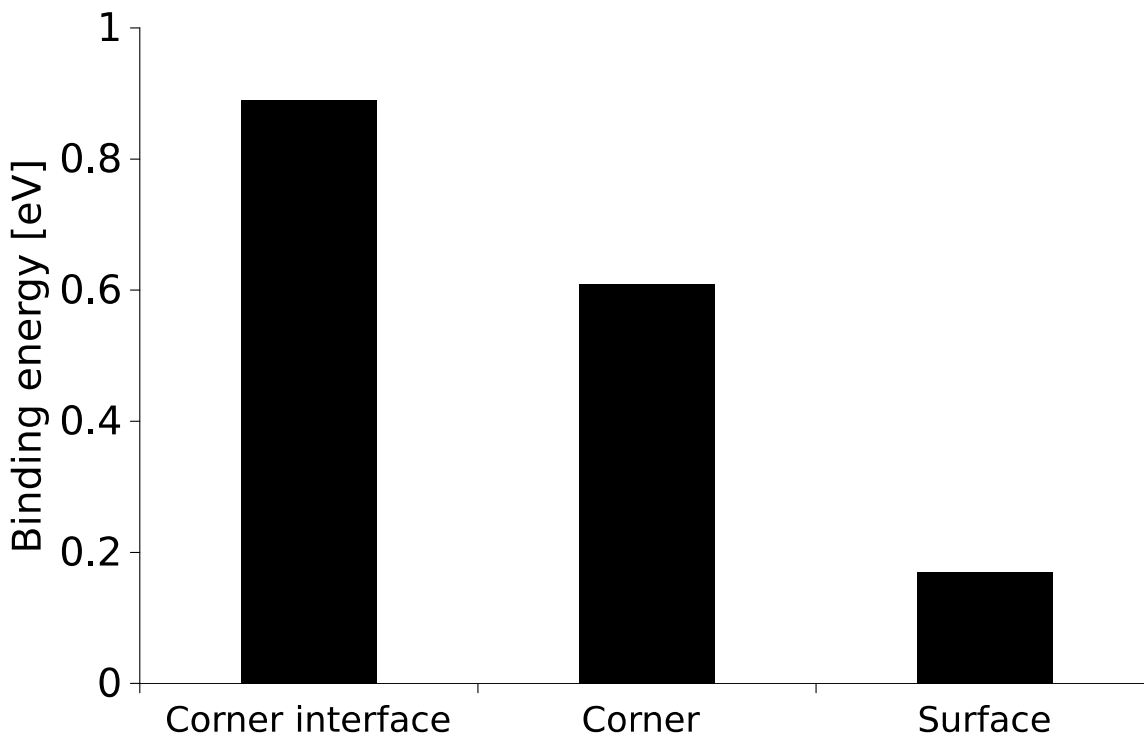
Fig. 4.5 Binding energies of hydrogen molecule in three different sizes of the 25 atom gold nanoparticle.

The adsorption configurations of H_2 on four different sites on the 119 atoms nanoparticle are shown in Fig. 4.6. The adsorption sites include the interface along the edge of the nanoparticle, a corner Au site at the interface between the Au nanoparticle and TiO_2 surface, a corner atom on the Au particle, and one site on the (111) face of the Au nanoparticle. The binding energies of H_2 on the 119 Au atoms system are shown in Fig. 4.7. The most stable configuration is the molecule absorbed on the edge interface site, followed by the corner interface site, corner, and lastly surface. For the 119 atoms nanocluster, the edge site has two corner site as neighbors, which could influence the stability of the molecule. Fig. 4.8 shows the optimized geometry of H_2 absorbed on a corner interface site on the 331 atoms nanoparticle. We did not model adsorption of H_2 at other sites on these nanoparticles due to the computational cost of the calculations.

| (a) | (b) | (c) | (d) |
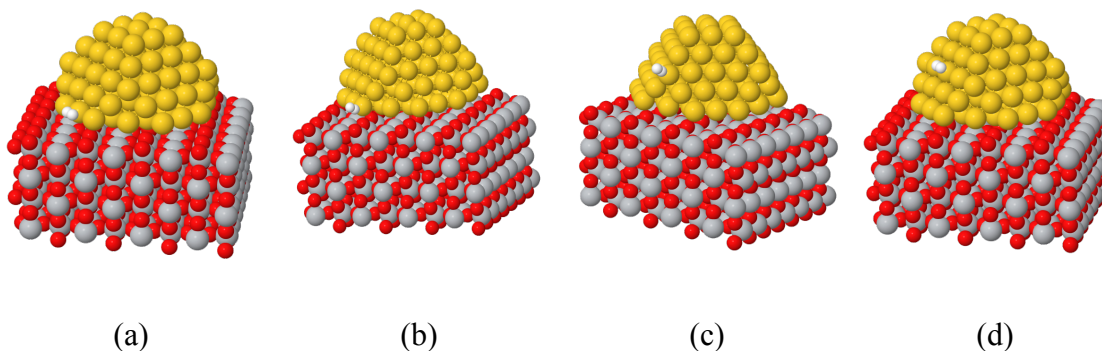
Fig. 4.6 Hydrogen molecule adsorption configuration on the 119 atom particle (a) adsorption at an edge interface site (b) adsorption at a corner interface site, (c) adsorption at a corner site, (d) adsorption on gold surface.
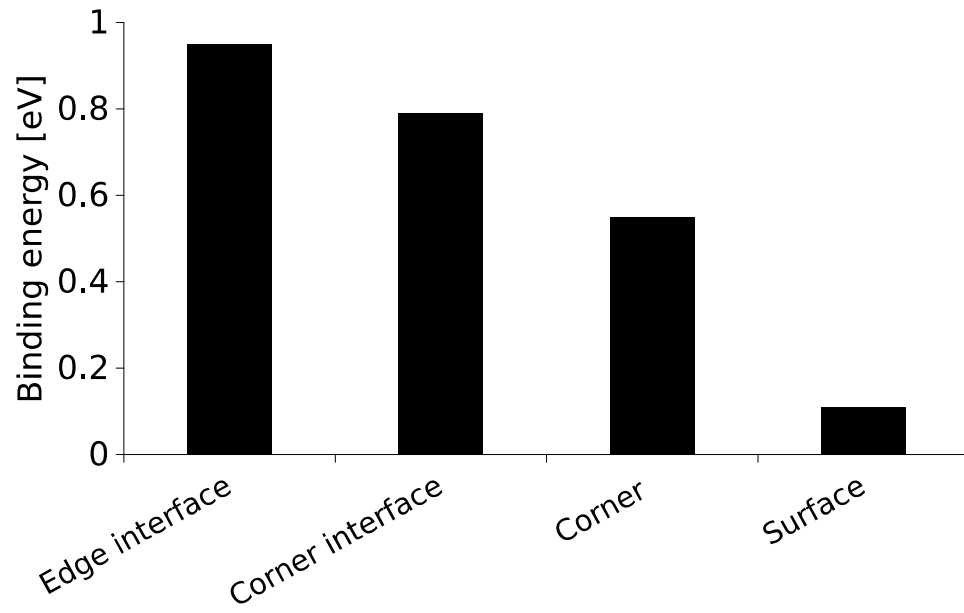
Fig. 4.7 Binding energy of hydrogen molecule at four different sites of the 119 atoms gold nanoparticle.
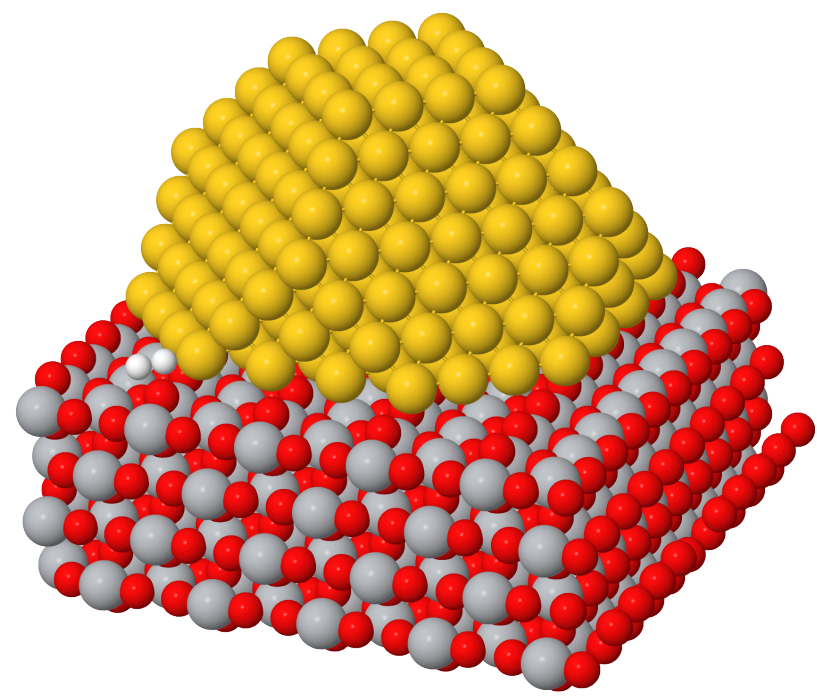
Fig. 4.8 Hydrogen atom adsorption configuration on 311 Au atom nanoparticle over rutile TiO$_2$ (110) surface system. Shown is a corner interface site.

Figure 4.9 shows a comparison of the different adsorption energies over the various Au particles. The adsorption energies at the same site over different particles are nearly the same. E.g. corner interface adsorption energies are nearly the same over all Au particles. We conclude that the size of the Au nanoparticle does not have a noticeable effect in the stability of absorbates. However, the choice of adsorption site within the Au nanoparticle does affect the stability of the absorbate. The difference between different particles can be attributed largely to the density of active sites. The smaller particles have a higher concentration of active corner sites, which leads to their greater activity per particle mass. These results suggest that the catalytic activity of the Au/TiO$_2$ system is determined largely by the density of special sites.
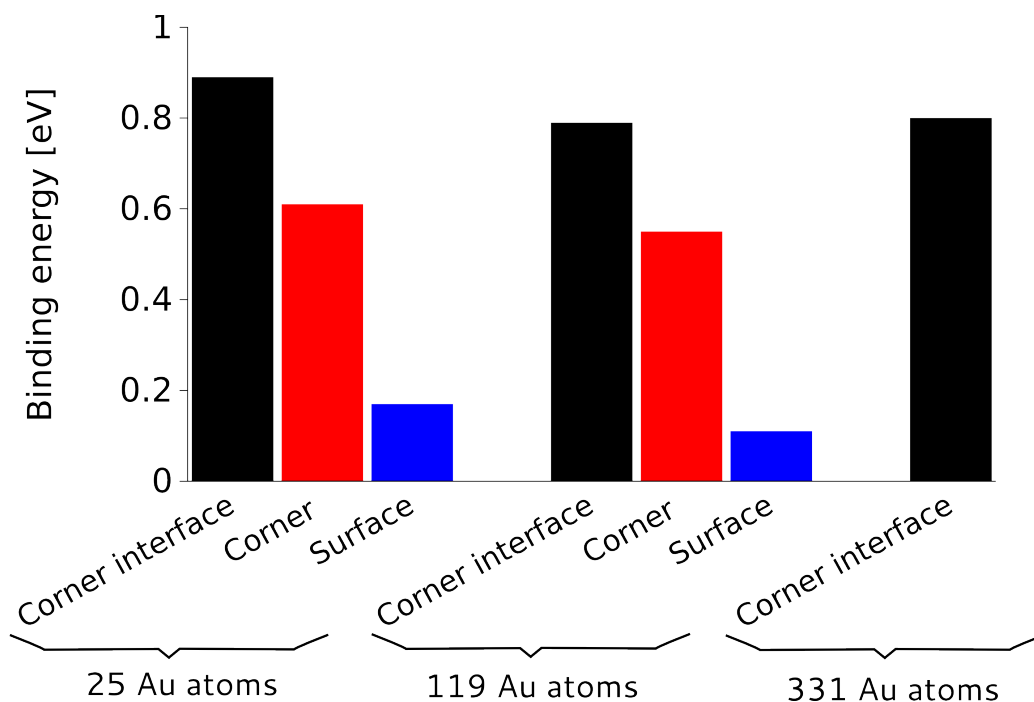
Fig. 4.9 Binding energies of a hydrogen molecule in three different sites of the various gold nanoparticle.

4.3.3 Adsorption of CO oxidation reaction intermediates

The adsorption energies of CO on four different sites on the 119 atom nanoparticle are shown in Fig. 4.10. We limit the analysis to this system because it is computationally tractable and it has a realistic size. The most stable configurations are the edge and corner interface perimeter sites just like the H_2 adsorption configuration. It is noteworthy that the CO molecule is more stable than H_2 in the surface of the gold particle.
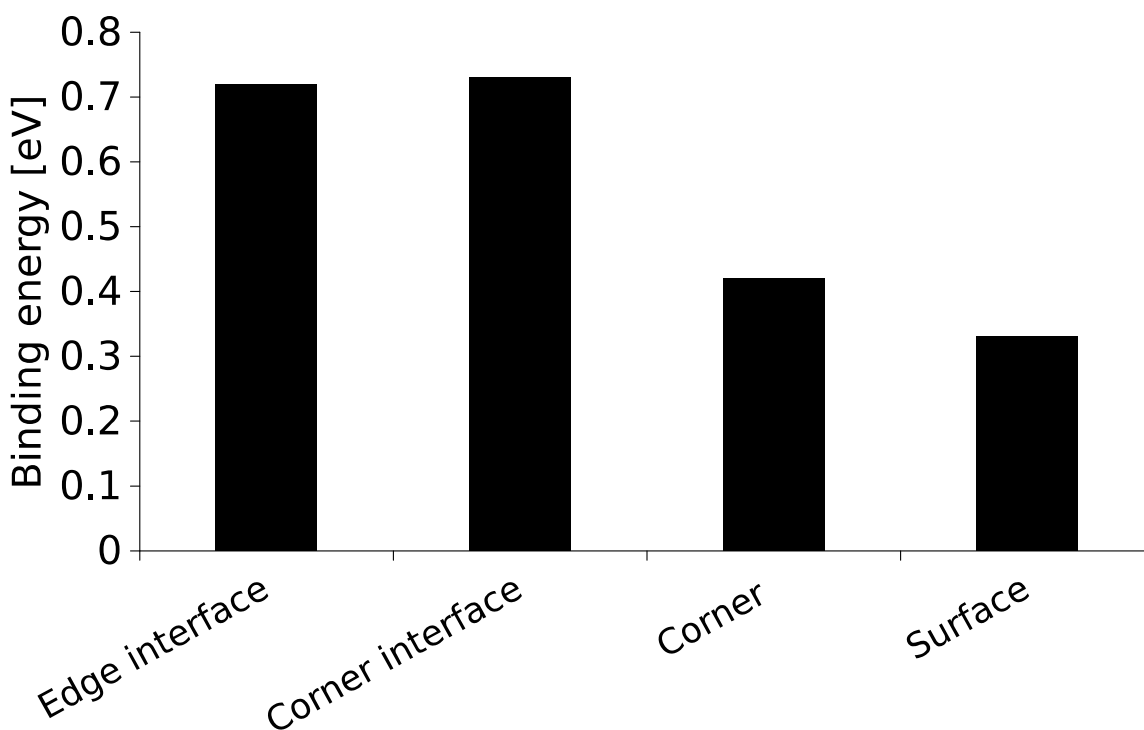
Fig. 4.10 Binding energy of CO molecule in three different sizes of the 119 atoms gold nanoparticle.

In order to show a possible application of our model we analyze the energetics of the CO oxidation reaction. The CO oxidation is assumed to take place via the following reaction steps: [180,185]

R1:	$CO + * \leftrightarrow CO*$
R2:	$O_2 + * \leftrightarrow O_2*$
R3:	$O_2* + * \leftrightarrow 2O*$
R4:	$CO* + O* \leftrightarrow CO_2 + 2*$
R5:	$CO* + O2* \leftrightarrow CO2 + O* + *$
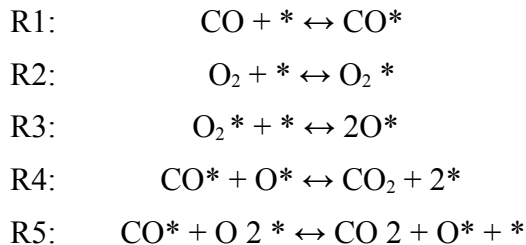
The reaction mechanism presents two possible routes for formation of CO_2. In the first route the oxidation of CO happens after O_2 is dissociated, whereas the second route to CO oxidation takes place via associative oxidation by O_2. Fig. 4.11 shows the potential energy surface for the two routes on a 119 atom cluster. The dissociated state of oxygen in the system is more stable. Then, is more likely to occur in the perimeter. CO was adsorbed in the corner sites and oxygen in the periphery of the nanoparticle. This results show that the reaction energies are all exothermic for CO oxidation, indicating that these special interface sites are indeed very active for catalysis.

We used the CO oxidation reaction as an example of the possible application of our model. We did not find significant differences in the adsorption energies of the intermediates of the CO oxidation with different Au nanoparticles. This support our main point on the independence of reactivity and particle size. The geometry of the 119 atom particle was a realistic model choice because the edge atoms are likely sites in the reactivity. Our results suggest that the reaction is viable at this special sites.

102
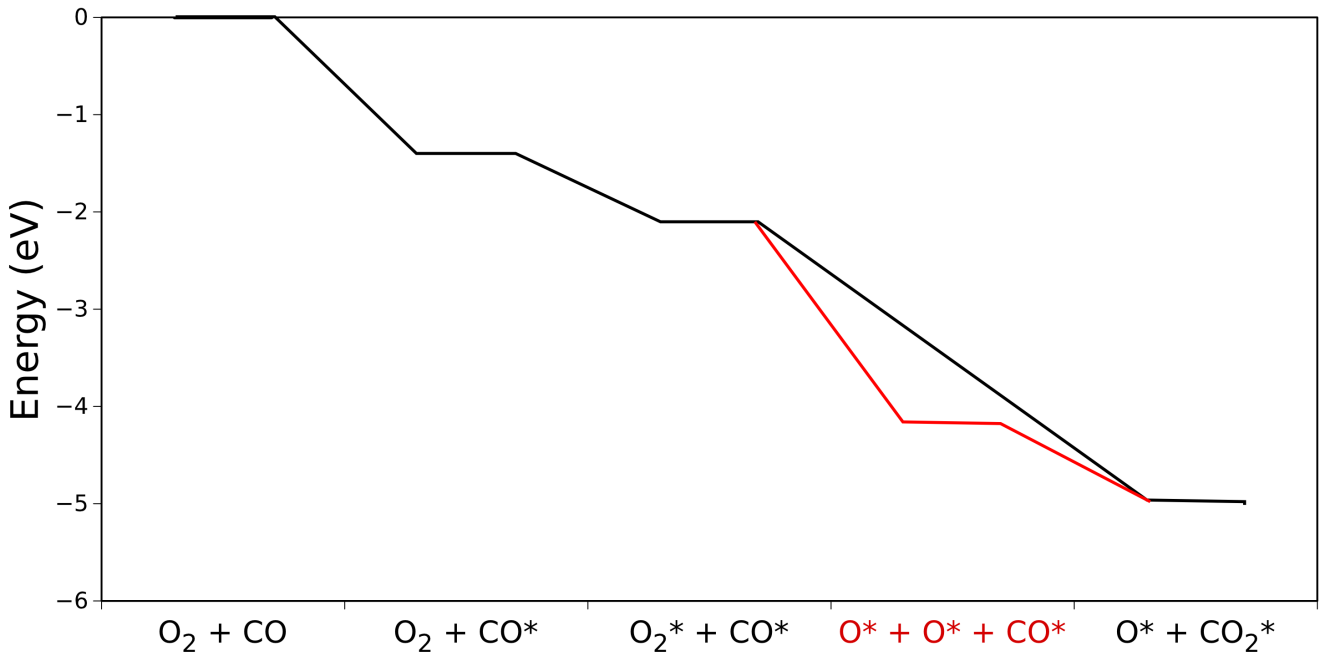
Fig.4.11 Potential reaction energy for CO oxidation on a 119 atoms Au cluster dispersed on TiO_2.

4.4 Conclusions

We have studied the adsorption of small molecules over different Au nanoparticles. We can conclude that the corner sites of supported Au nanoparticles lead to the most stable configuration of adsorption for small molecules. Thus, the reactivity of the whole system depends mostly in the number of those corner sites per unit area of catalyst. The corner sites at the interface between the support and the Au nanoparticle produce the strongest binding energies. The edges sites in the periphery of the Au clusters also were found to strongly bind the molecules. However, further research is required to assess the reactivity of this sites over a variety of reactions. We showed for a sample reaction, CO oxidation, that these non-terrace sites are very reactive.

We analyzed the influence of the size of the particle on the activity of the adsorption sites. We did not find a significant difference in the binding energy of the molecules on the same adsorption sites for nanoparticles of different sizes. Thus, we expect reaction sites on different particles to behave similarly, but that the density of active sites on smaller nanoparticles is higher. This explains the increased reactivity of systems with smaller Au nanoparticles.

Acknowledgments

Chapter 5: Conclusions

In this work we used molecular modeling (density functional theory) to study several key features of TiO_2 catalysts. First, we have examined the details of the localization and transfer of charge in several TiO_2 configurations. We have presented evidence that suggests ionosorption should occur over group IV metal oxides with electron-donating defects. Increased binding of absorbates is observed when the surface is reduced and unpaired electrons are present in the surface slab. These electrons transfer to absorbates forming an anion that may favorably interact with surface metal cations.

We have found that the charge transfer process from the surface to the surface depends on the difference of the electro-negativity of the surface and the adsorbate. We also found a correlation between the work function of the metal oxide, and the ionic adsorption of the oxygen molecule; surfaces with smaller work function values have larger adsorption energies for O_2. The ionic character of a surface, as measured by vacancy formation energy, also correlates well with the O_2 adsorption energy. Thus, if the work function or vacancy formation energy of a metal oxide surface is known, it may be possible to predict when electron transfer occurs and to what degree during adsorption.

We have simulated the interface between the anatase and rutile phases of TiO_2 using DFT+U in order to better characterize the nature of mixed-phase TiO_2 photocatalysts. We modeled realistic structures that contained thousands of atoms, rather than smaller, possibly irrelevant interfaces. Our results show the preferred direction of electron/hole flow (electrons to anatase, holes to rutile). Such preferred migration could

lower the electron/hole recombination rate, which would increase photo-reactivity. We also probed the electronic structure of our heterostructure and found a gap state caused by electrons localized in undercoordinated Ti atoms which were present within the interfacial region. Interfaces between bulk materials and between exposed surfaces both showed electron trapping at undercoordinated sites. These undercoordinated (typically four) atoms present localized electrons that could enable reduction reactions in the interfacial region, and could explain the increased reactivity of mixed-phase TiO_2 photocatalyst materials. Such sites have been experimentally predicted, but theoretical work now confirms their existence. We cannot exclude the possibility that defects (such as O vacancies or Ti interstitials) may affect the electronic properties of mixed-phase interfaces, and future work may examine interfaces with such structures.

We examined the reactivity of gold nanoparticles dispersed on TiO_2 surfaces. Our results show that different possible adsorption sites have different stabilities, but that according to our calculations the presence of low-coordinated Au sites seem to be crucial for the adsorption process. Low-coordinated corner Au sites are most active for binding adsorbates. This is in agreement with previous experimental results. We found that the binding energies of small molecules to the gold nanoparticles do not change significantly with the size of the nanoparticle. That is, adsorption energies at corner sites (or corner interface sites) are all nearly the same on all three Au nanoparticles. The effect of changing Au particle size thus appears to be changing the number and density of reactive corner (or corner-interface) sites. Larger particles will have less active sites per mass of particle, and thus will appear less reactive when normalized by amount of catalyst. We

expect that these insights will be of great help in understanding the catalytic activity of gold dispersed over titania.

To summarize we have studied the role of metal oxides during catalytic and photocatalytic processes. We have detailed three particular systems, namely, the anatase surface of TiO_2 and other group IV metal oxides, mixed phase TiO_2 surfaces, and gold decorated rutile TiO_2 surfaces. The electronic nature of TiO_2 plays a key role in all the processes examined. TiO_2 is an active photocatalyst and catalyst support.

My work may lead to several new avenues of research. The concept of ionosorption could be explored on other metal oxides to address how general this process is and what may be further governing principles. We recommend to continue investigating on the influence of the work function and the energy of formation of an oxygen vacancy of a material on the ionic adsorption process.

To gain further understanding of metal oxides as catalysts we recommend that future work investigate the stability of relevant intermediates for reactions in the interfacial region of mixed phase catalyst. The calculation of the work function for each phase could determine the potential activity of different parts of the mixed surface.

Finally, the challenging task in the development of supported gold nanoparticle catalysts is to understand how to stabilize undercoordinated Au sites. Future work may examine other particle shapes and address size effects, as well as the effect of different metal oxide supports. Further research is also needed to stablish the influence of the oxygen vacancies and other defects on the activity of the Au nanoparticles.

107

References

(1) Diebold, U.; Li, S. C.; Schmid, M. Oxide Surface Science. *Annu. Rev. Phys. Chem.* **2010**, *61*, 129–148.

(2) Hoffmann, M. R.; Martin, S. T.; Choi, W.; Bahnemann, D. W. Environmental Applications of Semiconductor Photocatalysis. *Chem. Rev.* **1995**, *95*, 69–96.

(3) Fujishima, A.; Zhang, X.; Tryk, D. A. TiO_2 Photocatalysis and Related Surface Phenomena. *Surf. Sci. Rep.* **2008**, *63*, 515–582.

(4) Boudart, M. From the Century of the Rate Equation to the Century of the Rate Constants: A Revolution in Catalytic Kinetics and Assisted Catalyst Design. *Catal. Letters* **2000**, *65*, 1–3.

(5) Carter, E. A. Challenges in Modeling Materials Properties Without Experimental Input. *Science (80-.).* **2008**, *321*, 800–803.

(6) Bell, A. T. The Impact of Nanoscience on Heterogeneous Catalysis. *Science (80-.).* **2003**, *299*, pp. 1688–1691.

(7) Lira, E.; Wendt, S.; Huo, P.; Hansen, J. Ø.; Streber, R.; Porsgaard, S.; Wei, Y.; Bechstein, R.; Lægsgaard, E.; Besenbacher, F. The Importance of Bulk Ti^{3+} Defects in the Oxygen Chemistry on Titania Surfaces. *J. Am. Chem. Soc.* **2011**, *133*, 6529–6532.

(8) Deskins, N. A.; Rousseau, R.; Dupuis, M. Distribution of Ti3+ Surface Sites in Reduced TiO_2. *J. Phys. Chem. C* **2011**, *115*, 7562–7572.

(9) Wendt, S.; Sprunger, P. T.; Lira, E.; Madsen, G. K. H.; Li, Z.; Hansen, J. Ø.; Matthiesen, J.; Blekinge-Rasmussen, A.; Lægsgaard, E.; Hammer, B. The Role of Interstitial Sites in the Ti3d Defect State in the Band Gap of Titania. *Science (80-.).* **2008**, *320*, 1755.

(10) Martinez, U.; Hammer, B. Adsorption Properties versus Oxidation States of Rutile TiO_2 (110). *J. Chem. Phys.* **2011**, *134*, 194703.

(11) Madsen, G. K. H.; Hammer, B. Effect of Subsurface Ti-Interstitials on the Bonding of Small Gold Clusters on Rutile TiO_2(110). *J. Chem. Phys.* **2009**, *130*, 044704.

(12) Chretien, S.; Metiu, H. Enhanced Adsorption Energy of Au_1 and O_2 on the Stoichiometric TiO_2(110) Surface by Coadsorption with Other Molecules. *J. Chem. Phys.* **2008**, *128*, 044714.

(13) Henrich, V. E.; Cox, P. A. *The Surface Science of Metal Oxides*; Cambridge University Press, 1994.

(14) Hofmann, P. *Solid State Physics: An Introduction*; Physics textbook; Wiley, 2008.

(15) Zhang, H.; Banfield, J. F. Understanding Polymorphic Phase Transformation Behavior during Growth of Nanocrystalline Aggregates: Insights from TiO_2. *J. Phys. Chem. B* **2000**, *104*, 3481–3487.

(16) Hanaor, D. H.; Sorrell, C. Review of the Anatase to Rutile Phase Transformation. *J. Mater. Sci.* **2011**, *46*, 855–874.

(17) Henderson, M. A. A Surface Science Perspective on Photocatalysis. *Surf. Sci. Rep.* **2011**, *66*, 185–297.

(18) Ramamoorthy, M.; Vanderbilt, D.; King-Smith, R. D. First-Principles Calculations of the Energetics of Stoichiometric TiO_2 Surfaces. *Phys. Rev. B* **1994**, *49*, 16721–16727.

(19) Diebold, U. The Surface Science of Titanium Dioxide. *Surf. Sci. Rep.* **2003**, *48*, 53–229.

(20) Munnix, S.; Schmeits, M. Electronic Structure of Ideal TiO_2 (110). *Phys. Rev. B* **1984**, *30*, 2202–2211.

(21) Mills, A.; Hunte, S. Le An Overview of Semiconductor Photocatalysis. *J. Photochem. Photobiol. A Chem.* **1997**, *108*, 1–35.

(22) Chi, L. P.; Lindsay, R.; Thornton, G. Chemical Reactions on Rutile $TiO_2(110)$. *Chem. Soc. Rev.* **2008**, *37*, 2328–2353.

(23) Dohnálek, Z.; Lyubinetsky, I.; Rousseau, R. Thermally-Driven Processes on Rutile TiO_2: A Direct View at the Atomic Scale. *Prog. Surf. Sci.* **2010**, *85*, 161–205.

(24) Zapol, P.; Curtiss, L. A. Organic Molecule Adsorption on TiO_2 Nanoparticles: A Review of Computational Studies of Surface Interactions. *J. Comput. Theor. Nanosci.* **2007**, *4*, 222–230.

(25) Sclafani, A.; Herrmann, J. M. Comparison of the Photoelectronic and Photocatalytic Activities of Various Anatase and Rutile Forms of Titania in Pure Liquid Organic Phases and in Aqueous Solutions. *J. Phys. Chem.* **1996**, *100*, 13655–13661.

(26) Vittadini, A.; Selloni, A.; Rotzinger, F. P.; Grätzel, M. Structure and Energetics of Water Adsorbed at TiO_2 Anatase (101) and (001) Surfaces. *Phys. Rev. Lett.* **1998**, *81*, 2954–2957.

(27) Vittadini, A.; Casarin, M.; Selloni, A. Chemistry of and on TiO_2-Anatase Surfaces by DFT Calculations: A Partial Review. *Theor. Chem. Acc.* **2007**, *117*, 663–671.

(28) Miller, K. L.; Musgrave, C. B.; Falconer, J. L.; Medlin, J. W. Effects of Water and Formic Acid Adsorption on the Electronic Structure of Anatase $TiO_2(101)$. *J. Phys.*

Chem. C **2011**, *115*, 2738–2749.

(29) Liu, L.-M.; Li, S.-C.; Cheng, H.; Diebold, U.; Selloni, A. Growth and Organization of an Organic Molecular Monolayer on TiO_2: Catechol on Anatase (101). *J. Am. Chem. Soc.* **2011**, *133*, 7816–7823.

(30) Gong, X.-Q.; Selloni, A.; Dulub, O.; Jacobson, P.; Diebold, U. Small Au and Pt Clusters at the Anatase TiO_2(101) Surface: Behavior at Terraces, Steps, and Surface Oxygen Vacancies. *J. Am. Chem. Soc.* **2007**, *130*, 370–381.

(31) Luo, X.; Demkov, A. A.; Triyoso, D.; Fejes, P.; Gregory, R.; Zollner, S. Combined Experimental and Theoretical Study of Thin Hafnia Films. *Phys. Rev. B.* **2008**, *78*, 245314.

(32) Fiorentini, V.; Gulleri, G. Theoretical Evaluation of Zirconia and Hafnia as Gate Oxides for Si Microelectronics. *Phys. Rev. Lett.* **2002**, *89*, 266101.

(33) Chen, R.; Kim, H.; McIntyre, P. C.; Bent, S. F. Self-Assembled Monolayer Resist for Atomic Layer Deposition of HfO_2 and ZrO_2 High-Kappa Gate Dielectrics. *Appl. Phys. Lett.* **2004**, *84*, 4017–4019.

(34) Stenzel, O.; Wilbrandt, S.; Schürmann, M.; Kaiser, N.; Ehlers, H.; Mende, M.; Ristau, D.; Bruns, S.; Vergöhl, M.; Stolze, M.; Held, M.; Niederwald, H.; Koch, T.; Riggers, W.; Burdack, P.; Mark, G.; Schäfer, R.; Mewes, S.; Bischoff, M.; Arntzen, M.; Eisenkrämer, F.; Lappschies, M.; Jakobs, S.; Koch, S.; Baumgarten, B.; Tünnermann, A. Mixed Oxide Coatings for Optics. *Appl. Opt.* **2011**, *50*, C69–C74.

(35) Giorgi, G.; Korkin, A.; Yamashita, K. Zirconium and Hafnium Oxide Interface with Silicon: Computational Study of Stress and Strain Effects. *Comput. Mater. Sci.* **2008**, *43*, 930–937.

(36) Peacock, P. W.; Robertson, J. Bonding, Energies, and Band Offsets of Si-ZrO_2 and HfO_2 Gate Oxide Interfaces. *Phys. Rev. Lett.* **2004**, *92*, 057601.

(37) Robertson, J. High Dielectric Constant Gate Oxides for Metal Oxide Si Transistors. *Rep. Prog. Phys.* **2006**, *69*, 327.

(38) Iskandarova, I. M.; Knizhnik, A. A.; Rykova, E. A.; Bagatur'yants, A. A.; Potapkin, B. V; Korkin, A. A. First-Principle Investigation of the Hydroxylation of Zirconia and Hafnia Surfaces. *Microelectron. Eng.* **2003**, *69*, 587–593.

(39) Syzgantseva, O.; Calatayud, M.; Minot, C. Hydrogen Adsorption on Monoclinic ($\bar{1}$11) and ($\bar{1}$01) ZrO_2 Surfaces: A Periodic Ab Initio Study. *J. Phys. Chem. C* **2010**, *114*, 11918–11923.

(40) Añez, R.; Sierraalta, A.; Martorell, G.; Sautet, P. Stabilization of the (110) Tetragonal Zirconia Surface by Hydroxyl Chemical Transformation. *Surf. Sci.* **2009**, *603*, 2526–2531.

(41) Hofmann, A.; Ganduglia-Pirovano, M. V.; Sauer, J. Vanadia and Water Coadsorption on Tetragonal Zirconia Surfaces. *J. Phys. Chem. C* **2009**, *113*, 18191–18203.

(42) Wang, C.-M.; Fan, K.-N.; Liu, Z.-P. Origin of Oxide Sensitivity in Gold-Based Catalysts: A First Principle Study of CO Oxidation over Au Supported on Monoclinic and Tetragonal ZrO2. *J. Am. Chem. Soc.* **2007**, *129*, 2642–2647.

(43) Haase, F.; Sauer, J. The Surface Structure of Sulfated Zirconia: Periodic Ab Initio Study of Sulfuric Acid Adsorbed on ZrO_2(101) and ZrO_2(001). *J. Am. Chem. Soc.* **1998**, *120*, 13503–13512.

(44) Foster, A. S.; Sulimov, V. B.; Lopez Gejo, F.; Shluger, A. L.; Nieminen, R. M. Structure and Electrical Levels of Point Defects in Monoclinic Zirconia. *Phys. Rev. B.* **2001**, *64*, 224108.

(45) Zheng, J. X.; Ceder, G.; Maxisch, T.; Chim, W. K.; Choi, W. K. First-Principles Study of Native Point Defects in Hafnia and Zirconia. *Phys. Rev. B.* **2007**, *75*, 104112.

(46) Pietrucci, F.; Bernasconi, M.; Laio, A.; Parrinello, M. Vacancy-Vacancy Interaction and Oxygen Diffusion in Stabilized Cubic ZrO_2 from First Principles. *Phys. Rev. B.* **2008**, *78*, 094301.

(47) Cramer, C. *Essentials of Computational Chemistry: Theories and Models*; Jhon Wiley and sons, USA, 2004.

(48) Szabo, A.; Ostlund, N. *Modern Quantum Chemistry: Introduction to Advanced Electronic Structure Theory*; Dover Publications, USA, 1996.

(49) Levine, I. N. *Quantum Chemistry*; Pearson Prentice Hall, 2009.

(50) Sakurai, J. J. *Advanced Quantum Mechanics*; Pearson Education, Incorporated, 2006.

(51) Hohenberg, P.; Kohn, W. Inhomogeneous Electron Gas. *Phys. Rev.* **1964**, *136*, B864–B871.

(52) Kohn, W.; Sham, L. J. Self-Consistent Equations Including Exchange and Correlation Effects. *Phys. Rev.* **1965**, *140*, A1133–A1138.

(53) Sholl, D.; Steckel, J. A. *Density Functional Theory: A Practical Introduction*; Wiley, 2009.

(54) Kurth, S.; Perdew, J. P. Role of the Exchange–correlation Energy: Nature's Glue. *Int. J. Quantum Chem.* **2000**, *77*, 814–818.

(55) Ohno, T.; Sarukawa, K.; Tokieda, K.; Matsumura, M. Morphology of a TiO_2 Photocatalyst (Degussa, P-25) Consisting of Anatase and Rutile Crystalline Phases. *J.Catal.* **2001**, *203*, 82–86.

(56) Yan, M.; Chen, F.; Zhang, J.; Anpo, M. Preparation of Controllable Crystalline

Titania and Study on the Photocatalytic Properties. *J. Phys. Chem. B.* **2005**, *109*, 8673–8678.

(57) Hurum, D.; Agrios, A.; Gray, K.; Rajh, T.; Thurnauer, M. Explaining the Enhanced Photocatalytic Activity of Degussa P25 Mixed-Phase TiO_2 Using EPR. *J. Phys. Chem. B.* **2003**, *107*, 4545–4549.

(58) Kang, J.; Wu, F.; Li, S.-S.; Xia, J.-B.; Li, J. Calculating Band Alignment between Materials with Different Structures: The Case of Anatase and Rutile Titanium Dioxide. *J. Phys. Chem. C.* **2012**, *116*, 20765–20768.

(59) Li, G.; Ciston, S.; Saponjic, Z.; Chen, L.; Dimitrijevic, N.; Rajh, T.; Gray, K. Synthesizing Mixed-Phase TiO2 Nanocomposites Using a Hydrothermal Method for Photo-Oxidation and Photoreduction Applications. *J. Catal.* **2008**, *253*, 105–110.

(60) Shi, L.; Weng, D. Highly Active Mixed-Phase TiO_2 Photocatalysts Fabricated at Low Temperature and the Correlation between Phase Compositionand Photocatalytic Activity. *J. Env. Sci.* **2008**, *20*, 1263–1267.

(61) Connelly, K.; Wahab, A.; Idriss, H. Photoreaction of Au/TiO2 for Hydrogen Production from Renewables: A Review on the Synergistic Effect between Anatase and Rutile Phases of TiO2. *Mater. Renew. Sustain. Energy* **2012**, *1*, 3.

(62) Zhang, J.; Xu, Q.; Feng, Z.; Li, M.; Li, C. Importance of the Relationship between Surface Phases and Photocatalytic Activity of TiO2. *Angew. Chemie Int. Ed.* **2008**, *47*, 1766–1769.

(63) Kawahara, T.; Konishi, Y.; Tada, H.; Tohge, N.; Nishii, J.; Ito, S. A Patterned TiO_2(Anatase)/TiO_2(Rutile) Bilayer-Type Photocatalyst: Effect of the Anatase/Rutile Junction on the Photocatalytic Activity. *Angew. Chem.* **2002**, *114*, 2935–2937.

(64) Li, G.; Gray, K. A. The Solid–solid Interface: Explaining the High and Unique Photocatalytic Reactivity of TiO2-Based Nanocomposite Materials. *Chem. Phys.* **2007**, *339*, 173–187.

(65) Hurum, D. C.; Agrios, A. G.; Crist, S. E.; Gray, K. A.; Rajh, T.; Thurnauer, M. C. Probing Reaction Mechanisms in Mixed Phase TiO_2 by EPR. *J. Electron Spectrosc. Relat. Phenom.* **2006**, *150*, 155–163.

(66) Kavan, L.; Grätzel, M.; Gilbert, S. E.; Klemenz, C.; Scheel, H. J. Electrochemical and Photoelectrochemical Investigation of Single-Crystal Anatase. *J. Am. Chem. Soc.* **1996**, *118*, 6716–6723.

(67) Kho, Y. K.; Iwase, A.; Teoh, W. Y.; Madler, L.; Kudo, A.; Amal, R. Photocatalytic H_2 Evolution over TiO_2 Nanoparticles. The Synergistic Effect of Anatase and Rutile. *J. Phys. Chem. C* **2010**, *114*, 2821–2829.

(68) Komaguchi, K.; Nakano, H.; Araki, A.; Harima, Y. Photoinduced Electron Transfer from Anatase to Rutile in Partially Reduced TiO_2 (P-25) Nanoparticles: An ESR Study. *Chem. Phys. Lett.* **2006**, *428*, 338–342.

(69) Leytner, S.; Hupp, J. T. Evaluation of the Energetics of Electron Trap States at the Nanocrystalline Titanium Dioxide/aqueous Solution Interface via Time-Resolved Photoacoustic Spectroscopy. *Chem. Phys. Lett.* **2000**, *330*, 231–236.

(70) Tersoff, J. Theory of Semiconductor Heterojunctions: The Role of Quantum Dipoles. *Phy. Rev. B.* **1984**, *30*, 4874–4877.

(71) Fall, C. J.; Binggeli, N.; Baldereschi, A. Deriving Accurate Work Functions from Thin-Slab Calculations. *J. Phys. Condens. Matter.* **1999**, *11*, 2689.

(72) Baldereschi, A.; Baroni, S.; Resta, R. Band Offsets in Lattice-Matched Heterojunctions: A Model and First-Principles Calculations for GaAs/AlAs. *Phys. Rev. Lett.* **1988**, *61*, 734–737.

(73) Colombo, L.; Resta, R.; Baroni, S. Valence-Band Offsets at Strained Si/Ge Interfaces. *Phys. Rev. B.* **1991**, *44*, 5572–5579.

(74) Rantala, H.-P. K. and E. A. and E. L. and T. T. Band Offset Determination of the GaAs/GaAsN Interface Using the Density Functional Theory Method. *J. Phys. Condens. Matter.* **2008**, *20*, 315004.

(75) De, P.; Deak, P.; Aradi, B.; Frauenheim, T. Band Lineup and Charge Carrier Separation in Mixed Rutile-Anatase Systems. *J. Phys. Chem. C* **2011**, *115*, 3443–3446.

(76) Li, G.; Dimitrijevic, N. M.; Chen, L.; Nichols, J. M.; Rajh, T.; Gray, K. a The Important Role of Tetrahedral Ti^{4+} Sites in the Phase Transformation and Photocatalytic Activity of TiO_2 Nanocomposites. *J. Am. Chem. Soc.* **2008**, *130*, 5402–5403.

(77) Agrios, A. G.; Gray, K. A.; Weitz, E. Photocatalytic Transformation of 2,4,5-Trichlorophenol on TiO_2 under Sub-Band-Gap Illumination. *Langmuir* **2003**, *19*, 1402–1409.

(78) Farnesi Camellone, M.; Kowalski, P. M.; Marx, D. Ideal, Defective, and Gold-Promoted Rutile TiO_2(110) Surfaces Interacting with CO, H_2, and H_2O: Structures, Energies, Thermodynamics, and Dynamics from PBE+U. *Phys. Rev. B* **2011**, *84*, 1–18.

(79) Haruta, M. Size- and Support-Dependency in the Catalysis of Gold. *Catal. Today* **1997**, *36*, 153–166.

(80) Okumura, M.; Nakamura, S.; Tsubota, S.; Nakamura, T.; Azuma, M.; Haruta, M. Chemical Vapor Deposition of Gold on Al_2O_3, SiO_2, and TiO_2 for the Oxidation of

CO and of H_2. *Catal. Letters* **1998**, *51*, 53–58.

(81) Deskins, N. A.; Rousseau, R.; Dupuis, M. Defining the Role of Excess Electrons in the Surface Chemistry of TiO_2. *J. Phys. Chem. C* **2010**, *114*, 5891–5897.

(82) Henderson, M. A.; Epling, W. S.; Peden, C. H. F.; Perkins, C. L. Insights into Photoexcited Electron Scavenging Processes on TiO_2 Obtained from Studies of the Reaction of O_2 with OH Groups Adsorbed at Electronic Defects on TiO_2(110). *J. Phys. Chem. B* **2002**, *107*, 534–545.

(83) Petrik, N. G.; Kimmel, G. A. Photoinduced Dissociation of O_2 on Rutile TiO_2(110). *J. Phys. Chem. Lett.* **2010**, *1*, 1758–1762.

(84) Barsan, N.; Schweizer-Berberich, M.; Göpel, W. Fundamental and Practical Aspects in the Design of Nanoscaled SnO_2 Gas Sensors: A Status Report. *Fresenius' J. Anal. Chem.* **1999**, *365*, 287–304.

(85) Wang, C.; Yin, L.; Zhang, L.; Xiang, D.; Gao, R. Metal Oxide Gas Sensors: Sensitivity and Influencing Factors. *Sensors* **2010**, *10*, 2088–2106.

(86) Gurlo, A. Interplay between O_2 and SnO_2: Oxygen Ionosorption and Spectroscopic Evidence for Adsorbed Oxygen. *ChemPhysChem* **2006**, *7*, 2041–2052.

(87) Nanto, H.; Minami, T.; Takata, S. Zinc-Oxide Thin-Film Ammonia Gas Sensors with High Sensitivity and Excellent Selectivity. *J. Appl. Phys.* **1986**, *60*, 482–484.

(88) Ahn, M.-W.; Park, K.-S.; Heo, J.-H.; Park, J.-G.; Kim, D.-W.; Choi, K. J.; Lee, J.-H.; Hong, S.-H. Gas Sensing Properties of Defect-Controlled ZnO-Nanowire Gas Sensor. *Appl. Phys. Lett.* **2008**, *93*, 263103.

(89) Tao, Y.; Cao, X.; Peng, Y.; Liu, Y. A Novel Cataluminescence Gas Sensor Based on MgO Thin Film. *Sens. Actuators, B* **2010**, *148*, 292–297.

(90) Pacchioni, G. Modeling Doped and Defective Oxides in Catalysis with Density Functional Theory Methods: Room for Improvements. *J. Chem. Phys.* **2008**, *128*, 182505.

(91) Ganduglia-Pirovano, M. V.; Hofmann, A.; Sauer, J. Oxygen Vacancies in Transition Metal and Rare Earth Oxides: Current State of Understanding and Remaining Challenges. *Surf. Sci. Rep.* **2007**, *62*, 219–270.

(92) Linsebigler, A.; Lu, G.; Yates, J. Photocatalysis on TiO_2 Surfaces: Principles, Mechanisms, and Selected Results. *Chem. Rev.* **1995**, *95*, 735–758.

(93) Lu, G.; Linsebigler, A.; Yates, J. J. T. The Adsorption and Photodesorption of Oxygen on the TiO_2(110) Surface. *J. Chem. Phys.* **1995**, *102*, 4657–4662.

(94) VandeVondele, J.; Krack, M.; Mohamed, F.; Parrinello, M.; Chassaing, T.; Hutter, J.

Quickstep: Fast and Accurate Density Functional Calculations Using a Mixed Gaussian and Plane Waves Approach. *Comput. Phys. Commun.* **2005**, *167*, 103–128.

(95) Lippert, G.; Hutter, J.; Parrinello, M. The Gaussian and Augmented-Plane-Wave Density Functional Method for Ab Initio Molecular Dynamics Simulations. *Theor. Chem. Acc. 103*, 124–140.

(96) VandeVondele, J.; Hutter, J. Gaussian Basis Sets for Accurate Calculations on Molecular Systems in Gas and Condensed Phases. *J. Chem. Phys.* **2007**, *127*, 114105.

(97) Goedecker, S.; Teter, M.; Hutter, J. Separable Dual-Space Gaussian Pseudopotentials. *Phys. Rev. B.* **1996**, *54*, 1703–1710.

(98) Hartwigsen, C.; Goedecker, S.; Hutter, J. Relativistic Separable Dual-Space Gaussian Pseudopotentials from H to Rn. *Phys. Rev. B.* **1998**, *58*, 3641–3662.

(99) Krack, M. Pseudopotentials for H to Kr Optimized for Gradient-Corrected Exchange-Correlation Functionals. *Theor. Chem. Acc.* **2005**, *114*, 145–152.

(100) Perdew, J. P.; Burke, K.; Ernzerhof, M. Generalized Gradient Approximation Made Simple [Phys. Rev. Lett. 77, 3865 (1996)]. *Phys. Rev. Lett.* **1997**, *78*, 1396–1396.

(101) Horn, M.; Schwerdtfeger, C.; Meaghe, E. No Title. *Z. Krist. 136*, 9.

(102) Teufer, G. The Crystal Structure of Tetragonal ZrO_2. *Acta Crystallogr.* **1962**, *15*, 1187.

(103) Adams, D. M.; Leonard, S.; Russell, D. R.; Cernik, R. J. X-Ray Diffraction Study of Hafnia under High Pressure Using Synchrotron Radiation. *J. Phys. Chem. Solids* **1991**, *52*, 1181–1186.

(104) Bader, R. *Atoms in Molecules: A Quantum Theory (International Series of Monographs on Chemistry)*; Oxford University Press, USA, 1994.

(105) Tang, W.; Sanville, E.; Henkelman, G. A Grid-Based Bader Analysis Algorithm without Lattice Bias. *J. Phys. Condens. Matter* **2009**, *21*, 084204.

(106) Sanville, E.; Kenny, S. D.; Smith, R.; Henkelman, G. Improved Grid-Based Algorithm for Bader Charge Allocation. *J. Comput. Chem.* **2007**, *28*, 899–908.

(107) Henkelman, G.; Arnaldsson, A.; Jónsson, H. A Fast and Robust Algorithm for Bader Decomposition of Charge Density. *Comput. Mater. Sci.* **2006**, *36*, 354–360.

(108) Cheng, H.; Selloni, A. Surface and Subsurface Oxygen Vacancies in Anatase TiO_2 and Differences with Rutile. *Phys. Rev. B.* **2009**, *79*, 092101.

(109) Safonov, A. A.; Bagatur'yants, A. A.; Korkin, A. A. Oxygen Vacancies in Tetragonal ZrO_2: Ab Initio Embedded Cluster Calculations. *Microelectron. Eng.* **2003**, *69*, 629–632.

(110) Zeng, W.; Liu, T.; Wang, Z.; Tsukimoto, S.; Saito, M.; Ikuhara, Y. Oxygen Adsorption on Anatase TiO2 (101) and (001) Surfaces from First Principles. *Mater. Trans.* **2010**, *51*, 171–175.

(111) Aschauer, U.; Chen, J.; Selloni, A. Peroxide and Superoxide States of Adsorbed O_2 on Anatase TiO_2 (101) with Subsurface Defects. *Phys. Chem. Chem. Phys.* **2010**, *12*, 12956–60.

(112) Lide, D. *CRC Handbook of Chemistry and Physics*; CRC Press: Maryland, USA ET - 85.

(113) Mattioli, G.; Filippone, F.; Amore Bonapasta, A. Reaction Intermediates in the Photoreduction of Oxygen Molecules at the (101) TiO_2 (Anatase) Surface. *J. Am. Chem. Soc.* **2006**, *128*, 13772–13780.

(114) Berger, T.; Sterrer, M.; Diwald, O.; Knözinger, E.; Panayotov, D.; Thompson, T. L.; Yates, J. T. Light-Induced Charge Separation in Anatase TiO_2 Particles. *J. Phys. Chem. B* **2005**, *109*, 6061–6068.

(115) Zhou, S.; Čižmár, E.; Potzger, K.; Krause, M.; Talut, G.; Helm, M.; Fassbender, J.; Zvyagin, S. A.; Wosnitza, J.; Schmidt, H. Origin of Magnetic Moments in Defective TiO_2 Single Crystals. *Phys. Rev. B.* **2009**, *79*, 113201.

(116) Pearson, R. G. Absolute Electronegativity and Hardness: Application to Inorganic Chemistry. *Inorg. Chem.* **1988**, *27*, 734–740.

(117) Li, W.; Liu, C.; Zhou, Y.; Bai, Y.; Feng, X.; Yang, Z.; Lu, L.; Lu, X.; Chan, K. Enhanced Photocatalytic Activity in Anatase/TiO_2(B) Core−Shell Nanofiber. *J. Phys. Chem. C.* **2008**, *112*, 20539–20545.

(118) Li, G.; Dimitrijevic, N.; Chen, L.; Nichols, J.; Rajh, T.; Gray, K. The Important Role of Tetrahedral Ti^{4+} Sites in the Phase Transformation and Photocatalytic Activity of TiO_2 Nanocomposites. *J. Am. Chem. Soc.* **2008**, *130*, 5402–3.

(119) Yin, W.-J.; Tang, H.; Wei, S.-H.; Al-Jassim, M. M.; Turner, J.; Yan, Y. Band Structure Engineering of Semiconductors for Enhanced Photoelectrochemical Water Splitting: The Case of TiO_2. *Phys. Rev. B.* **2010**, *82*, 45106.

(120) Ni, M.; Leung, M. K. H.; Leung, D. Y. C.; Sumathy, K. A Review and Recent Developments in Photocatalytic Water-Splitting Using for Hydrogen Production. *Renew. Sustain. Energy Rev.* **2007**, *11*, 401–425.

(121) Choi, W.; Termin, A.; Hoffmann, M. R. The Role of Metal Ion Dopants in Quantum-Sized TiO_2: Correlation between Photoreactivity and Charge Carrier Recombination Dynamics. *J. Phys. Chem.* **1994**, *98*, 13669–13679.

(122) Henderson, M. A Surface Science Perspective on TiO_2 Photocatalysis. *Surf. Sci*

Rep. **2011**, *66*, 185–297.

(123) Li, G.; Chen, L.; Graham, M. E.; Gray, K. A. A Comparison of Mixed Phase Titania Photocatalysts Prepared by Physical and Chemical Methods: The Importance of the Solid–solid Interface. *J. Mol. Catal. A Chem.* **2007**, *275*, 30–35.

(124) Deák, P.; Aradi, B.; Frauenheim, T. Band Lineup and Charge Carrier Separation in Mixed Rutile-Anatase Systems. *J. Phys. Chem. C* **2011**, *115*, 3443–3446.

(125) Scanlon, D. O.; Dunnill, C. W.; Buckeridge, J.; Shevlin, S. A.; Logsdail, A. J.; Woodley, S. M.; Catlow, C. R. A.; Powell, M. J.; Palgrave, R. G.; Parkin, I. P.; Watson, G. W.; Keal, T. W.; Sherwood, P.; Walsh, A.; Sokol, A. A. Band Alignment of Rutile and Anatase TiO$_2$. *Nat Mater* **2013**, *advance on*.

(126) Pfeifer, V.; Erhart, P.; Li, S.; Rachut, K.; Morasch, J.; Brötz, J.; Reckers, P.; Mayer, T.; Rühle, S.; Zaban, A.; Mora Seró, I.; Bisquert, J.; Jaegermann, W.; Klein, A. Energy Band Alignment between Anatase and Rutile TiO$_2$. *J. Phys. Chem. Lett.* **2013**, *4*, 4182–4187.

(127) Hoffling, B.; Schleife, A.; Fuchs, F.; Rodl, C.; Bechstedt, F. Band Lineup between Silicon and Transparent Conducting Oxides. *Appl. Phys. Lett.* **2010**, *97*, 32113–32116.

(128) Sayle, T.; Catlow, C.; Sayle, D.; Parker, S.; Harding, J. Computer Simulation of Thin Film Heteroepitaxial Ceramic Interfaces Using a near-Coincidence-Site Lattice Theory. *Philos. Mag. A.* **1993**, *68*, 565–573.

(129) Deskins, N. A.; Kerisit, S.; Rosso, K. M.; Dupuis, M. Molecular Dynamics Characterization of Rutile-Anatase Interfaces. *J. Phys. Chem. C* **2007**, *111*, 9290–9298.

(130) Akoagi, M.; Matsui, M. Molecular Dynamics Simulation of the Structural and Physical Properties of the Four Polymorphs of TiO$_2$. *Mol. Simul.* **1991**, *6*, 239.

(131) Collins, D. R.; Smith, W.; Harrison, N. M.; Forester, T. R. Molecular Dynamics Study of TiO2 Microclusters. *J. Mater. Chem.* **1996**, *6*, 1385–1390.

(132) Kresse, G.; Hafner, J. Ab Initio Molecular Dynamics for Liquid Metals. *Phys. Rev. B* **1993**, *47*, 558–561.

(133) Kresse, G.; Hafner, J. Ab Initio Molecular-Dynamics Simulation of the Liquid-Metal–amorphous-Semiconductor Transition in Germanium. *Phys. Rev. B* **1994**, *49*, 14251–14269.

(134) Kresse, G.; Furthmüller, J. Efficiency of Ab-Initio Total Energy Calculations for Metals and Semiconductors Using a Plane-Wave Basis Set. *Comput. Mater. Sci.* **1996**, *6*, 15–50.

(135) Kresse, G.; Furthmüller, J. Efficient Iterative Schemes for Ab Initio Total-Energy Calculations Using a Plane-Wave Basis Set. *Phys. Rev. B* **1996**, *54*, 11169–11186.

(136) Blöchl, P. E. Projector Augmented-Wave Method. *Phys. Rev. B* **1994**, *50*, 17953–17979.

(137) Kresse, G.; Joubert, D. From Ultrasoft Pseudopotentials to the Projector Augmented-Wave Method. *Phys. Rev. B* **1999**, *59*, 1758–1775.

(138) Perdew, J. P.; Burke, K.; Ernzerhof, M. Generalized Gradient Approximation Made Simple. *Phys. Rev. Lett.* **1996**, *77*, 3865–3868.

(139) Anisimov, V. I.; Zaanen, J.; Andersen, O. K. Band Theory and Mott Insulators: Hubbard U instead of Stoner I. *Phys. Rev. B.* **1991**, *44*, 943–954.

(140) Lichtenstein, V. I. A. and F. A. and A. I. First-Principles Calculations of the Electronic Structure and Spectra of Strongly Correlated Systems: The LDA + U Method. *J. Phys. Condens. Matter.* **1997**, *9*, 767.

(141) Chrétien, S.; Metiu, H. Electronic Structure of Partially Reduced Rutile TiO_2(110) Surface: Where Are the Unpaired Electrons Located? *J. Phys. Chem. C* **2011**, *115*, 4696–4705.

(142) Stausholm-Møller, J.; Kristoffersen, H. H.; Hinnemann, B.; Madsen, G. K. H.; Hammer, B. DFT+U Study of Defects in Bulk Rutile TiO_2. *J. Chem. Phys.* **2010**, *133*.

(143) Kowalski, P. M.; Camellone, M. F.; Nair, N. N.; Meyer, B.; Marx, D. Charge Localization Dynamics Induced by Oxygen Vacancies on the TiO_2(110) Surface. *Phys. Rev. Lett.* **2010**, *105*, 146405.

(144) Morgan, B. J.; Watson, G. W. A DFT+U Description of Oxygen Vacancies at the TiO_2 Rutile (110) Surface. *Surf. Sci.* **2007**, *601*, 5034–5041.

(145) Sanyal, T. S. and K. Y. and S. M. and B. A Systematic Study of Polarons due to Oxygen Vacancy Formation at the Rutile TiO_2 (110) Surface by GGA + U and HSE06 Methods. *J. Phys. Condens. Matter* **2012**, *24*, 435504.

(146) Finazzi, E.; Di Valentin, C.; Pacchioni, G.; Selloni, A. Excess Electron States in Reduced Bulk Anatase TiO_2: Comparison of Standard GGA, GGA+U, and Hybrid DFT Calculations. *J. Chem. Phys.* **2008**, *129*.

(147) Toroker, M. C.; Kanan, D. K.; Alidoust, N.; Isseroff, L. Y.; Liao, P.; Carter, E. a First Principles Scheme to Evaluate Band Edge Positions in Potential Transition Metal Oxide Photocatalysts and Photoelectrodes. *Phys. Chem. Chem. Phys.* **2011**, *13*, 16644–54.

(148) Nolan, M.; Elliott, S. D.; Mulley, J. S.; Bennett, R. A.; Basham, M.; Mulheran, P. Electronic Structure of Point Defects in Controlled Self-Doping of the TiO_2 (110) Surface: Combined Photoemission Spectroscopy and Density Functional Theory Study. *Phys. Rev. B.* **2008**, *77*, 235424.

(149) Patrick, C. and Giustin, F. GW Quasiparticle Bandgaps of Anatase TiO2 Starting from DFT + U. *J. Phys. Condens. Matter* **2012**, *24*, 202201.

(150) Penn, R. L.; Bansfield, J. F. Formation of Rutile Nuclei at Anatase (112) Twin Interfaces and the Phase Transformation Mechanism in Nanocrystalline Titania. *Am. Mineral.* **1999**, *84*, 871.

(151) Lee, G. H.; Zuo, J.-M. Growth and Phase Transformation of Nanometer-Sized Titanium Oxide Powders Produced by the Precipitation Method. *J. Am. Ceram. Soc.* **2004**, *87*, 473–479.

(152) Zhang, H.; Banfield, J. F. Understanding Polymorphic Phase Transformation Behavior during Growth of Nanocrystalline Aggregates: Insights from TiO_2. *J. Phys. Chem. B* **2000**, *104*, 3481–3487.

(153) Li, G.; Gray, K. A. The Solid–solid Interface: Explaining the High and Unique Photocatalytic Reactivity of TiO_2-Based Nanocomposite Materials. *Chem. Phys.* **2007**, *339*, 173–187.

(154) Nunzi, F.; Mosconi, E.; Storchi, L.; Ronca, E.; Selloni, A.; Gratzel, M.; De Angelis, F. Inherent Electronic Trap States in TiO_2 Nanocrystals: Effect of Saturation and Sintering. *Energy Environ. Sci.* **2013**, *6*, 1221–1229.

(155) Zhang, J.; Hu, Y.; Matsuoka, M.; Yamashita, H.; Minagawa, M.; Hidaka, H.; Anpo, M. Relationship between the Local Structures of Titanium Oxide Photocatalysts and Their Reactivities in the Decomposition of NO. *J. Phys. Chem. B* **2001**, *105*, 8395–8398.

(156) Xia, T.; Li, N.; Zhang, Y.; Kruger, M. B.; Murowchick, J.; Selloni, A.; Chen, X. Directional Heat Dissipation across the Interface in Anatase–Rutile Nanocomposites. *ACS Appl. Mater. Interfaces* **2013**, *5*, 9883–9890.

(157) Kullgren, J.; Huy, H. A.; Aradi, B.; Frauenheim, T.; Deák, P. Theoretical Study of Charge Separation at the Rutile--Anatase Interface. *Phys. status solidi (RRL)-Rapid Res. Lett.* **2014**.

(158) Li, W.-K.; Hu, P.; Lu, G.; Gong, X.-Q. Density Functional Theory Study of Mixed-Phase TiO_2: Heterostructures and Electronic Properties. *J. Mol. Model.* **2014**, *20*.

(159) Mitra, C.; Lange, B.; Freysoldt, C.; Neugebauer, J. Quasiparticle Band Offsets of Semiconductor Heterojunctions from a Generalized Marker Method. *Phys. Rev. B.* **2011**, *84*, 2–5.

(160) Van de Walle, C. G. Band Theory. *Phys. Rev. B.* **1989**, *39*, 1871–1883.

(161) Kang, J.; Wu, F.; Li, S.-S.; Xia, J.-B.; Li, J. Calculating Band Alignment between Materials with Different Structures: The Case of Anatase and Rutile Titanium Dioxide. *J. Phys. Chem. C.* **2012**, *116*, 20765–20768.

(162) Van de Walle, C. G.; Neugebauer, J. Universal Alignment of Hydrogen Levels in Semiconductors, Insulators and Solutions. *Nature* **2003**, *423*, 626–8.

(163) Deskins, N. A.; Dupuis, M. Intrinsic Hole Migration Rates in TiO_2 from Density Functional Theory. *J. Phys. Chem. C.* **2008**, *113*, 346–358.

(164) Li, G.-L.; Li, W.-X.; Li, C. Model Relation between the Energy-Band Edge and the Fermi Level of the Nondegenerate Semiconductor TiO_2: Application to Electrochemistry. *Phys. Rev. B.* **2010**, *82*, 235109.

(165) Deskins, N. A.; Dupuis, M. Electron Transport via Polaron Hopping in Bulk TiO_2: A Density Functional Theory Characterization. *Phys. Rev. B.* **2007**, *75*, 195212.

(166) Cordones, A.; Leone, S. Mechanisms for Charge Trapping in Single Semiconductor Nanocrystals Probed by Fluorescence Blinking. *Chem. Soc. Rev.* **2013**, *42*, 3209–3221.

(167) Posternak, M.; Baldereschi, A.; Delley, B. Dissociation of Water on Anatase TiO_2 Nanoparticles: The Role of Undercoordinated Ti Atoms at Edges. *J. Phys. Chem. C* **2009**, *113*, 15862–15867.

(168) Flytzani-Stephanopoulos, M.; Gates, B. C. Atomically Dispersed Supported Metal Catalysts. *Annu. Rev. Chem. Biomol. Eng.* **2012**, *3*, 545–574.

(169) Molina, L. M.; Hammer, B. Some Recent Theoretical Advances in the Understanding of the Catalytic Activity of Au. *Appl. Catal. A Gen.* **2005**, *291*, 21–31.

(170) Min, B. K.; Friend, C. M. Heterogeneous Gold-Based Catalysis for Green Chemistry: Low-Temperature CO Oxidation and Propene Oxidation. *Chem. Rev.* **2007**, *107*, 2709–2724.

(171) Janssens, T. W.; Clausen, B.; Hvolbæk, B.; Falsig, H.; Christensen, C.; Bligaard, T.; Nørskov, J. Insights into the Reactivity of Supported Au Nanoparticles: Combining Theory and Experiments. *Top. Catal.* **2007**, *44*, 15–26.

(172) Gong, J. Structure and Surface Chemistry of Gold-Based Model Catalysts. *Chem. Rev.* **2012**, *112*, 2987–3054.

(173) Valden, M.; Lai, X.; Goodman, D. W. Onset of Catalytic Activity of Gold Clusters on Titania with the Appearance of Nonmetallic Properties. *Science (80-.).* **1998**, *281*, pp. 1647–1650.

(174) Freund, H.-J.; Meijer, G.; Scheffler, M.; Schlögl, R.; Wolf, M. CO Oxidation as a Prototypical Reaction for Heterogeneous Processes. *Angew. Chemie Int. Ed.* **2011**, *50*, 10064–10094.

(175) Haruta, M.; Daté, M. Advances in the Catalysis of Au Nanoparticles. *Appl. Catal. A Gen.* **2001**, *222*, 427–437.

(176) Bond, G. C.; Thompson, D. T. Gold-Catalysed Oxidation of Carbon Monoxide. *Gold Bull.* **2000**, *33*, 41–50.

(177) Kung, H. H.; Kung, M. C.; Costello, C. K. Supported Au Catalysts for Low Temperature CO Oxidation. *J. Catal.* **2003**, *216*, 425–432.

(178) Rodriguez, J. A. Gold-Based Catalysts for the Water–gas Shift Reaction: Active Sites and Reaction Mechanism. *Catal. Today* **2011**, *160*, 3–10.

(179) Williams, W. D.; Shekhar, M.; Lee, W.-S.; Kispersky, V.; Delgass, W. N.; Ribeiro, F. H.; Kim, S. M.; Stach, E. A.; Miller, J. T.; Allard, L. F. Metallic Corner Atoms in Gold Clusters Supported on Rutile Are the Dominant Active Site during Water−Gas Shift Catalysis. *J. Am. Chem. Soc.* **2010**, *132*, 14018–14020.

(180) Schubert, M. M.; Hackenberg, S.; van Veen, A. C.; Muhler, M.; Plzak, V.; Behm, R. J. CO Oxidation over Supported Gold Catalysts—"Inert" and "Active" Support Materials and Their Role for the Oxygen Supply during Reaction. *J. Catal.* **2001**, *197*, 113–122.

(181) Chen, M. S.; Goodman, D. W. The Structure of Catalytically Active Gold on Titania. *Science (80-.).* **2004**, *306*, pp. 252–255.

(182) Liu, Z.-P.; Gong, X.-Q.; Kohanoff, J.; Sanchez, C.; Hu, P. Catalytic Role of Metal Oxides in Gold-Based Catalysts: A First Principles Study of CO Oxidation on TiO_2 Supported Au. *Phys. Rev. Lett.* **2003**, *91*, 266102.

(183) Vilhelmsen, L. B.; Hammer, B. Interfacial Oxygen under TiO_2 Supported Au Clusters Revealed by a Genetic Algorithm Search. *J. Chem. Phys.* **2013**, *139*, -.

(184) Vilhelmsen, L. B.; Hammer, B. Identification of the Catalytic Site at the Interface Perimeter of Au Clusters on Rutile TiO_2(110). *ACS Catal.* **2014**, *4*, 1626–1631.

(185) Remediakis, I. N.; Lopez, N.; Nørskov, J. K. CO Oxidation on Rutile-Supported Au Nanoparticles. *Angew. Chemie* **2005**, *117*, 1858–1860.

(186) Lopez, N.; Janssens, T. V. W.; Clausen, B. S.; Xu, Y.; Mavrikakis, M.; Bligaard, T.; Nørskov, J. K. On the Origin of the Catalytic Activity of Gold Nanoparticles for Low-Temperature CO Oxidation. *J. Catal.* **2004**, *223*, 232–235.

(187) Mavrikakis, M.; Stoltze, P.; Nørskov, J. K. Making Gold Less Noble. *Catal. Letters* **2000**, *64*, 101–106.

(188) Lopez, N.; Nørskov, J. K.; Janssens, T. V. W.; Carlsson, A.; Puig-Molina, A.; Clausen, B. S.; Grunwaldt, J.-D. The Adhesion and Shape of Nanosized Au Particles in a Au/TiO_2 Catalyst. *J. Catal.* **2004**, *225*, 86–94.

(189) Wahlström, E.; Lopez, N.; Schaub, R.; Thostrup, P.; R\onnau, A.; Africh, C.; L\aegsgaard, E.; N\orskov, J. K.; Besenbacher, F. Bonding of Gold Nanoclusters to Oxygen Vacancies on Rutile TiO_2 (110). *Phys. Rev. Lett.* **2003**, *90*, 26101.

(190) Matthey, D.; Wang, J. G.; Wendt, S.; Matthiesen, J.; Schaub, R.; Lægsgaard, E.; Hammer, B.; Besenbacher, F. Enhanced Bonding of Gold Nanoparticles on Oxidized $TiO_2(110)$. *Science (80-.).* **2007**, *315*, 1692–1696.

(191) Widmann, D.; Behm, R. J. Active Oxygen on a Au/TiO_2 Catalyst: Formation, Stability, and CO Oxidation Activity. *Angew. Chemie Int. Ed.* **2011**, *50*, 10241–10245.

(192) Green, I. X.; Tang, W.; Neurock, M.; Yates, J. T. Insights into Catalytic Oxidation at the Au/TiO_2 Dual Perimeter Sites. *Acc. Chem. Res.* **2014**, *47*, 805–815.

(193) Koga, H.; Tada, K.; Okumura, M. DFT Study of CO Oxidation over Au/TiO_2: The Extent of the Reactive Perimeter Zone. *Chem. Phys. Lett.* **2014**, *610–611*, 76–81.

(194) Rodriguez, P.; Plana, D.; Fermin, D. J.; Koper, M. T. M. New Insights into the Catalytic Activity of Gold Nanoparticles for CO Oxidation in Electrochemical Media. *J. Catal.* **2014**, *311*, 182–189.

(195) Li, X.-N.; Yuan, Z.; He, S.-G. CO Oxidation Promoted by Gold Atoms Supported on Titanium Oxide Cluster Anions. *J. Am. Chem. Soc.* **2014**, *136*, 3617–3623.

(196) VandeVondele, J.; Krack, M.; Mohamed, F.; Parrinello, M.; Chassaing, T.; Hutter, J. Quickstep: Fast and Accurate Density Functional Calculations Using a Mixed Gaussian and Plane Waves Approach. *Comput. Phys. Commun.* **2005**, *167*, 103–128.

(197) Williams, W. D.; Shekhar, M.; Lee, W.-S.; Kispersky, V.; Delgass, W. N.; Ribeiro, F. H.; Kim, S. M.; Stach, E. A.; Miller, J. T.; Allard, L. F. Metallic Corner Atoms in Gold Clusters Supported on Rutile Are the Dominant Active Site during Water−Gas Shift Catalysis. *J. Am. Chem. Soc.* **2010**, *132*, 14018–14020.

(198) Wang, Y.-G.; Yoon, Y.; Glezakou, V.-A.; Li, J.; Rousseau, R. The Role of Reducible Oxide–Metal Cluster Charge Transfer in Catalytic Processes: New Insights on the Catalytic Mechanism of CO Oxidation on Au/TiO_2 from Ab Initio Molecular Dynamics. *J. Am. Chem. Soc.* **2013**, *135*, 10673–10683.

(199) Wang, J. G.; Hammer, B. Role of Au^+ in Supporting and Activating Au_7 on $TiO_2(110)$. *Phys. Rev. Lett.* **2006**, *97*, 136107.

(200) Vilhelmsen, L. B.; Hammer, B. Systematic Study of Au_6 to Au_{12} Gold Clusters on MgO(100) F Centers Using Density-Functional Theory. *Phys. Rev. Lett.* **2012**, *108*, 126101.

(201) Sun, C.; Smith, S. C. Strong Interaction between Gold and Anatase $TiO_2(001)$ Predicted by First Principle Studies. *J. Phys. Chem. C* **2012**, *116*, 3524–3531.

(202) Romero Sarria, F.; Plata, J.; Laguna, O. H.; Marquez, A.; Centeno, M. A.;

Fernandez Sanz, J.; Odriozola, J. A. Surface Oxygen Vacancies in Gold Based Catalysts for CO Oxidation. *RSC Adv.* **2014**, -.

(203) Rodríguez, J. A.; Evans, J.; Graciani, J.; Park, J.-B.; Liu, P.; Hrbek, J.; Sanz, J. F. High Water−Gas Shift Activity in TiO_2(110) Supported Cu and Au Nanoparticles: Role of the Oxide and Metal Particle Size. *J. Phys. Chem. C* **2009**, *113*, 7364–7370.